

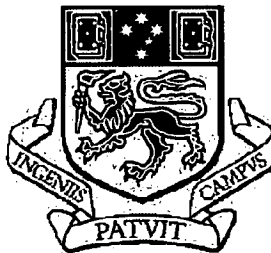
Hydrogen Production Performance Modelling Using Intelligent Techniques

By

Steffen Becker

Dipl. Wirtschafts-Ingenieur (Industrial Eng.)

**Submitted in Fulfilment of the Requirements for the Degree of
Doctor of Philosophy**



School of Engineering, University of Tasmania

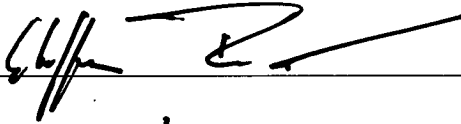
September 2010

STATEMENT OF ORIGINALITY AND AUTHORITY OF ACCESS

This thesis contains no material that has been accepted for a degree or diploma by the University of Tasmania or any other institution, except by way of background information that has been duly acknowledged in this thesis, and to the best of the author's knowledge and belief no material has previously been published or written by another person except where due acknowledgement is made in text of this thesis.

This thesis contains confidential information and is not to be disclosed or made available for loan or copy without the expressed permission of the University of Tasmania. Once released the thesis may be available for loan and limited copying in accordance with the Copyright Act 1968.

Signed: _____



Date: _____

17/03/2010

ABSTRACT

Electrolytic hydrogen production can be seen as the binding element in utilising and storing renewable energies towards a sustainable and environmentally compatible energy supply.

In this thesis comprehensive literature review on hydrogen production with emphasises on electrolysis of water and various conventional models has been conducted. Furthermore, literature survey on applied Artificial Neural Networks (ANN) and Adaptive Neuro-Fuzzy Inference Systems (ANFIS) elucidates architecture, functionality and application in detail.

This study provided predictive hydrogen production performance models for a commercial PEM-electrolyzer. Two different approaches using intelligent techniques have been conducted. The first employs ANN and the second uses a hybrid model ANFIS as time series prediction combining fuzzy logic and Neural Networks.

An experimental apparatus has been developed to measure and model specific performance parameters such as hydrogen flow rate, system-efficiency and stack-efficiency. A comprehensive range of experimental conditions were tested as part of the investigation that covers a wide range of input variables and their influence on the output performance. The various parameters have been obtained using the electrolyzers' internal software (windows diagnostic) and additional sensors measuring power and feed water parameters, such as water quality, water pressure, system temperature, stack current, stack voltage, system power consumption, system pressure, product pressure and lower explosive limit. Synchronous data-acquisition of all parameters was carried out with National Instruments LabVIEW software to build a database. The database formed the foundation for the predictive models, where experimental data were used to train and test the developed hydrogen production performance models. Verification of those models was carried out by comparison of predicted and measured data. It is argued that, due to the high costs associated with the hydrogen measuring equipment; these reliable predictive models can be implemented as virtual sensors.

Hydrogen production performance models were built using ANN and ANFIS for parameter prediction of hydrogen flow rate, system-efficiency and stack-efficiency respectively. The quantitative accuracy of the predictive models is appraised using statistical techniques. These mathematical models are found to be reliable predictive tools with a maximum RMS error of $\pm 3\%$ compared with the experimental values. The predictive nature of these models did not show any significant bias to either over prediction or under prediction.

These predictive models, built on a sound mathematical and quantitative basis, can be seen as a step towards establishing hydrogen performance prediction models as generic virtual sensors for wider safety and monitoring applications. This work is a significant advancement for understanding of dynamic electrolyzer behaviour and intelligent modelling to build virtual sensors.

ACKNOWLEDGEMENTS

First of all I would like to express my deepest gratitude to my mentor and supervisor Prof Vishy Karri. His guidance, knowledge and support proved to be invaluable for me and had an enormous impact towards the completion of this work. I also like to thank my co-supervisor Prof Michael Negnevitsky for his support and assistance in all matters regarding my candidature here at the School of Engineering. His rational thinking put things in the right perspective, whenever it was necessary.

I would like to express my gratitude towards the School of Engineering, especially former Head of School Prof Frank Bullen and acting Head of School Prof Chris Letchford, for the financial support during my candidature. Without the scholarship and funding for the research to be undertaken, this project would not have been possible. Greatly appreciated was also the help from Mrs. Mary Dixon and Mrs. Jenny O'Donohue in all administrative matters. In addition, I would like to thank the technical staff Mr. Bernhard Chenery, Mr. David Morley, Mr. Steven Avery, Mr. Russell Twining, Mr. Glenn Mayhew, Mr. Nathan Smith and Mr. Peter Seward for the generous and invaluable support during the developmental and experimental stage of this project. Special thanks also to Mr. Anders Rou from the Aalborg University in Denmark for the collaboration during the early stage of this project.

Furthermore, I would like to particularly thank my friends Ahsan, David, Jason, Obiwankenobi, Aman, Vien, Rob, Duncan, Rod, Matt for the unique experiences in social events and endless conversations and debates whilst having coffee and cigarettes. Their support during (also before and after) my PhD candidature definitely provided the anchor to cope with this challenge. Thanks to Dr Sushil Patil, I know mate, it was a long way to the top, for giving me the support and motivation whenever I needed it. I also would like to thank Mr. James Fox for his very useful comments during the final stage of my candidature.

In particular I would like to thank my family in Germany. Without their emotional and financial support, I would have achieved nothing. Also many thanks to my all time best friends JU, Tiedt and Stoecki. I will always be always with you guys, even

if I am in down under. Just to be sure, I would like to thank everyone who has supported and assisted me and I might have forgotten in this section.

Finally, I would like to show my appreciation to my beautiful partner and soul mate Laura Parsley for giving me the strength, advice and endless emotional support to complete this project. Thank you for being part of my life.

DEDICATION

*I dedicate this thesis to my parents,
Monika and Manfred Becker. Without them, I would not be here and this thesis
would have never been written.*

LIST OF PUBLICATIONS

1. Becker, S. and V. Karri. Neural network based predictive models for PEM-electrolyzer performance, Proceedings Hypothesis 8, Hydrogen Systems and Materials for Sustainability, Lisbon (2009), April 1-3
2. Becker, S. and V. Karri, Predictive models for PEM-electrolyzer performance using adaptive neuro-fuzzy inference systems. International Journal of Hydrogen Energy. In Press, Corrected Proof.
3. Becker, S. and V. Karri, Modelling of hydrogen production efficiency for a PEM-electrolyzer using Neural Networks. The 3rd International Workshop on Artificial Intelligence in Science and Technology (AISAT), Hobart (2009), 23-24 November
4. Becker, S. and V. Karri, Implementation of Neural Network Models for parameter estimation of a PEM-electrolyzer. Journal of Advanced Computational Intelligence and Intelligent Informatics (JACIII). (2010). Accepted, In Press
5. Negnevitsky, M., Haque, E., Gargoom, A., Haruni, O., Becker, S., Muttaqi, K., Hybrid remote area power supply systems with hydrogen energy storage for isolated and regional Communities, Annual Progress Report, Australian Research Council (ARC), 2008

TABLE OF CONTENTS

STATEMENT OF ORIGINALITY AND AUTHORITY OF ACCESS	II
ABSTRACT	III
ACKNOWLEDGEMENTS.....	V
DEDICATION.....	VII
LIST OF PUBLICATIONS.....	VIII
TABLE OF CONTENTS	IX
LIST OF FIGURES	XII
LIST OF TABLES.....	XV
NOMENCLATURE	XVI
CHAPTER 1 INTRODUCTION.....	1
1.1 Present Global Energy Supply and Forecast	2
1.2 Energy Supply Challenges.....	3
1.2.1 Pollution and global warming.....	3
1.2.2 Decrease of fossil fuels.....	5
1.3 Future Energy Supply	7
1.3.1 Renewable energies.....	7
1.3.2 Hydrogen as a prospective solution in a future energy supply	9
1.4 Thesis Objective and Structure.....	11
CHAPTER 2 LITERATURE SURVEY	12
2.1 Hydrogen Production.....	13
2.1.1 Introduction to hydrogen and production technologies	13
2.1.2 Properties of hydrogen as a fuel	14
2.1.3 Hydrogen production from fossil resources and biomass.....	16
2.1.4 Hydrogen from water.....	20
2.2 Electrolysis of Water	20
2.2.1 Thermodynamic fundamentals and general theory.....	21
2.2.2 Electrolyzer.....	26
2.2.2.1 Alkaline electrolyzer.....	27
2.2.2.2 PEM-electrolyzer.....	30
2.3 Use of PEM-Electrolysis and Broader Applications of Hydrogen Generation On-line	34
2.3.1 PEM-electrolysis as a preferred method in industrial use	34

2.3.2 PEM-electrolysis in conjunction with renewable energies	36
2.4 Concluding Remarks	38
CHAPTER 3 INTELLIGENT TECHNIQUES AS PREDICTIVE MODELS FOR VARIOUS NON-LINEAR PROCESSES	42
3.1 Introduction to Artificial Neural Networks	43
3.1.1 Biological function of neurons	43
3.1.2 Artificial neurons	45
3.2 Neural Network Classification	47
3.2.1 Feed-forward networks	47
3.2.2 Recurrent Neural Networks	48
3.3 Training of Neural Networks	49
3.3.1 Supervised learning of Neural Networks	50
3.3.2 Unsupervised learning of Neural Networks	51
3.4 Neural Network Models	52
3.4.1 Back-propagation Neural Network	52
3.4.2 Optimisation Layer-by-Layer Neural Network	57
3.5 Hybrid Intelligent Systems	64
3.6 Adaptive Neuro-Fuzzy Inference Systems	65
3.7 Application of ANN and ANFIS	68
3.8 Concluding Remarks	69
CHAPTER 4 EXPERIMENTAL SETUP AND DESIGN	70
4.1 Introduction	71
4.2 Hydrogen Test Rig Facility and Safety Aspects	71
4.3 Experimental Setup and Components	73
4.3.1 Hydrogen generator	73
4.3.2 Storage unit	77
4.3.2.1 Material and assembly	78
4.3.2.2 Permeability and sealing	82
4.3.2.3 Purification procedure and pressurisation	84
4.3.3 Water deionisation	86
4.3.4 Power analyser	88
4.4 Data-Acquisition	89
4.4.1 On board diagnostic software of electrolyzer	90
4.4.2 Determination of electrolyzer serial link parameters and data protocols	91
4.4.3 Implementation with National Instruments LabVIEW software	94

4.5 Range of Operating Conditions and Testing	97
4.6 Concluding Remarks	100
CHAPTER 5 PREDICTIVE MODELS FOR HYDROGEN PRODUCTION	
PERFORMANCE IN A PEM-ELECTROLYZER	101
5.1 Introduction	102
5.2 Hydrogen Production Performance Prediction Model of a PEM-Electrolyzer.....	102
5.2.1 Neural Network Analysis Package	103
5.2.2 General procedure of performance prediction modelling using ANN.....	105
5.2.3 ANFIS implementation.....	107
5.2.4 ANFIS parameter selection.....	107
5.3 Results and Model Evaluation	108
5.3.1 Stack-efficiency prediction model.....	108
5.3.2 Hydrogen flow rate prediction model.....	114
5.3.3 System-efficiency prediction model	119
5.4 Concluding Remarks	125
CHAPTER 6 FINAL CONCLUDING REMARKS AND PROPOSED FUTURE WORK 126	
REFERENCES	129
APPENDIX EXPERIMENTAL DATA.....	144

LIST OF FIGURES

Figure 1.1: Rising primary energy demand in Australia [1].....	2
Figure 1.2: Changes in Carbon Dioxide from Ice-Core from IPCC assessment report 2007 [3]	4
Figure 1.3: Discovery vs. Production [15].....	6
Figure 1.4: Share of renewable energy in gross energy consumption from in Denmark [18].	8
Figure 1.5: Example for a grid connected hydrogen application and research focus	10
Figure 2.1: Current hydrogen production methods.....	14
Figure 2.2: Hofmann voltameter.....	21
Figure 2.3: Principle of an electrolysis cell	22
Figure 2.4: Monopolar cell design.....	27
Figure 2.5: Bipolar cell design	28
Figure 2.6: PEM-electrolyzer cell.....	31
Figure 2.7: Examples of a PEM water electrolysis cell polarization curves using different anode electrocatalysts and Nafion 115 electrolyte	33
Figure 2.8: Example of a grid independent PV-hydrogen energy system	37
Figure 3.1: Biological structure of a nerve cell	44
Figure 3.2: Architecture of an artificial neuron	45
Figure 3.3: Activation functions	47
Figure 3.4: Feed-forward Neural Network	48
Figure 3.5: Recurrent Neural Network	49
Figure 3.6: Schematic of a Back-propagation Neural Network model with one hidden layer	53
Figure 3.7: Basic structure of an Optimisation Layer-by-Layer network with one hidden layer	58
Figure 3.8: Linearised network structure for hidden layer optimisation	61
Figure 3.9: Typical ANFIS structure with 2 inputs	66
Figure 4.1: UTAS hydrogen laboratory layout.....	72
Figure 4.2: Combustible gas sensor and wall fan.....	73
Figure 4.3: Hogen® 20 PEM-electrolyzer setup in hydrogen laboratory.....	74
Figure 4.4: Inside view of electrolyzer with location of components.....	76
Figure 4.5: Flow schematic of Hogen® 20 electrolyzer.....	77
Figure 4.6: Hydrogen storage unit trolley.....	78

Figure 4.7: Connected tanks and piping	80
Figure 4.8: Connector and weld connector assembly	81
Figure 4.9: Connector welded with thread for each storage tank including o-ring	81
Figure 4.10: Main needle valve with metal against metal solution for safety	82
Figure 4.11: Vacuum pump	85
Figure 4.12: Pressurisation with nitrogen	85
Figure 4.13: Hydrogen storage purification procedure before initial operation of the storage unit to ensure safety handling and quality of hydrogen.....	86
Figure 4.14: Water deionisation system with water container (1),RTD (resistance temperature device) (2), water deionisation (3), feed-water pump (4), pressure transducer (5), flow-meter (6) and data-acquisition connection box (7)	87
Figure 4.15: PM 3000 wiring diagram	88
Figure 4.16: Data-acquisition schematic	89
Figure 4.17: Electrolyzer diagnostic software	91
Figure 4.18: Hardware setup for deduction of interrogator byte sequence.....	92
Figure 4.19: Feed water parameters front panel	94
Figure 4.20: Power analyser setup front panel	95
Figure 4.21: Electrolyzer system parameter front panel.....	96
Figure 4.22: Virtual instrument front panel of main program	96
Figure 4.23: Experimental hydrogen flow for tank filling process.....	98
Figure 5.1: Performance Prediction Model (PPM) schematic	103
Figure 5.2: User interface of Neural Network Model Selection.....	104
Figure 5.3: General Neural Network structure for PPM.....	105
Figure 5.4: Back-propagation Neural Network (BP1) RMS error with changing architecture for prediction of Stack-efficiency	109
Figure 5.5: Two hidden layer Back-propagation Neural Network (BP2) RMS error with changing architecture for prediction of Stack-efficiency	110
Figure 5.6: OLL Neural Network RMS error with changing architecture for prediction of Stack-efficiency	111
Figure 5.7: ANFIS network with 3 membership functions for prediction of stack-efficiency	113
Figure 5.8: Back-propagation Neural Network (BP1) RMS error with changing architecture for prediction of Hydrogen flow rate.....	114
Figure 5.9: Two hidden layer Back-propagation Neural Network (BP2) RMS error with changing architecture for prediction of Hydrogen flow rate	116

Figure 5.10: OLL Neural Network RMS error with changing architecture for prediction of Hydrogen flow rate	117
Figure 5.11: Experimental and predicted data for OLL Neural Network with 8 neurons in hidden layer for Hydrogen flow rate prediction	119
Figure 5.12: Back-propagation Neural Network (BP1) RMS error with changing architecture for prediction of System-efficiency	120
Figure 5.13: Two hidden layer Back-propagation Neural Network (BP2) RMS error with changing architecture for prediction of System-efficiency.....	121
Figure 5.14: OLL Neural Network RMS error with changing architecture for prediction of System-efficiency	122
Figure 5.15: ANFIS network with 3 membership functions for prediction of system-efficiency	124

LIST OF TABLES

Table 2.1: Properties of hydrogen, methane, propane and gasoline	15
Table 2.2: Hydrogen production share by source (annual).....	17
Table 2.3: Typical composition of natural gas	18
Table 2.4: Overview of alkaline electrolyzer manufacturers.....	29
Table 2.5: Overview of PEM-electrolyzer manufacturers.....	32
Table 4.1: Specifications for Hogen®RE and Hogen®20.....	75
Table 4.2: Part list of hydrogen storage unit.....	79
Table 4.3: Permeability of hydrogen for several o-ring materials.....	83
Table 4.4: Concatenated data pairs (1-7) representing electrolyzer system parameters.....	93
Table 4.5: Data pairs (8-14) for electrolyzer system parameters.....	93
Table 5.1: ANFIS performance for prediction of stack-efficiency with variation of MFs and epochs based on RMS error.....	112
Table 5.2: Summary of best performing model in each category.....	113
Table 5.3: ANFIS performance for prediction of hydrogen flow rate with variation of MFs and epochs	117
Table 5.4: Summary of best performing model for hydrogen flow rate prediction in each category	118
Table 5.5: ANFIS hybrid network performance for prediction of system-efficiency with variation of MFs and epochs	122
Table 5.6: Summary of best performing model for system-efficiency in each category	123
Table 5.7: Selected models for the PPM of the PEM-electrolyzer	125

NOMENCLATURE

AI	Artificial Intelligence
ANFIS	Adaptive Neuro-Fuzzy Inference Systems
ANN	Artificial Neural Networks
APU	Auxiliary Power Unit
BP	British Petroleum
BP1	Back-propagation Neural Network with one hidden layer
BP2	Back-propagation Neural Network with two hidden layers
CH ₄	Methane
CO	Carbon Monoxide
CO ₂	Carbon Dioxide
O ₂	Oxygen
H ₂	Hydrogen
HC	Hydrocarbons
HHV	Higher Heating Value
IEA	International Energy Agency
IPPC	Intergovernmental Panel on Climate Change
KOH	Potassium Hydroxide
LEL	Lower Explosive Limit
LHV	Lower Heating Value
LPG	Liquefied Petroleum Gas
MF	Membership Function
NO _x	Nitrogen Oxides
OECD	Organization for Economic Co-operation and Development
OLL	Optimisation Layer-by-Layer
PEM	Proton Exchange Membrane
PO	Peak Oil
PPM	Performance Prediction Model
PPS	Product Pressure
PV	Photovoltaic
RBF	Radial Basis Function

RMS	Root Mean Square
SAPS	Stand Alone Power Systems
SCT	Stack Current
SMR	Steam Methane Reformation
SPS	System Pressure
STM	Electrolyzer System Temperature
SVG	Stack Voltage
SO ₂	Sulphur Dioxide
WTQ	Feed Water Quality

CHAPTER 1

INTRODUCTION

“I believe that water will one day be employed as fuel, that hydrogen and oxygen which constitute it, used singly or together, will furnish an inexhaustible source of heat and light, of an intensity of which coal is not capable.”

Jules Verne, *The Mysterious Island* (1874)

1.1 Present Global Energy Supply and Forecast

The primary energy is the energy contained in raw fuels and other forms of energy. It also includes renewable energies and is usually transformed to a more convenient form of energy such as electricity and petrol. The global primary energy demand is mainly driven by conventional use of fossil fuels, such as coal, crude oil, natural gas and nuclear resources. As an example, Australia's primary energy demand or generation from 1984- 2004 is shown in figure 1.1 [1]. The graph shows, that the main provider for electricity in Australia comes from conventional thermal and hydro power. About 75% of generated electricity in Australia is derived from coal. A small fraction of renewable energies is displayed in the figure at the beginning of 2000. There is a steady increase in overall generation or consumption over the last 20 years, in other words it has doubled from 1984-2004.

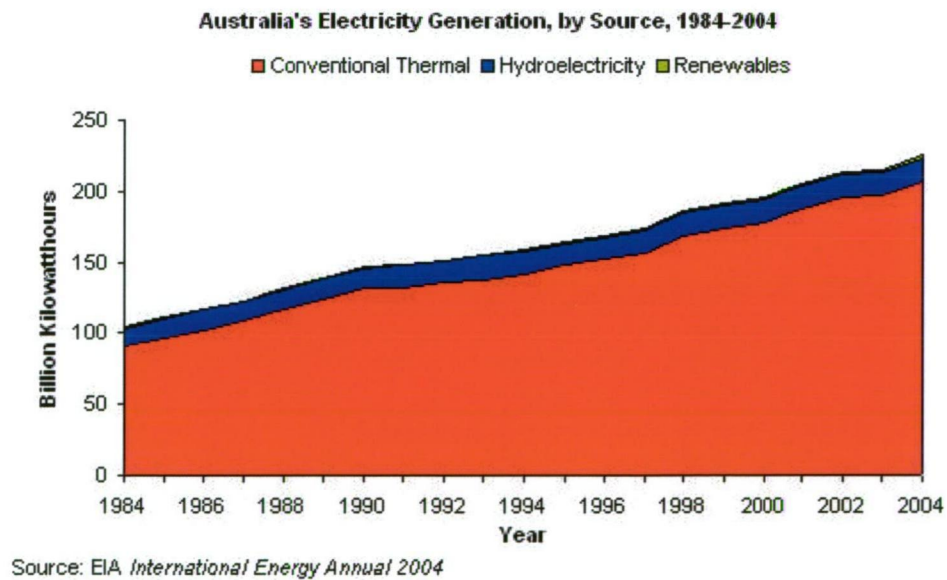


Figure 1.1: Rising primary energy demand in Australia [1]

An outlook over the transportation sector established the dependency on fossil resources of our oil based economies, as most of the fuels to power cars and trucks are also derived from fossil energy resources, such as crude oil.

The International Energy Agency (IEA) states, in the latest energy outlook for the transportation sector, an average increase of 2.7% for non-OECD (Organization for Economic Co-operation and Development) nations compared to an average growth of 0.3% per year for OECD countries from 2006- 2030. The transportation systems are generally well established in OECD countries, hence a comparative higher growth in energy consumption in developing countries, such as non-OECD nations [2].

1.2 Energy Supply Challenges

1.2.1 Pollution and global warming

The cause for global warming has been clearly identified by increasing rates of greenhouse gases such as carbon dioxide into the atmosphere since the industrialisation of the early 19th century. This fact directly reflects human activity through burning of fossil fuels as the cause for greenhouse gas emissions according to the latest report of the Intergovernmental Panel on Climate Change (IPCC) [3].

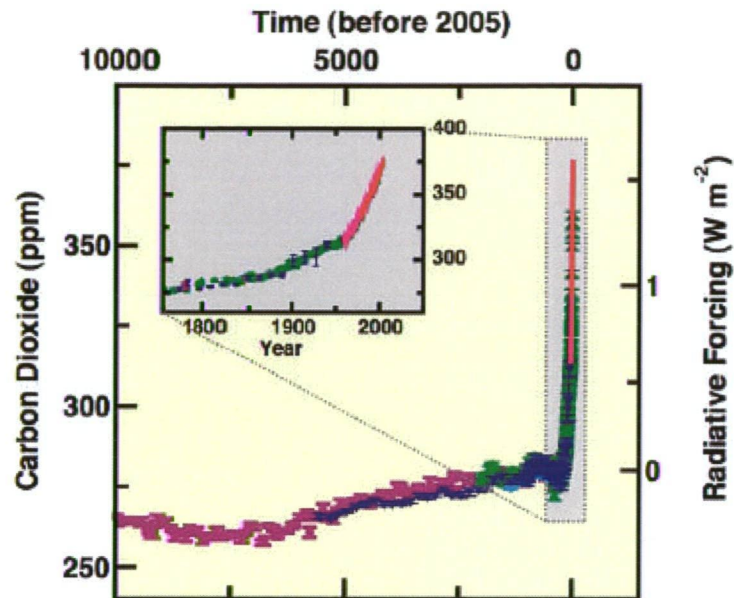


Figure 1.2: Changes in Carbon Dioxide from Ice-Core from IPCC assessment report 2007 [3]

Figure 1.2 shows the increase of carbon dioxide as one particular greenhouse gas over the last 10000 years. The evidence supporting this fact has been discovered by ice-core drilling. The figure shows a slow increase of carbon dioxide from the atmosphere until the mid 18th century. An exponential increase from the beginning of the industrial revolution 250 years ago is due to burning of fossil fuels.

The burning of fossil fuels is polluting on a global scale. The impacts of pollution from burning of fossil fuels are widely felt on personal and political levels. Major cities are experiencing lower air quality, which is directly linked to emissions from power generation, residential heating and motor vehicles [4-6]. Motor vehicles emit carbon dioxide into the atmosphere contributing to global warming. Other harmful emissions include Carbon Monoxide (CO), Hydrocarbons (HC), Nitrogen Oxides (NO_x) and Sulphur Dioxide (SO₂). A number of these compounds have mutagenic and carcinogenic effects in humans [7]. Carbon Monoxide produces severe health effects in humans reducing the oxygen carrying capacity of blood. This can cause

chronic poisoning and shows first symptoms as headaches, blurry vision and difficulty in concentration [8]. Some HC's have been proven to be carcinogenic (lung cancer) [9]. Nitrogen Oxides, especially nitrogen dioxide, contribute to morbidity and mortality as affects the lung directly and can lead to inflammatory reactions [10].

1.2.2 Decrease of fossil fuels

Fossil fuels are exhaustible resources. Reports on fossil fuel reserves vary, as released data about production and depletion rates are scarce and uncertain. British Petroleum (BP) and OPEC (Organisation of Petroleum Exporting Countries) for example, frequently vary their assumptions of undiscovered reserves, keeping in mind that controversial statistics have political and economical impact. A recent model by Topal and Sharhriar [11] assumes a continuous compound rate and computes depletion times for oil, coal and gas of approximately 35, 107 and 137 years respectively [11]. The models for oil and gas show a positive and significant relationship with consumption, compared to a negative and significant relationship with price [11]. As the transport sector heavily relies upon oil production, the 35 years to come indicate a growing gap between production and demand.

A phenomenon termed Peak Oil (PO) describes the associated with growing demand and maximum production capacity and was initially introduced by Hubbert [12]. The concept was at first disputed, but the general idea is now well accepted [13, 14]. However, the time frame for the PO production is still under discussion and varies from “already happening” to the next 2-3 decades.

According to Hubbert [12] it is impossible to keep up with rising energy demand as new discoveries of oil and gas fields are decreasing. Even if mankind will not run out of fossil resources in the next decades, the effect of shortage in global energy supply will increase the price of those resources [11]. For example, the price of crude oil rose 57% to about \$100 USD per barrel in 2007, increasing to \$147 USD in 2008.

The high price could be a result of fewer discoveries in crude oil deposits and growing demand as expected by Hubbert [12].

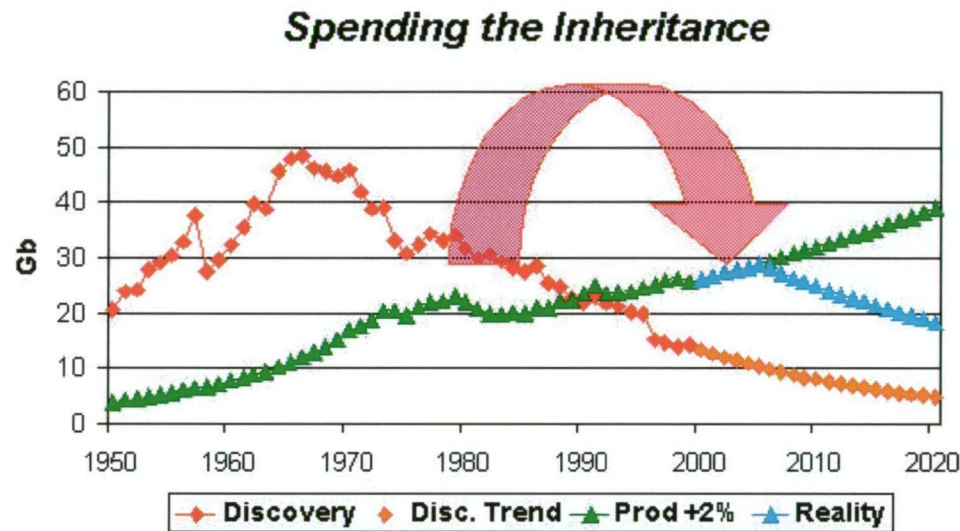


Figure 1.3: Discovery vs. Production [15]

Figure 1.3 [15] illustrates the basic idea of the Peak Oil scenario according to Campbell [15, 16]. The red line shows the discovery of crude oil deposits with a ten year moving average. It shows a decline since the 1970's with a clear downward trend. The green line shows the production with an extrapolated 2% growth in demand. The 'inheritance' or reserves is defined as the area between the red and green line. As the discovery trend crosses the production trend in the early 1990's, the 'inheritance' is declining as discoveries are insufficient to match the growing demand. Therefore production will peak at some point in future, indicated at the downward trend of the blue line (reality) [15, 16]. The crude oil peak scenario shows another need for alternatives in the energy sector of our oil based economies. This is turning point for mankind. At the actual peak production, little or no time for reaction remains to find alternatives for oil and the economic pressure will be enormous [15].

1.3 Future Energy Supply

1.3.1 Renewable energies

Renewable energies, such as hydro power, wind power and solar power offer the potential for a new form of energy supply compared to the traditional approach based on fossil fuels. The term renewable applies as they are freely available and “renew” themselves on a steady basis, so the supply will not suddenly come to an end compared to the non-renewable fossil energy resources. Renewable energies can greatly assist in cutting greenhouse gas emissions as technology available allows to produce electricity directly, without emitting greenhouse gases compared to electricity generation from coal and oil. Renewable energies provide a substantial part in the primary energy generation in several countries around the world. In addition, those technologies help to develop new industries and create new jobs, which ultimately provide diversity in energy supply and economic growth.

Denmark for example has a share of renewable energies in primary energy consumption of approximately 15% in 2005 as shown in figure 1.4. The figure also shows a steady increase from 1980 until 2005. Some of their share is covered by net imports, e.g. the import of feed stock for biomass production. The government of Denmark laid the foundation for the growth of renewable energies and industries by government incentives in response to the oil crisis in 1973 [17].

Production and Consumption of Renewable Energy - Share of Gross Energy Consumption

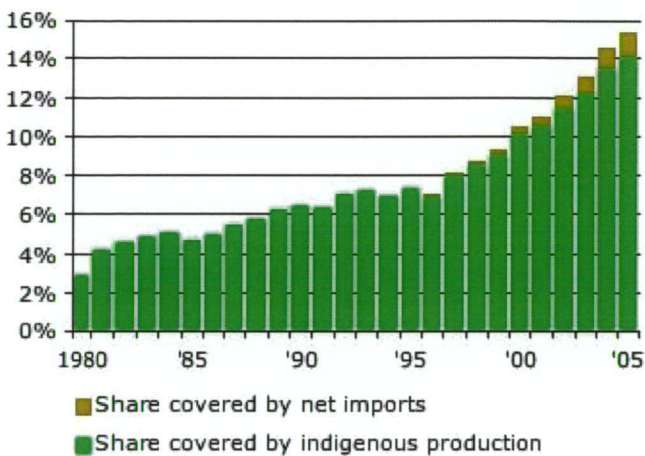


Figure 1.4: Share of renewable energy in gross energy consumption from in Denmark
[18]

In Australia, Tasmania provides approximately 90% of primary energy from hydro power [19] compared to the national power generation, which generates 75% electricity from coal [1]. The dominance of coal as the primary energy source demonstrates the necessity of a nation wide (and global) energy strategy to cut greenhouse gas emission to an acceptable level. A 50-60% global reduction by 2050 has been recommended by the IPCC in order to bring climate changes back under control [3].

The drawback with renewable energies is often seen in their fluctuating nature as wind and solar radiation are not always present. An energy mix, such as the combination of solar power and wind power can provide a step towards a more sustainable system, but still it is not a definite solution. There is need for a storage medium to store renewable energies in times of greater supply than needed, in order to compensate for insufficient supply times.

1.3.2 Hydrogen as a prospective solution in a future energy supply

Hydrogen is the most abundant element on the earth, however it is mostly bound to other elements such as hydrocarbons and water. It has some distinct benefits for its high energy content per mass basis compared to hydrocarbon fuels, hence its application in electricity generation, combustion engines and aerospace. It is especially of great interest in such applications as there is nearly zero pollution in its conversion, e.g. fuel cell vehicles only emit water.

Hydrogen is considered to play a key role in the future energy supply, as it can be used as an energy storage and transportation medium. It has the potential as a renewable and sustainable solution for reducing fossil fuel consumption and emissions and thus combating global warming and pollution [20, 21]. Due to its bonds to other elements it has to be produced. Several technologies are available for the production of hydrogen, to name the most common such as the steam reforming of natural gas and electrolysis of water. As the reformation of natural gas is further exploiting fossil energy resources and the need for alternative energy supply has been described in section 1.2, the electrolysis of water only uses electric current and water as resources. If the electric current for the electrolytic hydrogen generation is provided by renewable sources, emissions are cut severely and a step towards a more sustainable energy supply can be established.

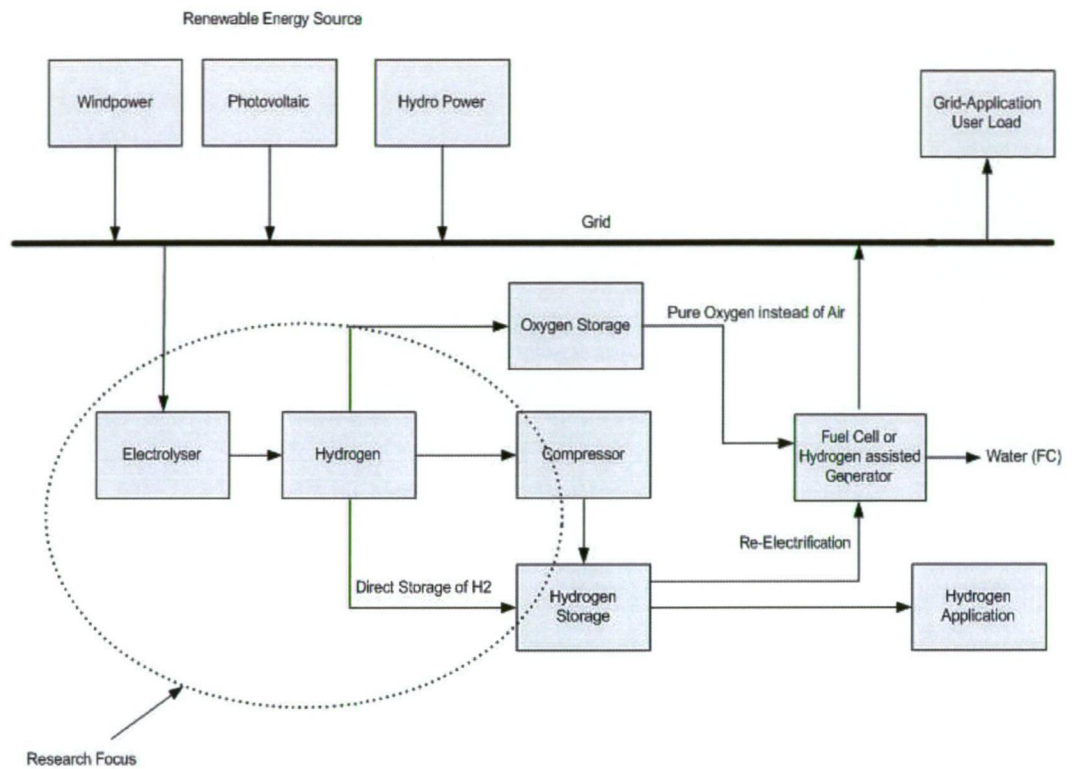


Figure 1.5: Example for a grid connected hydrogen application and research focus

Figure 1.5 shows an example for a possible hydrogen application in conjunction with renewable energies. The renewable sources such as wind power or solar power are connected to the grid. In times of over supply of electricity an electrolyzer is converting the electricity to a more suitable storage medium, hydrogen gas. Depending on the setup of the overall system, it can either be compressed and stored or directly stored. When the energy demand cannot be matched by the renewable sources, the stored hydrogen can be re-electrified, e.g. by a fuel cell or hydrogen assisted generator and fed back into the grid. In other words hydrogen can be seen as the binding element for the exploitation of renewable energies as a storage medium to compensate for the fluctuating nature of renewable sources.

1.4 Thesis Objective and Structure

The specific objectives of this thesis are the investigation of a commercial Proton Exchange Membrane (PEM)-electrolyzer and then to apply the experimental findings from a custom designed test rig to several models based on intelligent techniques. The developed neural network based models, after sufficient training and testing, operate as a virtual sensor to accurately predict basic electrolyzer performance parameters.

This work also investigates the potential application of intelligent technologies, such as Artificial Neural Networks (ANNs) and Adaptive Neuro-Fuzzy Inference Systems (ANFIS), as an alternative modelling approach to predict hydrogen production performance parameters. In order to develop the predictive models, a comprehensive range of experimental conditions is tested to build a database. The experimental data cover a wide range of input variables and their influence on the output performance and represent a realistic industrial hydrogen production process.

The thesis is structured in 6 chapters. Chapter 2 represents literature reviews on hydrogen production with emphasis on electrolysis of water, fundamentals and conventional modelling techniques. Chapter 3 elucidates applied alternative modelling approaches based on intelligent techniques, such as ANNs and ANFIS, with respect to architecture, functionality and application in detail. That is followed by chapter 4, which describes the design and construction of the experimental rig, including data-aquisition and -collection of various system parameters. The obtained experimental data build the foundation for the applied neural network based modelling approaches previously discussed in chapter 3. Construction, results and discussion of developed predictive models for hydrogen production performance are presented in chapter 5. Final concluding remarks and proposed future work are discussed in chapter 6.

CHAPTER 2

LITERATURE SURVEY

2.1 Hydrogen Production

2.1.1 Introduction to hydrogen and production technologies

Declining crude oil supplies, environmental problems and political instability in regions with large oil deposits are creating a need for alternative fuels in our oil based economies. Within a number of potential alternative fuels such as biodiesel, methanol, ethanol, natural gas, liquefied petroleum gas (LPG), it seems hydrogen is having the best prospective to fulfil the attributes of alternative fuels to be technically feasible, economically competitive, environmentally friendly and available [22].

Historically, hydrogen was first discovered by von Hohenheim, also known as Paracelsus (1493–1541). He was the first to artificially produce hydrogen via the mixing of metals with strong acids, unaware that the flammable gas produced by this chemical reaction was a new chemical element. About a century later, in 1671, Robert Boyle's research describes the reaction between iron fillings and diluted acids, resulting in the production of hydrogen gas. Another century had to pass by, before Henry Cavendish first recognized hydrogen gas as “inflammable air” and produces water when burned. He also was able to accurately describe several key properties of hydrogen gas as a discrete substance. Although he is usually given credit for hydrogen discovery, its name was given by Antoine Lavoisier in 1783. In conjunction with the prior findings of Cavendish and his own experiments its name was derived from the Greek words of “hydro” and “genes”, which means “water” and “born of” [23, 24].

Hydrogen is the most abundant element on the earth, but it is usually bound to other elements. Therefore it requires a production or generation method. The schematic in figure 2.1 gives an overview about current production methods. The present hydrogen generation can be divided into three major methods: thermal, electrochemical and biological respectively. These primary production methods can be further divided. Characteristically every generation method depends on the feedstock or the source of hydrogen and the procedure respectively.

Properties for hydrogen as an alternative fuel have been briefly outlined in the next subsection, followed by a number of quantitatively significant methods for present hydrogen production. A special emphasises is given to the electrolysis of water, as it can be seen as a step towards utilising intermitted renewable energy sources into a sustainable future energy management.

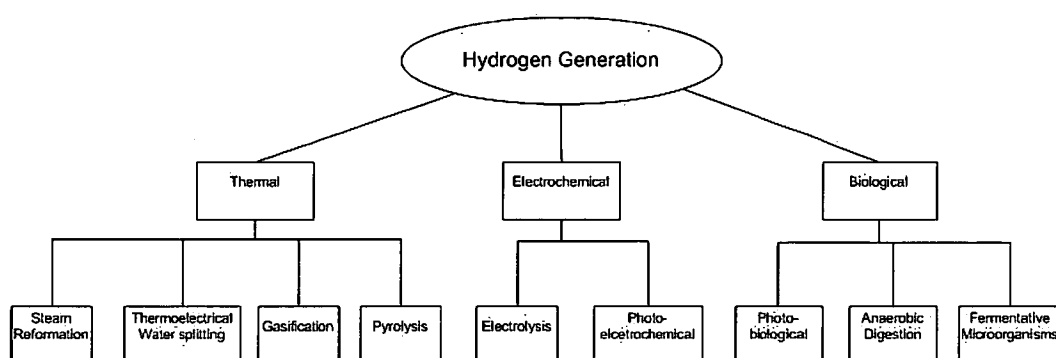


Figure 2.1: Current hydrogen production methods

2.1.2 Properties of hydrogen as a fuel

Hydrogen is an odourless, colourless, tasteless and non-toxic gas. It can be found in air at concentrations of approximately 100ppm or 0.01% respectively. The universe composes of 75% of normal matter by mass and over 90% by number of atoms of hydrogen, making it the most abundant element [25]. Table 2.1 [25] shows the combustion and explosion properties of hydrogen in comparison to other fuels such as methane, propane and gasoline vapour. However, it should be noted that gasoline is normally used in its liquid form and is approximately 12000 times denser and contains about 4000 times more energy per unit of volume compared to hydrogen. Some distinct properties that contribute to its use as a fuel can be derived from the table. Hydrogen accounts for a high energy density by mass ranging from $119.93 \times 10^3 \text{ kJ/kg}$ (Lower Heating Value, LHV) to $141.8 \times 10^3 \text{ kJ/kg}$ (Higher Heating Value, HHV), which is about 2.5 times greater compared to other hydrocarbon fuels.

Conversely hydrogen is also the lightest element with a very low density of 0.08988g/l indicating its energy content by volume is very small with approximately 2.9×10^{-3} kWh/l (LHV) under standard conditions (100kPa and 15.5°C). This fact leads to challenges within the automotive sector, in particular to store a sufficient amount of hydrogen in vehicles to provide adequate driving ranges [26]. The storage options for hydrogen in general and especially vehicles vary from high pressure gas storage, liquidation of hydrogen to absorption by metal hydrides [27-29]. It should also be noted that the flammability limits for hydrogen are exceptionally wide, ranging from 4-75% of hydrogen concentration in air. Hydrogen's use in combustion engines allows high compression ratios and efficiencies in addition to less nitrogen oxide emissions compared to gasoline operated engines [30]. Fuel cell operated vehicles have indeed negligible emissions as hydrogen reacts with oxygen, directly produces electricity and only emits water.

Table 2.1: Properties of hydrogen, methane, propane and gasoline

	Hydrogen	Methane	Propane	Gasoline
Density of gas at standard conditions [kgm⁻³(STP)]	0.084	0.65	2.42	4.4 (100kPa and 15.5°C)
Heat of vaporisation [kJ kg⁻¹]	445.6	509.9		250-400
Lower heating value [kJ kg⁻¹]	119.93×10^3	50.02×10^3	46.35×10^3	44.5×10^3
Higher heating value [kJ kg⁻¹]	141.8×10^3	55.3×10^3	50.41×10^3	48×10^3
Thermal conductivity of gas at standard conditions [m W cm⁻¹ K⁻¹]	1.897	0.33	0.18	0.112
Diffusion coefficient in air at standard conditions [cm² s⁻¹]	0.61	0.16	0.12	0.05
Flammability limits in air [vol%]	4.0-75	5.3-15	2.1-9.5	1-7.6
Detonability limits in air [vol%]	18.3-59	6.3-13.5		1.1-3.3

Chapter 2: Literature Survey

Limiting oxygen index [vol%]	5	12.1		11.6 (average value for a mixture)
Stoichiometric composition in air [vol%]	29.53	9.48	4.03	1.76
Minimum energy for ignition in air [MJ]	0.02	0.29	0.26	0.24
Autoignition temperature [K]	858	813	760	500-744
Flame temperature in air [K]	2318	2148	2385	2470
Maximum burning velocity in air at standard conditions [m s⁻¹]	3.46	0.45	0.47	1.76
Detonation velocity in air at standard conditions [km s⁻¹]	1.48-2.15	1.4-1.64	1.85	1.4-1.7 (based on properties of n-pentane and benzene)
Energy of explosion, mass- related [gTNT g⁻¹]	24	11	10	10

Furthermore hydrogen has a very high diffusion coefficient which represents its ability to disperse in air. This fact in particular is of advantage for two reasons [26]. One, it supports the formation of a uniform mixture in the combustion process and two, it is advantageous if possible leaks within the fuel or storage system occur, as it disperses rapidly. This fact also supports the safety aspects for use and handling of hydrogen. For a more detailed compilation of hydrogen safety characteristics and hazard on handling see references [32 -33].

2.1.3 Hydrogen production from fossil resources and biomass

Principally hydrogen can be derived from all primary energy sources [23]. As shown in table 2.2 [34], most of the hydrogen produced today, approximately 96% worldwide, is derived from fossil energy resources such as natural gas, oil and coal.

The hydrogen of present production is mainly used in oil refineries and petrochemical plants to refine fuels and to manufacture industrial commodities such as ammonia, steel and polymers. Furthermore hydrogen can be utilised for generator cooling, as rocket fuel in liquid form because of its high energy content by mass and in several other industries, e.g. pharmaceutical, glass, ceramic, electronic etc. [35].

Table 2.2: Hydrogen production share by source (annual)

Source	Billion Nm ³ /year	Share (%)
Natural gas	240	48
Oil	150	30
Coal	90	18
Water (Electrolysis)	20	4
Total	500	100

The most common and widely used methods for hydrogen production from fossil fuels are the Steam Methane Reformation (SMR) [36-39] and partial oxidation [40-44] of hydrocarbon fuels.

The feedstock for the SMR process is usually natural gas, which accounts for almost 48% of the entire hydrogen production (table 2.2). The chemical composition of natural gas consists primarily of methane, hence SMR, but includes also significant quantities of ethane, butane and pentane as shown in table 2.3. Natural Gas (NG), which contains hydrocarbons other than methane, is often referred in the literature as wet NG compared to dry natural gas that only consists of methane. SMR is currently the least expensive method with an energy consumption rate of about 1.23-1.35GJ-NG per GJ hydrogen [45]. It is a three step process, involving a catalytic reformation of methane at elevated temperature and pressure to produce a mixture (syngas) of hydrogen and Carbon Monoxide (CO) in the first step, followed by a catalytic shift reaction to combine CO and water to produce the hydrogen

product. In the third step purification of the hydrogen product is carried out by adsorption. The reforming reaction can be described as follows:



Table 2.3: Typical composition of natural gas

Component	Typical weight [%]
Methane (CH ₄)	70-90
Ethane (C ₂ H ₆)	5-15
Propane (C ₃ H ₈) and Butane (C ₄ H ₁₀)	<5
CO ₂ , N ₂ , H ₂ S, etc.	Balance

Partial oxidation of hydrocarbons is usually achieved by a reaction of the hydrocarbon with steam and air at high temperature. The process requires energy to produce steam and heat for the steam-fuel mixture. A controlled amount of air (oxygen) allows partial oxidation (equation 2.2) of the fuel during the heating process of the mixture, followed by adding steam in the downstream process in order to complete the water-gas shift and fully oxidize the carbon (see equation 2.3). An example of the partial oxidation for methane is given below [44].



Hydrogen production from coal accounts for 18% of the world's hydrogen production. Gasification is the dominant process for hydrogen production from coal

and petroleum products [46-49], but other feedstock materials such as waste [50, 51] and biomass [52-54] can also be used. Generally speaking gasification is mature compared to SMR, with an energy consumption of about 1.54-1.69GJ-coal per GJ hydrogen [45]. Recent developments in the field of carbon capturing and sequestration [55, 56] give the opportunity for this method to keep the emissions to a minimum. Nevertheless the gasification process is complex and expensive, especially when carbon capturing technologies are implemented. Gasification of coal for hydrogen production can be supportive matching the hydrogen demand in a future hydrogen economy mainly in the transition stage [57, 58].

Additionally hydrogen can also be produced from biomass by a number of processes, such as pyrolysis [59-61], partial oxidation [62], steam reforming [63-65] and biological conversion methods [66-68]. Yields are generally low, since the hydrogen content of biomass is approximately 6% compared to methane with 25% [69]. This fact demonstrates the limitations of hydrogen production from biomass. Another concerning fact related to hydrogen and alternative fuel production from biomass fact can be seen in the exploitation of valuable agricultural land for fuel production. The increasing world population and the accompanied rising demand for food oppose the hydrogen production from biomass.

Hydrogen production from fossil energy sources exploits those declining resources and increases CO₂ emissions, especially when hydrogen is used as a fuel, centrally produced and distributed to its end users [70]. Carbon capture technologies are relatively new and expensive. Long-term testing of these technologies is necessary to proof their reliability and success. The production of hydrogen from fossil resources is also highly dependent on the price of the feedstock, which is subject to demand and availability. The most economical productions methods today might not be sustainable in a possible future hydrogen economy, but can assist in the transition phase to match the future hydrogen demand.

2.1.4 Hydrogen from water

Hydrogen production from water offers a possible alternative to hydrogen production from fossil resources, especially in conjunction with renewable energies towards a sustainable energy management [25]. The electrolysis of water is an electrochemical method to produce hydrogen and was found to be major technology for hydrogen production from sea water and fresh water, respectively [71]. Currently electrolysis accounts for about 4% of the global hydrogen production [34], with varying reports on system efficiencies ranging from 39-73% [72]. System efficiencies include auxiliaries and consider the power of the entire electrolysis system required to produce hydrogen based on the HHV.

As water is an available resource in most areas, the necessary electricity can be supplied by a number of sources. Nuclear energy has been taken into consideration for large scale hydrogen production in order to match the future hydrogen demand [73-76]. In particular, hydrogen production from renewable sources such as solar [77-79], wind [80-82], geothermal [83, 84] and hydropower [85-87] offer the potential for energy storage of fluctuating renewable sources and an emission free hydrogen production.

The fundamentals of electrolysis, their application in technology and several modelling approaches have been further discussed in the next sections.

2.2 Electrolysis of Water

The history of electrolysis can be seen within the history of electrochemistry. William Nicholson and Johann Ritter were the first who succeeded in decomposing water into hydrogen and oxygen in 1800. Ritter discovered the process of electroplating and also observed that the amount of metal deposited and the amount of oxygen produced during an electrolytic process depended on the distance between

the electrodes. After the invention of the voltaic pile, one of the early batteries, Nicholson and Ritter utilised it for the electrolysis of water [88].

Strictly speaking electrolysis is a method of separating bonded elements by passing electric current through an electrolyte. Figure 2.2 [89] shows the so called Hoffmann voltameter. Developed by August Wilhelm von Hofmann (1818–1892), it demonstrates the principle for electrolytic hydrogen production as one of the early alkaline electrolyzers.

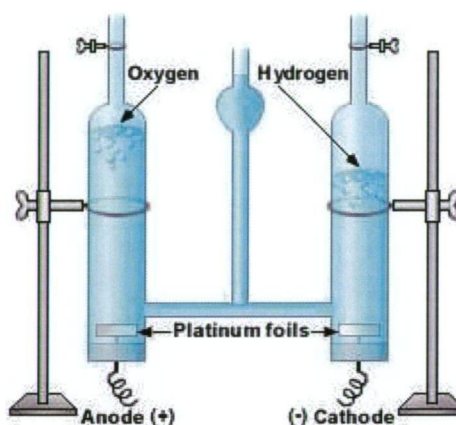


Figure 2.2: Hofmann voltameter

Pure water or distilled water is normally a non electrolyte. A few drops of an ionic compound like sulphuric acid makes it become an electrolyte. The electrodes, anode and cathode respectively, have a platinum layer and are connected to a battery. The cell generates a small current of a few milliamps, which generates hydrogen gas on the cathode (negative electrode) side and oxygen (positive electrode) on the anode side [89].

2.2.1 Thermodynamic fundamentals and general theory

The thermodynamic fundamentals for the electrolysis process are briefly described in this section. Generally speaking, the general process in all technologies for

electrolysis of water is the same. Figure 2.3 shows the basic principle of an electrolysis cell. Water supply to an electrochemical cell produces hydrogen at the cathode and oxygen at the anode when a sufficient voltage, which is above the zero-current potential E_0 , is provided. The released ions travel through an electrolyte and a diaphragm ensures the separation of oxygen and hydrogen.

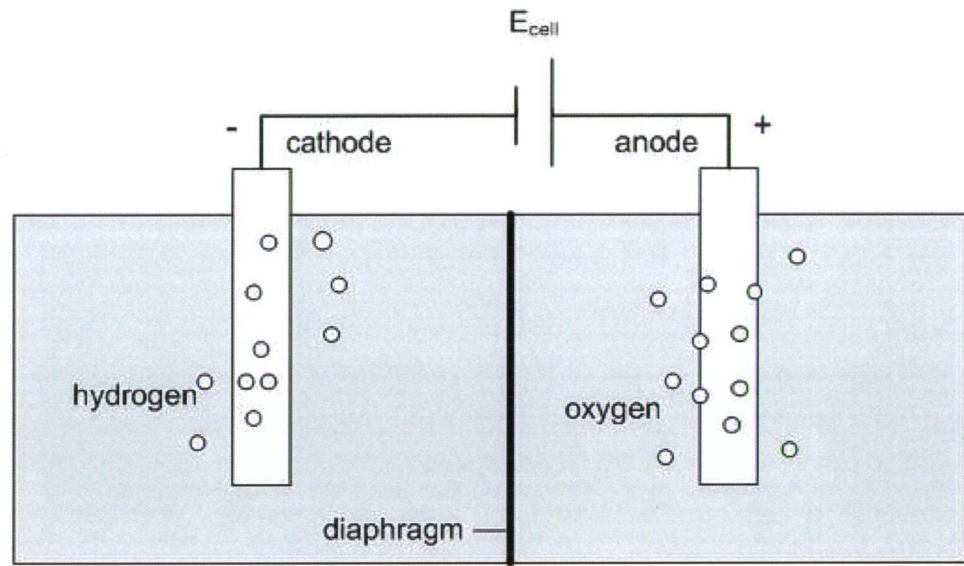
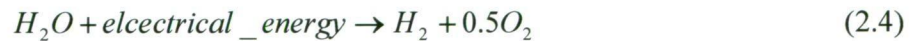


Figure 2.3: Principle of an electrolysis cell

The total reaction for splitting water can be expressed as



where the minimum electrical energy required to split water is given by the Gibbs energy ΔG_R of the reaction in equation 2.4. At standard conditions (298.15K and 101.3kPa) ΔG_R for splitting water is 237.19kJ mol⁻¹. The change in Gibbs energy is positive since it is a non-spontaneous reaction as reported by Ulleberg [90]. Consequently the zero-current cell potential E_0 can be derived as follows [25]:

$$E_0 = \frac{\Delta G_R}{nF} \quad (2.5)$$

where F represents the Faraday constant ($96\,485\text{C mol}^{-1}$) and n the number of electrons exchanged per mole of water split ($n = 2$). Therefore the standard zero-cell potential (at standard conditions) for the formation of hydrogen and oxygen from water is 1.23V.

As standard conditions are mostly applied in theory, it should be noted that Gibbs energy is dependent on temperature and pressure and thus also affect the zero-cell potential E_0 . Higher pressure increases the cell potential E_0 , whereas increasing temperatures decreases E_0 .

The energy contained in one mole of water is defined by its enthalpy of reaction ΔH_R (286kJ mol^{-1}), which is equivalent total amount of energy needed for the reaction to take place. A part of the enthalpy of reaction can be applied as thermal energy $T\Delta S_R$, which is equal to the heat demand for a reversible process. The thermal energy $T\Delta S_R$ is the amount of energy related to the entropy of reaction ΔS_R at thermodynamic temperature T as given in equation 2.6 [25].

$$\Delta H_R = \Delta G_R + T\Delta S_R. \quad (2.6)$$

Therefore the rest of the energy required to achieve ΔH_R or thermo-neutral potential E_{th} is supplied as thermal energy $T\Delta S_R$ (equation 2.6) and can be formulated as in equation 2.7 [90].

$$E_{th} = \frac{\Delta H_R}{nF} \quad (2.7)$$

The thermo-neutral potential E_{th} under standard conditions is 1.48V. The total energy required for the reaction to take place can be provided by electricity and heat. Where heat is available as by-product, the electrical power required, can be reduced at higher operating temperatures, e.g. high temperature electrolysis process [91-93].

Under real conditions the electrical energy required is significantly higher compared to the theoretical minimum of the zero-current cell potential from equation 2.5. The total voltage of an electrolysis cell E_{cell} under real conditions can be expressed as follows [25]:

$$E_{cell} = E_0 + iR + |E_{cath}^{ov}| + |E_{an}^{ov}| \quad (2.8)$$

As a result the total cell voltage depends on

- the current in the cell,
- the voltage drop iR ,
- and overvoltages of anode E_{an}^{ov} and cathode E_{cath}^{ov} , respectively.

The voltage drop iR is caused by Ohmic resistance and can be seen as a function of conductivity of electrodes, electrolyte and diaphragm, the distance between electrodes and the contact resistance between cell components. The anodic and cathodic overvoltages E_{an}^{ov} and E_{cath}^{ov} correspond to the surplus of electrical energy required to activate the electrode reactions and to conquer concentration gradients [94].

The efficiency of an electrolysis process can be estimated by the energetic ratio of the generated amount of hydrogen over a period of time P_{H_2} over the electrical power consumed P_{el} as stated in equation 2.9.

$$\eta = \frac{P_{H_2}}{P_{el}} \quad (2.9)$$

The electrical power consumed P_{el} can either refer to the power consumption of the cell stack or the entire electrolysis system, including auxiliaries. In the first case the efficiency is regarded as stack-efficiency and as system-efficiency for the latter.

It should be noted, that efficiency reports vary in literature and in most cases the Lower Heating Value (LHV) of hydrogen is used. Theoretically, the energy needed to split water is 39kWh per kg of hydrogen. This value represents the Higher Heating Value (HHV) of hydrogen. In order to overcome misrepresentations, the HHV should be used instead of the LHV for steam with 33.3kWh per kg of hydrogen; hence the produced hydrogen is derived from water. Even for an electrolyzer with no losses, the maximum efficiency that can be achieved is 84.5%, which can be derived by dividing the LHV by the HHV [72].

Aside from the approach stated in equation 2.9, efficiencies of the electrolysis process can be described more in detail. The cell efficiency η_{cell} of an electrolytic cell is defined as the ratio between the actual cell voltage E (at operating conditions with temperature T and pressure p) and the minimum theoretical voltage or E_0 as shown in equation 2.10 [25].

$$\eta_{cell} = \frac{E(T, p)}{E_0(T_0, p_0)} \quad (2.10)$$

Furthermore, the Faraday efficiency describes the ratio of produced hydrogen gas (real operating conditions) and the theoretical amount of produced hydrogen based on the current flow in the cell. It accounts for parasitic current losses in the cell and also for diffusion losses caused by hydrogen travel between cathode and anode and oxygen travel respectively (anode to cathode). Barbir [95] reports these currents and

diffusion losses to be less than 1% of operating current density and as a result Faraday efficiencies of over 90% are typically achieved [95]. Faradays law of electrolysis relates the current needed to split water directly to moles of gas produced. Therefore the Faraday efficiency $\eta_{Faraday}$ for ideal gases can be described as stated in equation 2.11 [25]:

$$\eta_{Faraday} = \frac{\dot{V}_{H_2,real}}{\dot{V}_{H_2,ideal}} \text{ with } \dot{V}_{H_2,ideal} = \frac{I}{nF} \cdot M_{mol} \quad (2.11)$$

where F and n are the same as in equation 2.5., I is current of the electrolyzer and M_{mol} being the molar mass of the hydrogen atom with 1.00797g/mol and 2.01588g/mol for the hydrogen molecule, respectively, which includes the number of atoms per molecule as a factor.

In order to describe the overall or system efficiency η_{system} of an electrolyzer, power losses due to the operation of peripheral devices $\eta_{peripheral}$ have also to be taken into account as shown in equation 2.12 [25].

$$\eta_{system} = \eta_{cell} \cdot \eta_{Faraday} \cdot \eta_{peripheral} \quad (2.12)$$

2.2.2 Electrolyzer

Electrolyzers are the technical realisation of hydrogen production through water electrolysis. The general theory has been elucidated in the previous section 2.2.1. Presently, two types of electrolyzers are commercially available for the electrolysis of water. Distinction can be made according to the state of electrolyte. The first type involves an aqueous solution (electrolyte), usually potassium hydroxide (KOH), and is often referred to as alkaline electrolyzer. The second type involves a Proton

Exchange Membrane or Polymer Electrolyte Membrane (PEM) as a solid electrolyte instead of an aqueous potassium hydroxide solution.

2.2.2.1 Alkaline electrolyzer

The alkaline electrolysis is a mature technology using aqueous potassium hydroxide solution as electrolyte. The concentration usually applied ranges between 20-30wt.%, because of optimal conductivity and extraordinary corrosion resistance of stainless steel [94]. Typical operating temperatures range between 70 and 100°C, while product pressures of hydrogen vary from 0.3psig for atmospheric electrolyzers up to usually 360psi and even up to 10,000psig for ultra high pressure electrolyzer systems (see table 2.4).

From the physical point of view an electrolyzer stack consists of several cells linked in series. Two separate cell designs, specifically monopolar (unipolar) and bipolar can be distinguished [96, 97]. In the monopolar design shown in figure 2.4 [90], electrodes are either positive or negative with parallel electrical connection of each cell.

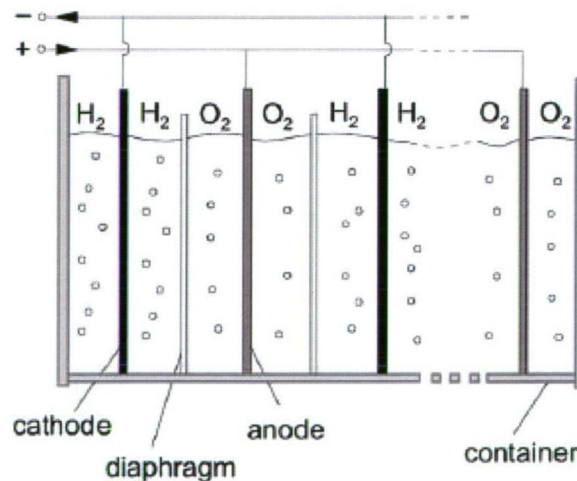


Figure 2.4: Monopolar cell design

Alternative to the monopolar design, bipolar technology is presently used in most alkaline electrolyzers. The bipolar cell design from figure 2.5 [90] demonstrates this design principle, where the individual cells are electrically and geometrically linked in series and one electrode serves as anode and cathode at the same time. This compact design has a number of advantages opposed to the monopolar design:

- Ohmic losses are reduced as the distance between electrodes and diaphragm are greatly reduced (equation 2.7)
- operation at high pressures (monopolar systems operate usually at atmospheric pressure) allow compression work for storage to be reduced.

Therefore the electrolyzer efficiency can be increased by using the bipolar design concept [96, 97].

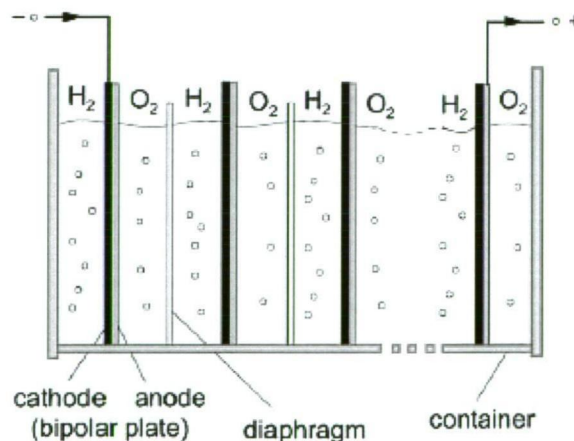


Figure 2.5: Bipolar cell design

In the so called zero-gap design of advanced alkaline electrolyzers, (bipolar) electrodes are directly placed on the diaphragm, which further reduces the distance of electrodes and the contact resistance of cell components. The aim of those advanced systems is to increase the current density (reduce investment costs as more

hydrogen is produced) and also reduce of cell voltages to reduce the power consumed and so reduce operation costs.

The technical realisation from the above stated aim leads to a conflict of interest, as increased current densities yield in increased cell voltages because of increased Ohmic resistance and overpotentials of anode and cathode. In order to overcome those problems a number of improvements had to be made. The application of low resistance diaphragms, operation at higher process temperatures to increase the conductivity of the electrolyte and so reduce the electric cell resistance and the development of new electrocatalysts such as mixed-metal coating containing cobalt oxide for anode and Raney-nickel at the cathode are partially employed in current advance alkaline electrolyzer systems to improve their performance [96,97].

The stack assembly of individual cells in an electrolyzer allows the generation of hydrogen in various quantities ranging from a few litres per hour to several hundred Nm^3 per hour. An overview of some manufacturers for alkaline electrolyzers is shown in table 2.4 [72, 98-100]. Most of them listed in the table 2.4 using bipolar technology with varying pressures. The system energy requirement gives an indication of the efficiency of the overall system, ranging from 4.3-6.1 kWh per Nm^3 or 57-81% efficiency (HHV) respectively.

Table 2.4: Overview of alkaline electrolyzer manufacturers

Manufacturer	Technology	Hydrogen production rate, min-max (Nm^3/hr)	Hydrogen product pressure (psig)	System Energy requirement (kWh/Nm^3)
Norsk Hydro ASA	Bipolar, alkaline, atmospheric	50-485	0.3	4.8
Norsk Hydro ASA	Bipolar, alkaline, high pressure	10-60	232	4.8

Chapter 2: Literature Survey

Stuart Energy Systems	Bipolar, alkaline	1-90	360	4.8-4.9
Teledyne Energy Systems	Bipolar, alkaline	2.8-42	60-115	5.3-6.1
Avalence LLC	Monopolar, alkaline	0.45-5	Up to 10,000	5.07-5.44
ELT Elektrolyse Technik GmbH [78]	Bipolar, alkaline, atmospheric	3-330	0.3	4.3-4.6
Linde AG [79]	Bipolar, alkaline	5-250	145-363	-
Hydrogenics Corporation [80]	Bipolar, alkaline	10-60	363	5.4

Aside from the cell stack, a number of peripheral devices are included in the electrolyzer system. Feed water needs to undergo deionisation to facilitate non-fouling of the system. Furthermore the electrolyte has to maintain its ideal concentration. For this purpose a process control system is employed, which controls feed water supply as well as lye (electrolyte) management. As the power supply for the stack is direct current (DC) and most systems use AC power supply, an internal AC/DC converter (rectifier) is necessary. Purification systems have to be employed, if high purity levels of the product hydrogen are necessary, e.g. for fuel cell application.

2.2.2.2 PEM-electrolyzer

Proton Exchange Membrane or Polymer Exchange Membrane (PEM)-electrolyzers use a solid electrolyte instead of an aqueous solution. General Electric was the original developer of the Solid Polymer Electrolyte (SPE) in 1967, another synonym for PEM. The material typically used is perfluorinated sulphuric acid polymer, such as Nafion® from DuPont. Those membranes act as a diaphragm and electrolyte simultaneously and are widely used in PEM fuel cells and water electrolyzers [101].

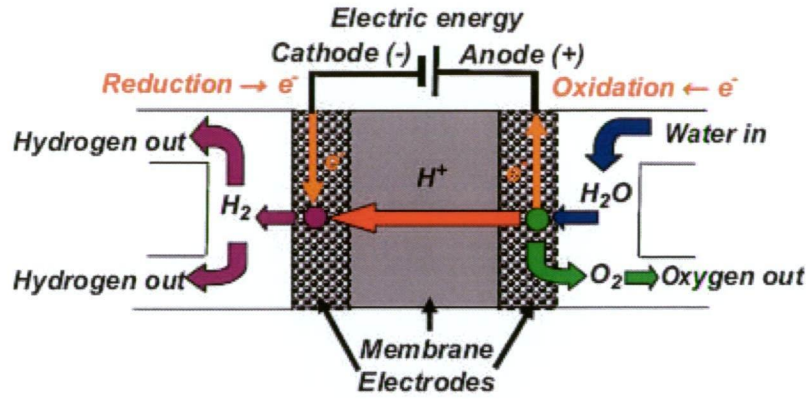


Figure 2.6: PEM-electrolyzer cell

Figure 2.6 [115] shows the schematic of a PEM-electrolyzer cell. The electrodes are directly applied on the PEM as a thin layer and deionised water is circulated in the cell. At the anode side (the positive pole) oxidation or electron loss occurs and oxygen is produced as in equation 2.13.



The membrane, containing H^+ ions for electricity conductivity, supports the proton exchange (electron transfer) to the cathode side where reduction or electron gain occurs and hydrogen is produced (see equation 2.14).



An overview about a number of current PEM-electrolyzer manufacturers is given in table 2.5 [102-106]. Few commercial systems besides the Hogen® series from Proton Energy Systems are currently available, but the development of prototypes indicate high potential for further future development. The compact design of PEM-

electrolyzer including the use of solid electrolytes instead of an alkaline solution allow better sealing options and offer the possibility for high pressure hydrogen production [107].

Table 2.5: Overview of PEM-electrolyzer manufacturers

Manufacturer	Model/ Development status	Hydrogen production rate, min-max (Nm³/hr)	Hydrogen product pressure (psig)	System Energy requirement (kWh/Nm³)
Proton Energy Systems (Distributed Energy Systems)	Hogen GC series	0.018-0.036	200	-
	Hogen S series	0.265-1.05	200	6.7
	HP (high pressure)	0.265-1.05	2400	-
	Hogen H series	2-6	218-435	6.8-7.3
Giner, Inc	Prototypes	3.7	Up to 1250	5.4
Treadwell Corporation	Prototype	1.2-10.2	Up to 1100	-
Mitsubishi Corporation	Prototype	2.5	5000	-
h-tec Wasserstoff- Energie-Systeme GmbH	Prototype	Up to 2.4	Up to 435	-

Compared to alkaline electrolysis different electrode materials (compounds) such as platinum for the anode electrode and iridium for the anode are used. The application of noble metals in PEM-electrolysis lead to higher material costs compared to conventional alkaline electrolysis. Efficiencies and hydrogen generation volumes (up to 10Nm³ per hour) of PEM-electrolyzers are generally lower as their alkaline counterparts. Nevertheless, PEM-electrolyzer cover the range of low production capacities with efficiencies reported from research and development

projects of above 80% per cell [108]. This was achieved on laboratory scale using different compositions of electrocatalysts for anode electrodes with the cell operating temperature at 80°C and low current densities as depicted in figure 2.7 [108].

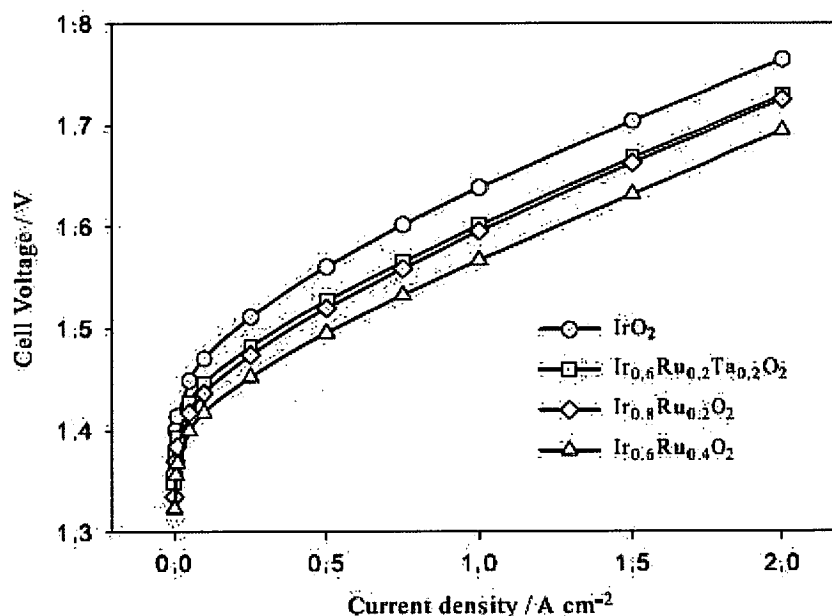


Figure 2.7: Examples of a PEM water electrolysis cell polarization curves using different anode electrocatalysts and Nafion 115 electrolyte

The performance benefits of PEM-electrolyzer offer the potential for further development and improvement in the near future. The next sections describe the application of PEM-electrolysis as a preferred method in industrial use with a view on future development followed by electrolyzer modelling approaches.

2.3 Use of PEM-Electrolysis and Broader Applications of Hydrogen Generation On-line

PEM-electrolysis technology offers some significant advantages compared to conventional alkaline electrolysis. Those advantages along with applications in industry and sustainable energy management will be discussed in detail in the following subsections.

2.3.1 PEM-electrolysis as a preferred method in industrial use

Extended incremental application of PEM-electrolyzers can be found in analytical instrument making, hydrogen welding, correction systems of a water-chemical mode of nuclear reactors, manufacturing of pure substances in electronic industry, analytical chemistry and fuel cells [109].

The inherent advantages from PEM-electrolysis over alkaline electrolysis can be summarised as follows:

- membrane sustainability of high differential pressures, whilst inhibiting mixing of product gases,
- greater safety and reliability, since no caustic electrolyte is circulated in the cell stack,
- operation of cells under high current density (up to several amps per square centimetre) is possible,
- higher gas quality with purity levels up to 99.999% and more, especially in part load operation.

As PEM technology uses solid electrolytes, a recycling of an alkaline solution is unnecessary. Furthermore the proton exchange membrane maintains a constant electrolyte concentration, which in turn needs to be addressed in alkaline systems where a lye management control system is usually employed.

Significant improvements in high pressure PEM-electrolysis ($\leq 70\text{bar}$) have been made and are currently in research and development phase [107, 110]. Such improvements are possible due to the chemical modification of the membrane, to sustain high differential pressures and reduce cross-permeation of the product gases, which increases under high pressure operation. The generation of high pressure hydrogen allows a storage option without a compressor and thus reduce the complexity of hydrogen generation and storage system and additionally increase the overall efficiency [111].

The implemented compact zero-gap design of PEM-electrolyzer stacks accompanied by the improved durability of the membrane allows the operation of high current densities of up to 2A cm^{-2} in the cells and also low energy consumption of $4.0\text{-}4.2\text{kW Nm}^{-3}$ [107]. Therefore more hydrogen per active electrode area can be produced compared to alkaline systems, where usually lower current densities and voltages are applied.

The high purity levels, around 99.999% of the produced hydrogen and oxygen make a direct application in the upcoming market of fuel cells attractive and possible, as impurities of hydrogen gas in fuel cells significantly shorten their life time span. Besides hydrogen, oxygen can be alternatively used instead of air in the fuel cell, since both gases are produced in the electrolysis process.

Although costs are still higher for PEM-electrolysis, costs are expected to be further reduced as research and development on low-cost electrocatalysts is ongoing and new families of cheap compounds are being developed and expected to appear in the short-term as reported by Millet et al. [113]. Additionally reduced energy consumption by improved electrocatalysts further increases the performance and efficiencies of PEM-electrolysis [115]. Many materials for catalysts and cell components in PEM-electrolyzer could also benefit from large scale PEM fuel cell production; hence PEM fuel cells are similar in design [112]. The principle of a PEM-electrolyzer cell operation can be seen as the reverse process to a PEM fuel cell. According to Barbir [95] and Grigoriev et al [109, 112] few modifications are necessary to convert a PEM-electrolyzer cell into a PEM fuel cell, as same membrane and catalysts on the bases of platinum metals and same production

techniques of catalyst synthesis are applied. Research is currently undertaken in the development of reversible fuel cell-electrolyzer systems, in order to combine the technologies in one compact system for hydrogen or electricity generation respectively [114].

2.3.2 PEM-electrolysis in conjunction with renewable energies

Hydrogen production via PEM-electrolysis can be realised with renewable energy sources. Most of the systems described in the literature refer to Stand Alone Power Systems (SAPS) in remote areas with no grid connection, where hydrogen is generated from renewable sources and used as energy storage before re-electrification on power demand, e.g. in fuel cells.

Barbir [95] and Clarke et al. [117] state, that PEM-electrolysis is a viable alternative for hydrogen production from photovoltaic (PV), where it may be coupled directly to the electrolyzer if polarisation curves of both systems are well matched [95, 117]. Figure 2.8 [95] shows an example of a grid independent SAPS. Handling of variable power input to the electrolyzer requires a DC/DC power regulator, which powers the cell stack, and must be part of the power conditioning and controls as depicted in figure 2.8. In this particular case, hydrogen can be generated via electrolysis from PV and either stored for re-electrification on demand by a fuel cell or used as a fuel for various applications, such as cooking, heating, cars. One essential task of the power conditioning and control is to match and optimise the polarisation curves of electrolyzer and PV array, to ensure stable and efficient operation. Additionally a permanent AC connection may be required to run the auxiliaries of the electrolyzer [95].

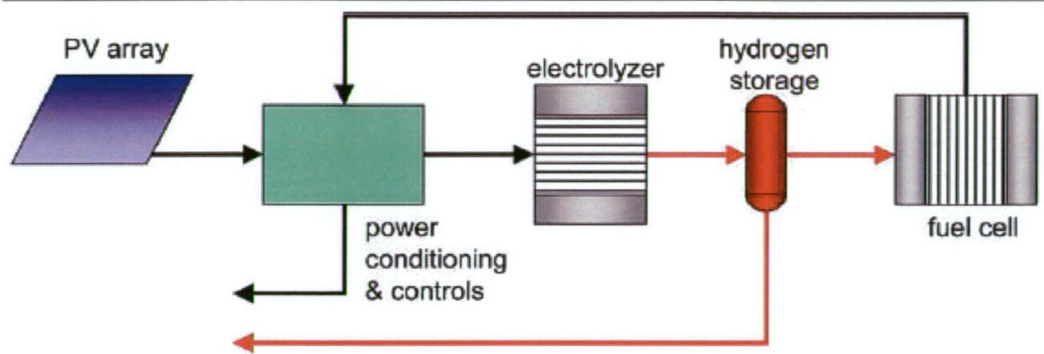


Figure 2.8: Example of a grid independent PV-hydrogen energy system

Such a system could also be grid coupled and supply high quality back-up power, where high reliability of power needs is desired [95, 116]. The combination of photovoltaic, PEM-electrolyzer and fuel cell system as an Auxiliary Power Unit (APU) has been investigated by Doucet et al. [118]. The maximum output power of the fuel cell was limited to 1kW and potential application as domestic power source and remote power supply were suggested for this APU.

The research in the field of SAPS currently deals with optimal coupling of PV arrays to PEM-electrolyzers [117, 119] and power management or control strategies of the individual system components, such as wind, photovoltaic, electrolyzer, hydrogen storage, fuel cell etc. in order to optimise such systems [120, 121]. Solar to hydrogen conversion efficiency of 18% have been reported by Peharz, Dimroth and Wittstadt [122] from the Fraunhofer Institute/ Germany. These prototypes of solar-hydrogen systems used solar cells with optical concentrator system that were directly connected to the electrodes of a PEM-electrolyzer cell. Further research focuses on improvement of the conversion efficiencies and also cost competitive development of cheaper polymer materials for large scale production.

2.4 Concluding Remarks

Several dynamic modelling approaches have been carried out based on mathematical and fundamental theory, such as thermodynamics and thermal behaviour of the electrolyzer components with different viewpoints for application, e.g. in control, monitoring, safety and overall system integration.

Models of system components, in this case an electrolyzer, are used to express their general behaviour under different operating conditions. They are also useful for determine optimal operating conditions or efficiencies respectively. Integrated in transient system simulation programs, they can be particularly used for design and optimisation of control strategies for sustainable energy systems or SAPS.

Ulleberg [90] developed a dynamic mathematical model for an advanced alkaline electrolyzer. It is based on a combination of fundamental thermodynamics, heat transfer theory and empirical electrochemical relationships. The model predicts system parameters such as cell voltage, hydrogen production, electrolyzer system temperature and efficiencies with varying reported RMS errors ranging from 0.15-5.3% between measured and predicted values. It can be applied for system design or re-design and for optimisation of control strategies [90].

Görgün [123] proposed a dynamical modelling approach based on a PEM-electrolyzer consisting of four ancillaries, anode, cathode, membrane and voltage. Physical experiments were not carried out; however, a simulation was conducted with Matlab simulink software with a view to integrate the proposed model in renewable energy systems [123].

Onda et al. [124] investigated the performance of a single electrolysis cell and applied his findings to a large cell-stack. This approach is mainly built on conservation equations of mass, mole balance at anode and cathode, charge, energy flow and membrane characteristics [124].

The safety handling and monitoring of hydrogen gas is becoming increasingly important with an emphasis on its use as alternative fuel or energy carrier. Whether the application of hydrogen is in automobiles [125, 126] or for stationary

applications, the need for equipment to monitor and measure explosion limit of any leakage increases with the pressure and flow. Lecœuche and Lebbal [127] developed a hybrid model dedicated to control and monitoring for a PEM-electrolyzer based on an analytical model and experimental data from open literature to estimate dynamic model parameters. Following this a model-based diagnosis was used to monitor the system and ensure its safety [127].

An intelligent model proposed by Karri et al. [128] predicts hydrogen pressure which is directly related to the flow rate. In this work accurate estimation of hydrogen pressure as a function of different input conditions of power supplied (voltage, current), the feed of de-ionized water and various PEM-electrolyzer system parameters is carried out. The predictive capability tested encompasses a range of hydrogen pressure that represents varied production rates. It is argued, that the reliable estimation greatly assists in avoiding expensive instrumentation for safety measurements [128].

However, most of the relevant electrolyzer models used conventional analytical approaches, empirical curve fitting techniques based on mathematical and fundamental relationships [90, 96, 123, 124, 129]. Those models are highly complex and using regression analysis or statistical modelling based on ‘empirical approach’, which makes a decision on the performance for a given set of process variables. From control point of view, the quantitative accuracy of the regression models is directly dependent on the number of process variables tested (data from open literature is often applied) and the rigour to which the complex curve fitting techniques are applied [130]. The decision on the performance will be of doubtful accuracy when an ‘alien’ process variable, not previously tested, is introduced into the decision making process. The strength of a regression model is dependent on the extent of experimental investigation and the number of process variables covered to develop such complex curve fitting techniques. The reliability of the predictive equations depend on the number of process parameters included in the equation and the extent of investigation will often result in expensive and prohibitive investigation to build such models. There is no ‘intelligence’ or ‘training’ as inherent features

within the models. They are used as mere ‘mathematical tool’ for a ‘quick answer’ from the developed empirical equations.

Neural Network based models or intelligent models, by contrast, differ to conventional models by the way the algorithm is built. They undergo a process of ‘training’, which essentially covers a comprehensive range of inputs provided to develop a decision making model. This training stage involves a constant up date of ‘inherent weights’ to match the provided target value, which otherwise is not part of regression analysis. This ‘training’ stage constantly updates all the weights in the algorithm to ‘settle for’ a minimum RMS error. This iterative process towards arriving at optimum minimum is not a feature in the regression models. Moreover, the decision making is carried out by ‘pattern recognition’ techniques that usually require minimum number of process parameters to make a comparable decision to the statistical models. This makes them most suitable for industrial cases where a data-acquisition is an expensive exercise which otherwise is not catered by the regression models. The Neural Networks provide a ‘testing stage’ which is a final stage for assessment of the developed model after the training event. This stage is a result of ‘most up dated’ weights that best represent and suit the given target values to estimate the performance. This dual stage is not part of the regression models where ‘once off’ curve fitting is carried out with out any ‘second chance’ for either adjustment or ‘super fitting’.

From a control point of view, when we have over 7 process variables, in the case of electrolysis process, that affect any given performance, any reliable regression model would need to be extremely complex with no chance for any ‘on line’ adjustment or improvement. When only few process variables are given for neural network models, the extent to which they interpolate results and arrive at decisions are more quantitatively reliable than the regression models.

This chapter presented an overview about the most common and widely used hydrogen production technologies. Special emphasises is given to the process of water electrolysis via electrolyzer. Furthermore, electrolyzer modelling approaches for hydrogen production have been discussed. Due to the complexity of those mathematical models, which rely on extensive and expensive experimental

Chapter 2: Literature Survey

investigations, an approach with intelligent techniques, such as Neural Networks and hybrid models is suggested. Intelligent techniques and their application in various non-linear dynamic processes will be further elucidated in the next chapter.

CHAPTER 3
INTELLIGENT TECHNIQUES AS PREDICTIVE MODELS FOR
VARIOUS NON-LINEAR PROCESSES

3.1 Introduction to Artificial Neural Networks

By definition, an Artificial Neural Network (ANN) is type of information processing system adopted from the functionality of the human brain or biological nervous system. The average human brain of an adult has probably about 100 billion neurons of which each is connected by approximately 5000 synapses. A brain is able to create or break one million connections per second, making it one of the most remarkable processing mechanism created by nature.

An ANN derives its computational power through a massively parallel distributed structure and its learning ability, inspired by the way the biological nervous system works. The learning ability and structure of ANNs, which is composed of a large number of highly interconnected neurons enables them to solve complex, non-linear problems. The ANN system learns to perform a function from data, e.g. an input/output map. Generally, Neural Networks are adaptive systems, where system parameters are changed during operation in the training phase and learning occurs. Following the training phase the ANN parameters are fixed and the system is tested to solve a specific problem (testing phase). As the ability to learn requires some sort of intelligence, ANNs have also been allocated to the field of Artificial Intelligence (AI) and intelligent systems [131-133].

3.1.1 Biological function of neurons

Figure 3.1 [134] shows the biological structure of a nerve cell (neuron). The neuron consists of the cell body or soma including the nucleus, a number of dendrites (incoming fibres) and the axon (outgoing fibre) with its connection (synapse) to the neighbouring cell.

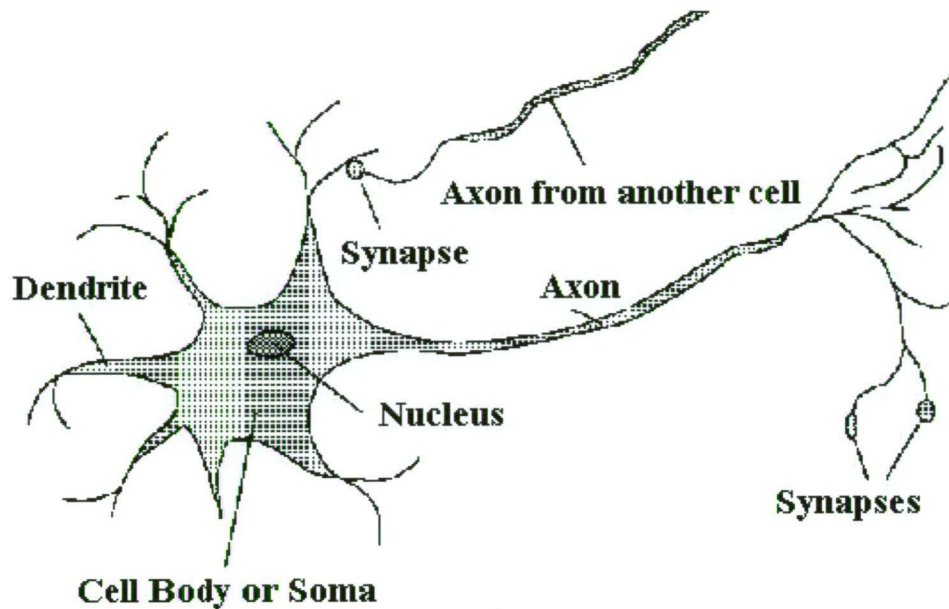


Figure 3.1: Biological structure of a nerve cell

The cell body can be seen as the main processing unit. It accepts various inputs through incoming dendrites from other neurons and processes these inputs. Outputs are sent via the axon through synapses to dendrites of other neurons. The communication or electrical signal transmission across the synapse occurs when chemical substances (neurotransmitter) in the synapse are released. This effect causes a change in the electrical potential of the cell body until a threshold value is reached and an electrical pulse is sent through the axon. The electrical pulse in turn changes the potential of the synapse. A large number of synapses show plasticity behaviour. In other words their potential can increase or decrease in strength and therefore have different strength and synaptic weights [135]. The learning mechanism of the human brain is most probably connected to the ability of changing synaptic weights of the synapses [136].

3.1.2 Artificial neurons

An artificial neuron is a fundamental information processing unit of a neural network, which consists of a number of interconnected neurons. It should be noted, that artificial neurons are truly primitive compared to their biological counterparts. Where ANNs try to imitate the sophisticated biological neural system, they are presently are not capable of actually replicate the human brain.

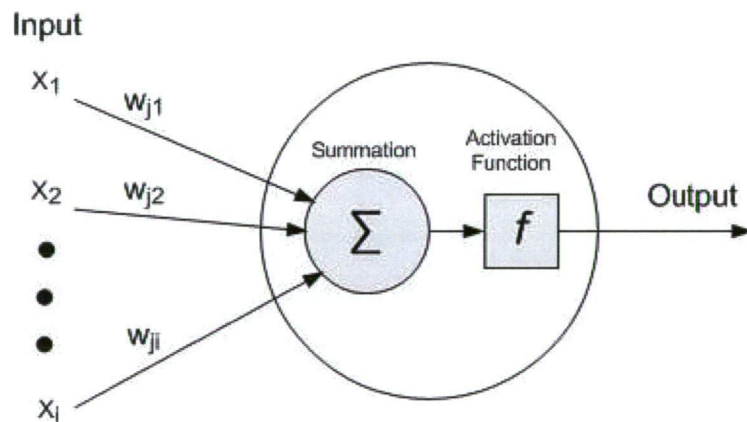


Figure 3.2: Architecture of an artificial neuron

The basic architecture of an artificial neuron is depicted in figure 3.2. The various inputs to the network are represented by the symbol x_i . Each input is multiplied by a connection weight, w_{ji} , where the index j represents the index and array of the neuron and i the index of the input of the neuron (source neuron). The neuron computes the output, after summation of the input products and feeding through an activation function occurs.

Mathematically, this process can be described as follows:

$$net_j = \sum_{i=1}^n x_i w_{ji} \quad (3.1)$$

$$output = f(net_j) = \begin{cases} +1 & \text{if } net_j \geq \theta \\ -1 & \text{if } net_j < \theta \end{cases} \quad (3.2)$$

where

- net_j: net weighted input
- n: number of inputs
- x: input
- w: connection weight
- f: activation function
- θ: threshold of neuron.

The activation function used in the above case is referred to as a sign function, where the net input net_j is either greater or less than the threshold θ and the corresponding output is +1 (activated neuron) or -1, respectively.

Apart from the sign function, several other types of activation functions, such as linear, step and sigmoid functions are commonly used as depicted in figure 3.3.

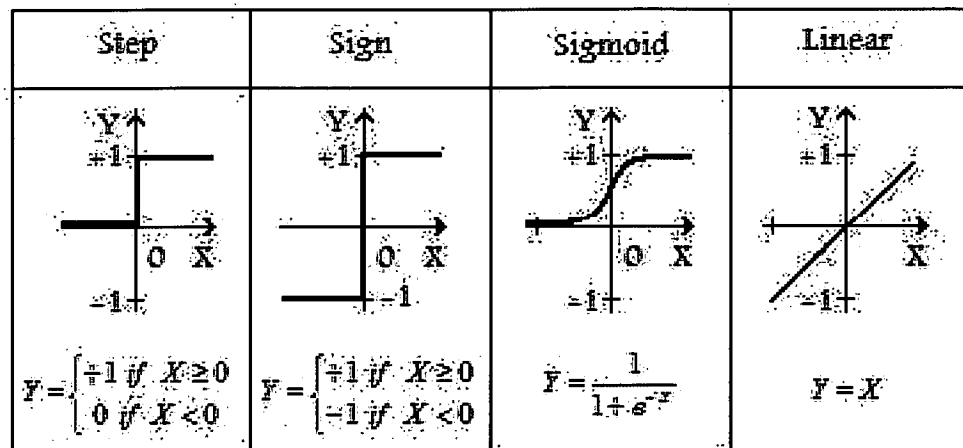


Figure 3.3: Activation functions

3.2 Neural Network Classification

Neural network models differ in the way they operate. They are classified as either feed-forward or recurrent Neural Networks.

3.2.1 Feed-forward networks

A feed-forward network is said to be one of the simplest form of Neural Networks, where source nodes (neurons) of an input layer are projected onto an output layer. Inputs are connected to each neuron in the hidden layer with corresponding weights. The information only moves one-directional, hence feed-forward. In other words, there are no lateral connections between neurons in a given layer and also none back to previous layers [131, 132]. A basic feed-forward network is shown in figure 3.4. In this case it consists of three layers, such as input, hidden and output layer.

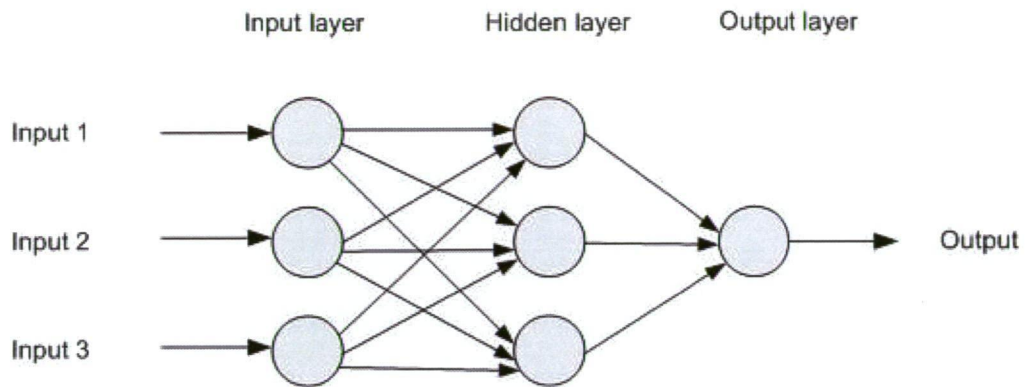


Figure 3.4: Feed-forward Neural Network

The output of a feed-forward network at any given instance is a function the inputs at that instance. The Back-propagation network [137] is one of the most popular networks among feed-forward networks.

3.2.2 Recurrent Neural Networks

In contrast to a feed-forward Neural Network, a recurrent Neural Network utilises at least one feedback loop. The output of a neuron is fed back in a previous layer. This process is repeated until the network converges. Therefore the output of a recurrent network is a function of inputs from previous layers and its own generated output (input) from an earlier time. In other words, those networks demonstrate some kind of short-term memory. Figure 3.5 illustrates such a recurrent Neural Network with external inputs and feedback loops (time-delayed) from generated outputs.

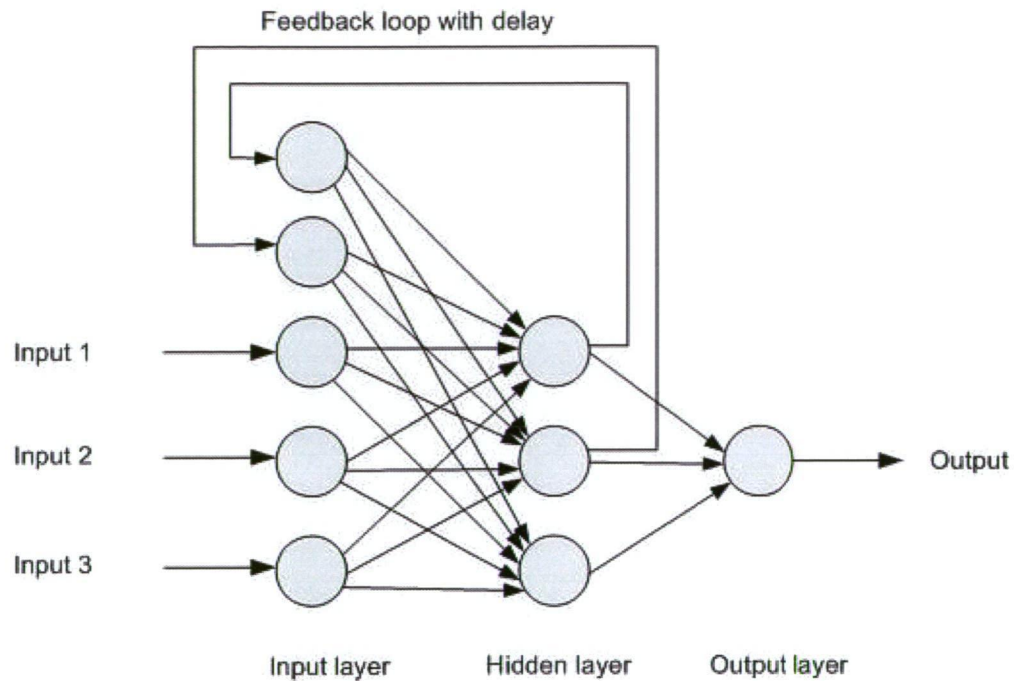


Figure 3.5: Recurrent Neural Network

Recurrent networks are used to solve computationally intense problems. They demonstrate dynamic behaviour due to the feedback loop and their outputs reflect current inputs as well as previous outputs (input). Feedback algorithms have been incorporated in a number of networks, such as the Hopfield [138] and Elman networks [139].

3.3 Training of Neural Networks

Prior to training of an ANN, the data set has to be normalized. Normalisation is a critical step in ANN as it converts input and output data to the same order of magnitude. Since original data sets (before normalisation) and their variables have values in various ranges, their corresponding influence to the predicted output might

vary and could be incorrect. In order to overcome this problem normalization of the data set to the range of 0-1 is generally performed as described in equation 3.3:

$$V_N = \frac{V_A - V_{\min}}{V_{\max} - V_{\min}} \quad (3.3)$$

where

V_N : normalised value in range from 0 to 1

V_A : actual value

V_{\min} : minimum value

V_{\max} : maximum value.

After the normalisation process, training of Neural Networks can be commenced. ANN is using a representative training data set and learns the connection weights from training patterns. This is done by creating rules through iteratively updating the inherent connection weights. Two types of training in Neural Networks can be differentiated: supervised learning and unsupervised learning, which will be discussed in the following sections.

3.3.1 Supervised learning of Neural Networks

Supervised learning of Neural Networks involves an external supervisor or teacher. The teacher controls the learning and provides information, which could a training set of data with actual inputs and their corresponding outputs. The performance of the network is graded by comparison of the actual output and the target output.

Initially the network weights are randomly set and gradually adjusted for each iteration or epoch in a way to minimise the error of actual and predicted values. Once an acceptable error is reached, which is usually a minimum error given by the supervisor the weights are set permanently before the network is tested by a set of data excluded from the training set. The testing phase ensures that the network has learned the patterns from the training phase. The testing error determines whether the training phase has been successful.

Examples of supervised learning algorithms include the Back-propagation network [137], Radial Basis Function network [140] and Optimisation Layer-by-Layer network (OLL) [141].

3.3.2 Unsupervised learning of Neural Networks

In comparison to supervised learning, unsupervised learning of Neural Networks does not require an external teacher. It is also referred to as self-organising learning, where the system organises itself by internal criteria local information. The performance is monitored internally and adaptations are made according to the function of the network.

The Kohonen network represents an example of an unsupervised learning network [142]. During the training phase the network discovers significant features in the input patterns and automatically learns to classify them into categories with similar features. In other words learning takes place by observation and discovery, where regularities and trends are extracted and explain the observation.

3.4 Neural Network Models

Up to date, an enormous number of Neural Network models have been developed. Since ANNs represent an alternative approach in solving complex non-linear dynamic problems, their application is extremely broad.

As the scope of this research lays in the development of predictive models for performance parameter estimation of a PEM-electrolyzer, the following Neural Networks have been selected to perform this task and being described in detail.

3.4.1 Back-propagation Neural Network

A Back-propagation Neural Network is classified as a multi-layered feed-forward network. It is utilising the supervised training method called the error back-propagation procedure.

An example of a Back-propagation network is depicted in figure 3.6. The network consists of an input layer with i number of inputs, the hidden layer with j neurons and the output layer neurons k .

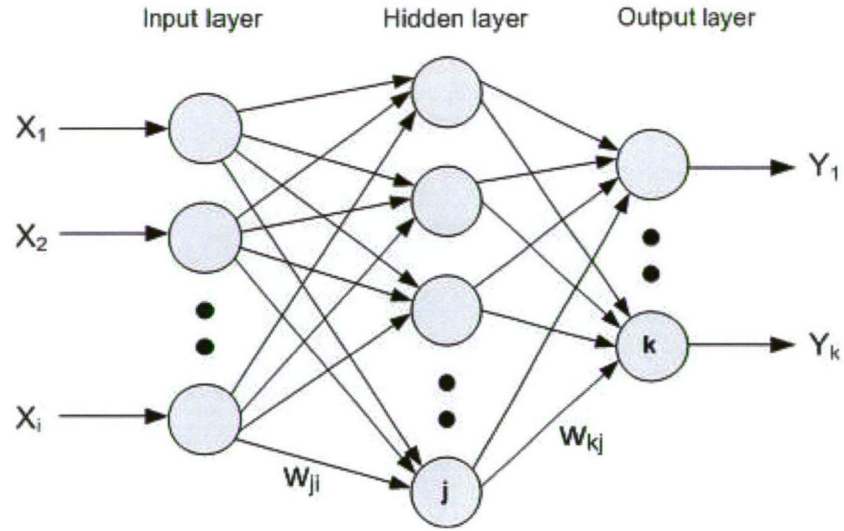


Figure 3.6: Schematic of a Back-propagation Neural Network model with one hidden layer

As the Back-propagation network is a feed-forward network, the information flow is one directional and the inputs are passed through hidden layer to the output layer. The weight of the connection between the neurons is represented by the letter w , where the first index indicates the target neuron and the second index the source neuron.

Similarly to section 3.1.2, three functions are assigned to each neuron: input function, activation function and output function.

Input function

The input function is shown in equation (3.4) and is derived by the sum of products of inputs and their corresponding weights as following:

$$net_j = \sum_i x_i w_{ji} \quad (3.4)$$

where

net_j : sum of weighted input (neuron j)

x_i : input to neuron j

w_{ji} : connection weight.

Activation function

A commonly used activation function in Back-propagation Neural Network is the non-linear sigmoid function:

$$f(net) = \frac{1}{1 + e^{(-net)}} \quad (3.5)$$

The output function basically passes the output of the activation function to the neuron of the following layer.

While the information flow of the input data is feed-forward, the network output errors generate a backward flow from output layer to the input layer (error back-propagation). A gradient descent method is being used by the error back-propagation training, where weights are being adjusted by an amount proportional to the partial derivative of the error function [133]. The calculation of the errors at the output layer and hidden layer is given in equation 3.6 and 3.7 respectively.

Errors in output layer

$$\delta_k = (t_k - y_k) f'(net_k) \quad (3.6)$$

The error value δ_k is calculated by the product of the difference between the target output t_k and the actual output y_k (of neuron k , see figure 3.6) and the derivative of the activation function $f'(net_k)$.

Errors in hidden layer

$$\delta_j = \left[\sum_k \delta_k w_{kj} \right] f'(net_j) \quad (3.7)$$

For the calculation of the neuron k error value, δ_j in the hidden layer, equation 3.7 can be applied. The connection weight from neuron j to k is represented by w_{kj} .

The connection weight adjustment is being performed by taking into account the error value of the input receiving neuron. It can be mathematically expressed as follows:

$$\Delta w_{ji} = \eta \delta_j x_i \quad (3.8)$$

where w_{ji} is the connection weight from neuron i to j , η is the learning rate constant ranging from 0 to 1 and x_i is the input i of neuron j . The learning rate is usually varied during training as high values can cause instability and low values of η could slow down the training process [143].

In order to improve the training process of the network, a momentum constant has been incorporated in the weight adjustment formula of equation 3.9 as follows [144]:

$$\Delta w_{ji}^n = \eta \delta_j x_i + \alpha \Delta w_{ji}^{n-1} \quad (3.9)$$

where

α :	momentum constant from 0 to 1
Δw_{jk}^n	weight adjustment at iteration n
Δw_{jk}^{n-1}	weight adjustment at n-1 iteration

Each portion of the weight adjustment n-1 is applied at the next iteration n. As a consequence the fluctuation in weight changes are minimised and the convergence of the weight training is enhanced.

A commonly used evaluation method of the training process is the calculation of the root mean square error (RMS). RMS error values below 10% are usually considered acceptable. The RMS error is commonly used as a measure of accuracy and can be derived from equation 3.10 below [143].

$$\%RMS\ error = \sqrt{\frac{\sum_p \sum_k (t_{kp} - y_{kp})^2}{PK}} \times 100\% \quad (3.10)$$

From the above equation P represents the number of training data, K is the number of output neurons, t_{kp} is the target output of neuron k and y_{kp} is the actual output of neuron k after the training data p has been presented.

The general training algorithm for a Back-propagation Neural Network can be summarised as follows:

- Step 1** Initialisation of connection weights at small random numbers
- Step 2** Presentation of initial input pattern (inputs and outputs) to the network
- Step 3** Outputs are computed by using input function (equation 3.4) and activation function (equation 3.5)

- Step 4** Calculation of error values from output layer (equation 3.6) and hidden layer (equation 3.7)
- Step 5** Weight adjustment calculation using the error back-propagation algorithm from equation 3.8 or 3.9 (introduced momentum constant)
- Step 6** Repetition of steps 2 to 5 with the complete set of input pattern including actual outputs and calculation of % RMS error using equation 3.10.
- Step 7** Termination of training process only if the error is in acceptable range. In all other cases repeat steps 2 to 6.

3.4.2 Optimisation Layer-by-Layer Neural Network

The Optimisation Layer-by-Layer (OLL) Neural Network is a supervised feed-forward learning process similar to Back-propagation models [132, 133]. It was initially introduced by Ergezinger and Thomsen [141] and has been identified to reduce the amount of time the Back-propagation algorithm would normally take for the network to converge. Its learning process is accelerated since the weights during training are optimised layer-by-layer. In other words, there is a dependency of individually weights per layer on each other, but no influence of weights from other layers. By doing so, the OLL network is creating an accurately solvable linear problem from the connection weight optimisation process in each layer. Linearisation errors are compensated by the introducing a penalty term to the algorithm, where optimisation of layers takes place in alternating method [141]. Applications of OLL Neural Networks have been proven to be a reliable tool for parameter estimation in several industrial processes [145, 146].

The architecture of an OLL network is shown in Figure 3.7. It consists of an input layer, one or more hidden layers and an output layer. All input nodes (neurons) are connected to all hidden nodes through weighted connections, W_{ji} , and all hidden nodes are connected to all output nodes through weighted connections, V_{kj} .

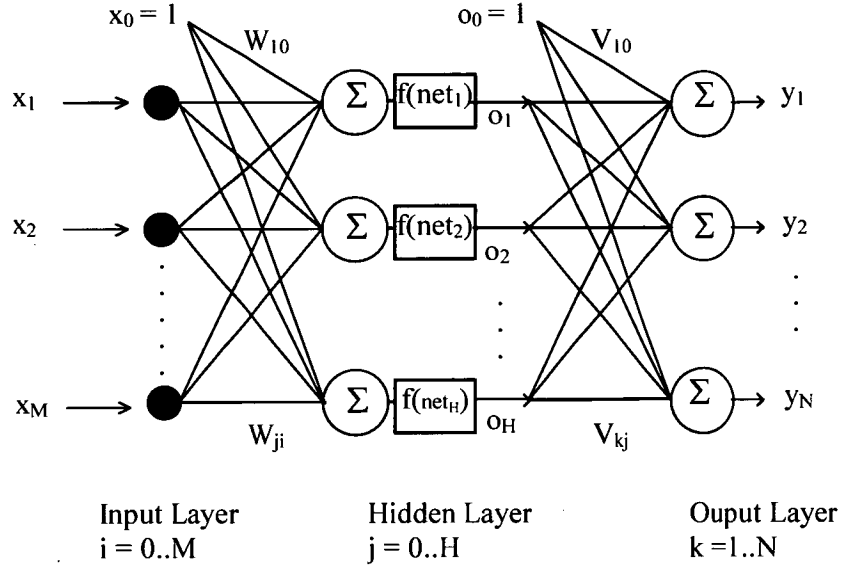


Figure 3.7: Basic structure of an Optimisation Layer-by-Layer network with one hidden layer

The sigmoid function (equation 3.5) is used as the activation function in the hidden layer, where linear activation function is used by output neurons as shown in equation 3.11 below:

$$f(\text{net}) = \text{net} \quad (3.11)$$

where net represents the sum of the weighted input to the neuron (see equation 3.1).

The weight matrix W of the input connections to the hidden layer and the weight connection V to the output layer is optimised by minimisation of the cost function. The cost function is the mean squared error between actual and target output and can be expressed as follows:

$$E(W, V) = \frac{1}{P} \sum_{p=1}^P \frac{1}{2} (t^p - y^p)^2 \quad (3.12)$$

where t^p is the target output (training data p) and y^p is the predicted (actual) output. The number of training data is represented by P .

Adjustments of the weight matrix from hidden layer and output layer respectively have to be performed individually (layer-by-layer).

Output layer optimisation

In order to find the optimum weight V of the output layer, the gradient of the cost function (equation 3.12) with respect to v is calculated and set to 0, where the input weights of the hidden layer W are regarded as constant values for the optimisation of the output layer.

$$\frac{dE}{dv} = 0 = \frac{1}{P} \sum_{p=1}^P (v^T o^p - t^p) o^p \quad (3.13)$$

The network output y^p of the training data p from number of training data P is written as $v^T o^p$ in the above equation, o^p represents the scalar output of the hidden neuron from training data p and t^p is the target output as in equation 3.12.

The optimised weight matrix V^{opt} of the output layer can be generated from the following equation:

$$V^{opt} = A^{-1} b \quad (3.14)$$

where

$$A = \{a_{ji}\}; \quad a_{ji} = \sum_{p=1}^P o_j^p o_i^p \quad j, i = 0, \dots, H$$

$$b = \{b_j\}; \quad b_j = \sum_{p=1}^P t^p o_j^p \quad j = 0, \dots, H$$

V^{opt} from the above equation 3.14 represents the optimal output layer weights for the current value of the hidden layer weights W .

Hidden layer optimisation

In order to estimate the optimal hidden layer weight matrix W^{opt} it is necessary to transform the non-linear sigmoid activation functions into linear equations. The linearisation is being performed using Taylor series expansion. By using equation 3.15, the linearised connection weights between hidden and output layer ($Vlin_j$) can be calculated as follows:

$$Vlin_j = f'(net_j) v_j \quad (3.15)$$

For the above equation, the first derivative of the summed weighted inputs to neuron j is represented by $f'(net_j)$ and v_j is the connection weight from neuron j to the output layer. The optimisation of the hidden layer weight matrix is based on the linearised network structure shown in figure 3.8. The change of the linearised network output Δy_k can be expressed in the following equation 3.16 [141]:

$$\Delta y_k = \sum_{j=1}^H Vlin_j \times \sum_{i=0}^M \Delta W_{ji} x_i \quad (3.16)$$

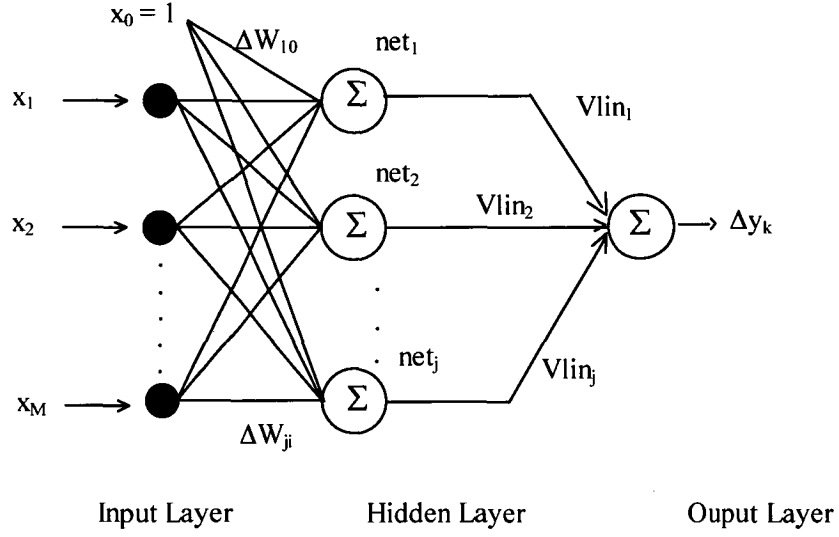


Figure 3.8: Linearised network structure for hidden layer optimisation

Following the linearisation process of hidden layer weights, the overall error function (cost function) for the hidden layer is defined as [141]:

$$E_{hid} = E_{lin} + \mu E_{pen} \quad (3.17)$$

where

E_{lin}	error function of linearised activation function
E_{pen}	penalty term to compensate the linearisations error
μ	penalty constant.

The minimisation of the cost function in equation 3.17 is carried out similarly to the optimisation of output layer cost function in equation 3.12. However, the

calculation of the partial derivatives of E_{hid} is performed separately for E_{lin} and E_{pen} . It should also be noted, that the penalty constant μ determines the influence of penalty term E_{pen} to compensate for the linearisation errors [141].

The optimal solution for the weight change matrix in the hidden layer connection can be calculated by using the following equation:

$$\Delta W^{opt} = \tilde{A}^{-1} \tilde{b} \quad (3.18)$$

where

$$\tilde{A} = \{a_{ji,hm}\};$$

for $j \neq h$

$$a_{(ji,hm)} = \sum_{p=1}^P \sum_{k=1}^N [(Vlin_{kj} x_i)(Vlin_{kh} x_m)]$$

for $j = h$

$$a_{(ji,hm)} = \sum_{p=1}^P \sum_{k=1}^N \left[(Vlin_{kj} x_i)(Vlin_{kh} x_m) + \frac{\mu}{H} |V_{kj}| \|f''(net_j)\| x_i x_m \right]$$

$$i, m = 0, \dots, M; j, h = 0, \dots, H; k = 1, \dots, N$$

$$\tilde{b} = \text{vector } \{b_{ji}\}$$

$$b_{ji} = \sum_{p=1}^P \sum_{k=1}^N [(t_k - y_k) Vlin_{kh} x_m]$$

$$i, m = 0, \dots, M; j, h = 0, \dots, H; k = 1, \dots, N$$

For training data p in the above equations, the linearised weights from neuron k in the output layer to neuron j and h in the hidden layer is represented by $Vlin_{kj}$ and $Vlin_{kh}$, the input of neuron l and m in the input layer are x_i and x_m , V_{kj} is the connection weight from neuron k (output layer) to neuron j (hidden layer) and

$f''(\text{net}_j)$ is the second derivative of the sigmoid activation function of net_j . The target output for the output neuron k is given by t_k and the network (actual) output is y_k .

Following the calculation of ΔW^{opt} the new weight matrix W^{new} can be identified:

$$W^{\text{new}} = W^{\text{old}} + \Delta W^{\text{opt}} \quad (3.19)$$

In order to find the optimal weights W and V for the entire network, iterative and alternating optimisation procedure for input and output layers is necessary. The overall training algorithm for the OLL Neural Network summarised as follows [141]:

- Step 1** Initialisation of network weights (W , V) for hidden and output layer at small random values; define number of iterations, set penalty constant μ ($\mu=0.0001$) and select desired prediction error.
- Step 2** Optimisation of the output layer weights by using equation 3.14 for V^{opt} , update output layer weight matrix and calculate RMS error.
- Step 3** Optimisation of the hidden layer weights by calculating optimal weight change ΔW^{opt} (equation 3.18). Compute new updated weight W^{test} from equation 3.19.
- Step 4** Determine the new RMS error E^{test} from weight matrix W^{test} and output layer weight matrix V or V^{opt} . Compare E^{test} with current RMS error E^{current} from step 2.
 - If $E^{\text{test}} < E^{\text{current}}$**
Update the hidden layer weight matrix to $W=W^{\text{test}}$ and decrease the influence of the penalty term by reducing the penalty constant according to $\mu = \mu\beta$, where $0 < \beta < 1$ ($\beta=0.9$). Continue to step 5.
 - If $E^{\text{test}} \geq E^{\text{current}}$**
Increase the penalty constant μ using $\mu = \mu\gamma$, where $\gamma > 1$ ($\gamma=1.2$) and continue with step 3.

Step 5 If RMS error is within the desired range, terminate the training process and save final network parameters. Otherwise go back to step 2.

3.5 Hybrid Intelligent Systems

Hybrid intelligent systems are a combination of at least two intelligent technologies. The application of such a system to solve a single problem can be of advantage as thoughtfully combined systems may overcome problems and boundaries of individual subsystems leading towards a more successful end result. In order to produce a successful end result, the system requirements as well as advantages and disadvantages of the individual subsystems have to be taken into consideration. On the other hand inadequately combined technologies can have the opposite effect and may lead to a poorer end result [133].

ANN and fuzzy systems have been recognised as complementary technologies for hybrid intelligent systems. Fuzziness concerns the uncertainty associated with a system and is based on the premise that nothing can be predicted with the exact precision. With the introduction of fuzzy set theory from Lofti in 1965 [147], a more flexible sense of membership could be achieved to adequately express uncertainty or vagueness. Fuzzy logic is designed to represent knowledge and human reasoning in an appropriate way to be processed by a computer. In other words, it allows the system to compute data with a degree of imprecision, specified by phrases of human reasoning such as fairly, very and quite possible conversely to traditional predicate logic of true or false [131].

Neural Networks are simple computational structures with the ability to solve complex tasks through learning, but they do not have good explanation capability. In contrast, fuzzy logic has a higher level of human reasoning and can facilitate consistent outcomes, but require the ability to learn and self adjustment of Neural Networks. In consequence, these two intelligent technologies naturally complement

each other and provide the possibility of predictive modelling approaches for non-linear dynamic processes, such as electrolyzer performance.

3.6 Adaptive Neuro-Fuzzy Inference Systems

Adaptive Neuro-Fuzzy Inference Systems (ANFIS) are hybrid systems incorporating the technologies of Neural Networks and fuzzy systems. First introduced by Jang in 1993 [148], the ANFIS is able to construct an input-output mapping based on fuzzy if-then rules and stipulated input-output data pairs in order to be employed to model non-linear functions, identify non-linear components and predict chaotic time series with remarkable results [148].

The basic idea behind neuro-adaptive learning techniques is simple. ANFIS provides a method for the fuzzy modelling procedure to learn information about a data set. Through this learning and training procedure, the membership function parameters and the number of epochs can be estimated by trial and error that best allow the associated fuzzy inference system to track the given input/output data. While the learning (training) method works correspondingly to that of Neural Networks [133, 149], the system operation (after the training process) is identical to a fuzzy expert system using the developed rules during the training procedure.

ANFIS is usually represented by a six-layer supervised feed forward neural network. Figure 3.9 depicts an example of a typical ANFIS architecture that corresponds to the first order Sugeno-fuzzy model [133]. The following sequence of mathematical representations has been adopted from the following references [133, 148].

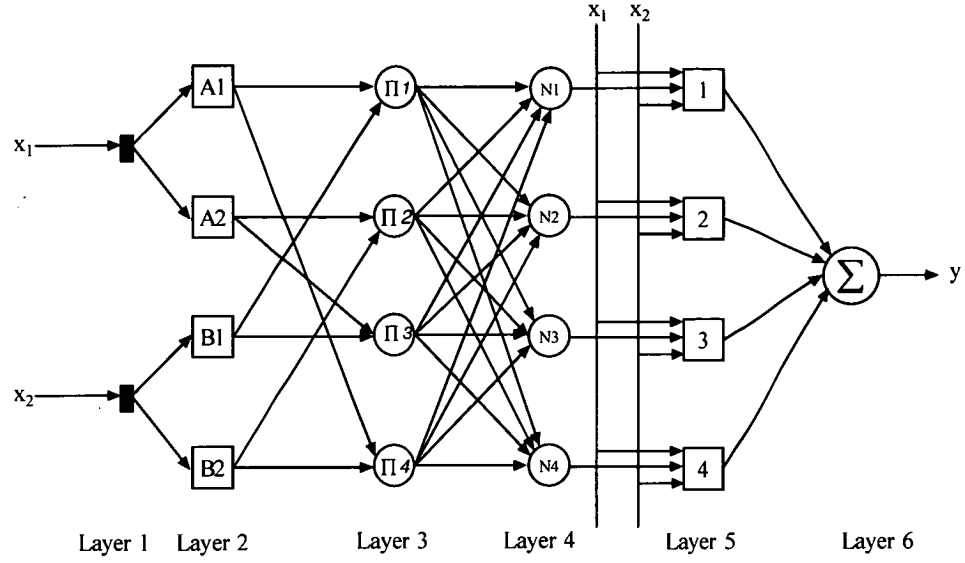


Figure 3.9: Typical ANFIS structure with 2 inputs

In layer 1 (input layer) inputs x_1 and x_2 are passed to a number of neurons in the second Layer. In the second layer, known as the fuzzification layer, the neurons perform fuzzification of the incoming inputs (equation 3.20).

$$\begin{aligned} y_{Ai} &= \mu_{Ai} \\ y_{Bi} &= \mu_{Bi} \end{aligned} \quad (3.20)$$

The third layer can be described as the rule layer. Each neuron corresponds to a single Sugeno-fuzzy type fuzzy rule. The firing strength calculated by the rule neurons then is determined by the product of the incoming signals (equation 3.21).

$$y_m = \prod_{j=1} x_{ji} \quad (3.21)$$

The output of the first neuron in layer 3 is calculated as follows:

$$y_{\Pi 1} = \mu_{A1} \mu_{B1} \quad (3.22)$$

where μ_{A1} is the firing strength of rule 1.

Layer 4 is known as the normalisation layer. Here the neurons receive inputs from all neurons of the third layer in order to calculate the normalised firing strength of a given rule. This firing strength is determined as the ratio of the firing strength of a given rule to the sum of all rules (equation 3.23). In other words, the output stands for the contribution of a particular rule to the final result.

$$y_{Nii} = \frac{\mu_i}{\sum_{j=1}^n \mu_j} = \overline{\mu_i} \quad (3.23)$$

Layer 5 is the so called defuzzification layer. Each neuron in this layer receives the outputs of the 4th layer as well as the original inputs x_1 and x_2 . Here, the neuron (defuzzification neuron) calculates the weighted consequent value of a particular rule and can be mathematically described in the following equation:

$$y_i = \overline{\mu_i} (k_{i0} + k_{i1}x_1 + k_{i2}x_2) \quad (3.24)$$

Where $\overline{\mu_i}$ is the input of the defuzzification neuron i in layer 5; y_i is the output of layer 5 and k_{i0} , k_{i1} and k_{i2} represent a set of consequent parameters of rule i .

Layer 6 contains a single summation neuron. Here, the sum of all defuzzification outputs is calculated and the overall ANFIS output y is obtained as in equation 3.25.

$$y_{ANFIS} = \sum_{i=1}^n y_i \quad (3.25)$$

3.7 Application of ANN and ANFIS

The applications of Neural Networks and hybrid systems such as ANFIS are numerous, ranging from character recognition to signal processing and financial problems. Through their ability of finding complex, non-linear relationships between input and output data, they are of great interest by researchers worldwide to be integrated into current technologies.

From an engineering perspective, ANN and ANFIS have been successfully applied to solve and optimise various engineering related problems in several industrial processes, such as arc furnace response prediction [153], parameter estimation of thrust and torque in drilling applications [145, 146, 154] and several other manufacturing applications [155].

Within the field of this research the potential use of intelligent techniques for electrolyzer performance prediction has been investigated. As reviewed in section 2.4, only very few studies can be found in the literature investigating the potential application of predictive models for electrolyzer performance [150-152] and associated hydrogen safety [128] using intelligent techniques. As the electrolytic hydrogen production represents a dynamic process with a large number of process parameters, the application of intelligent techniques to accurately predict electrolyzer performance parameters achieved promising results.

3.8 Concluding Remarks

This chapter presented a general knowledge about ANNs and hybrid system ANFIS including their theoretical concepts. The neural network based models explored throughout the scope of this research, such as Back-propagation, OLL and ANFIS have been explained in detail. Amongst those models, the OLL network and the ANFIS network are fast learning networks.

Furthermore this chapter has also provided information about applying intelligent techniques to solve engineering related problems. The lack of literature investigating the potential use of predictive models for electrolyzer performance and safety shows the need for predictive modelling utilising intelligent techniques as an alternative approach in this area.

In the following chapter, the design and development of the experimental test rig will be described. The focus of chapter 4 will be on investigating the capability of electrolyzer performance prediction using the models examined in this chapter. Those models are to be incorporated into the experimental rig to perform prediction of electrolyzer performance parameters and act as virtual sensors.

CHAPTER 4

EXPERIMENTAL SETUP AND DESIGN

4.1 Introduction

This chapter describes the experimental setup in the hydrogen laboratory. The experiments provide the database for the development of the predictive models, which can be employed as virtual sensors. Extensive testing and data-acquisition is necessary to assist the learning stage of the models and to provide a wide range of operating conditions to prove their applicability and practicality. Components of the test rig are being described including the data-acquisition of experiments. Furthermore the range of conditions is being presented.

4.2 Hydrogen Test Rig Facility and Safety Aspects

The experimental setup is located in the UTAS hydrogen laboratory. The laboratory was designed for applied hydrogen use with the latest safety equipment due to the hydrogen gas properties. It also complies with Australian and International standards [31, 156]. The layout of the laboratory is shown in Figure 4.1 [156].

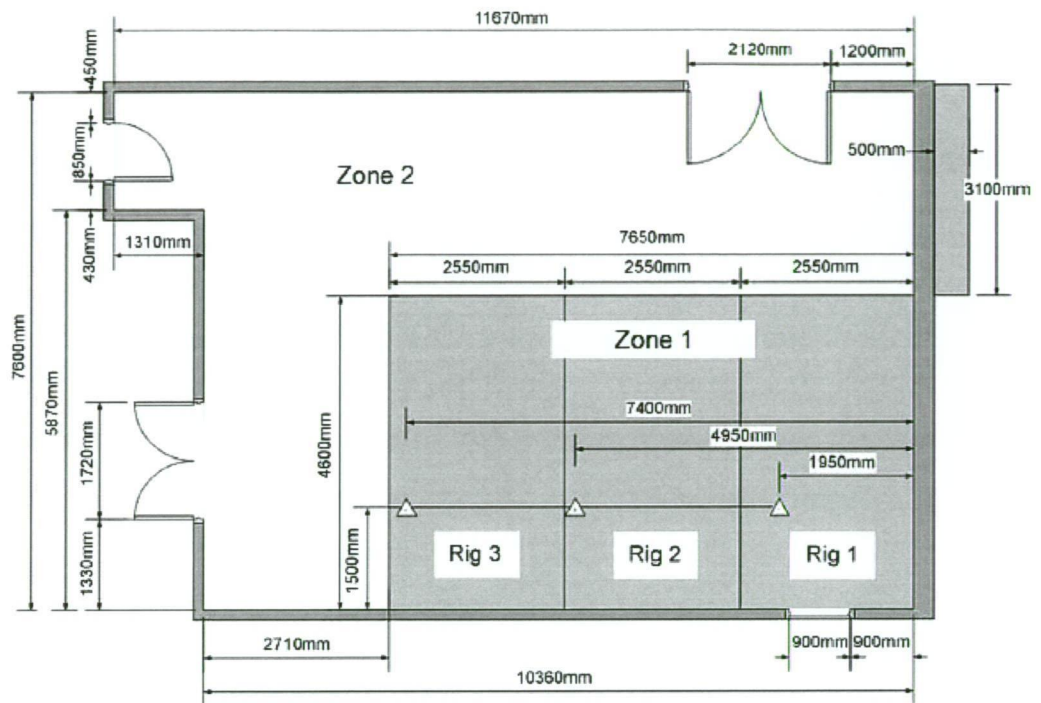


Figure 4.1: UTAS hydrogen laboratory layout

The test rig was placed into zone 2 (figure 4.1) according to Australian Standard AS 2430.1-1987 [31]. A combustible gas sensor, type R61-0203-02RK, was used to determine and monitor the hydrogen concentration in air. As shown in figure 4.2 [157] the fan was placed at the highest point of the ceiling in front of a ventilation fan, type Bal-400 wall fan (Pacific Fans), as the low density characteristics of hydrogen allow higher concentration in the highest point. Furthermore the fan airflow characteristics with an air drag of 1700l/s ensures safe operation environment [157].

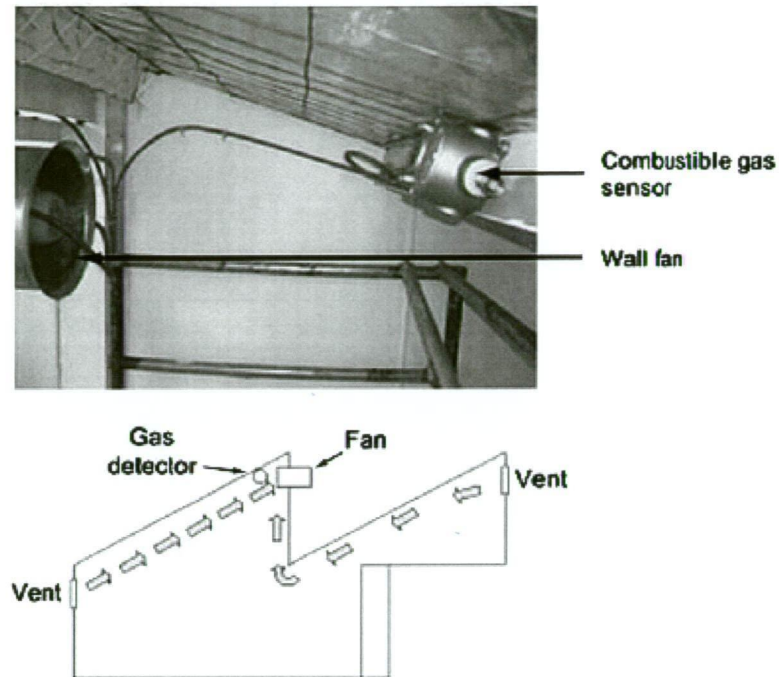


Figure 4.2: Combustible gas sensor and wall fan

4.3 Experimental Setup and Components

This section illustrates the experimental setup and gives a description of the applied components used in the experiments.

4.3.1 Hydrogen generator

The hydrogen generator used in the experiments (see figure 4.3) is a PEM-electrolyzer, type Hogen® 20 from Distributed Energy Systems, based in the United States. The PEM cell stack consists of 10 cells linked in series with a Nafion® 115 membrane [158].

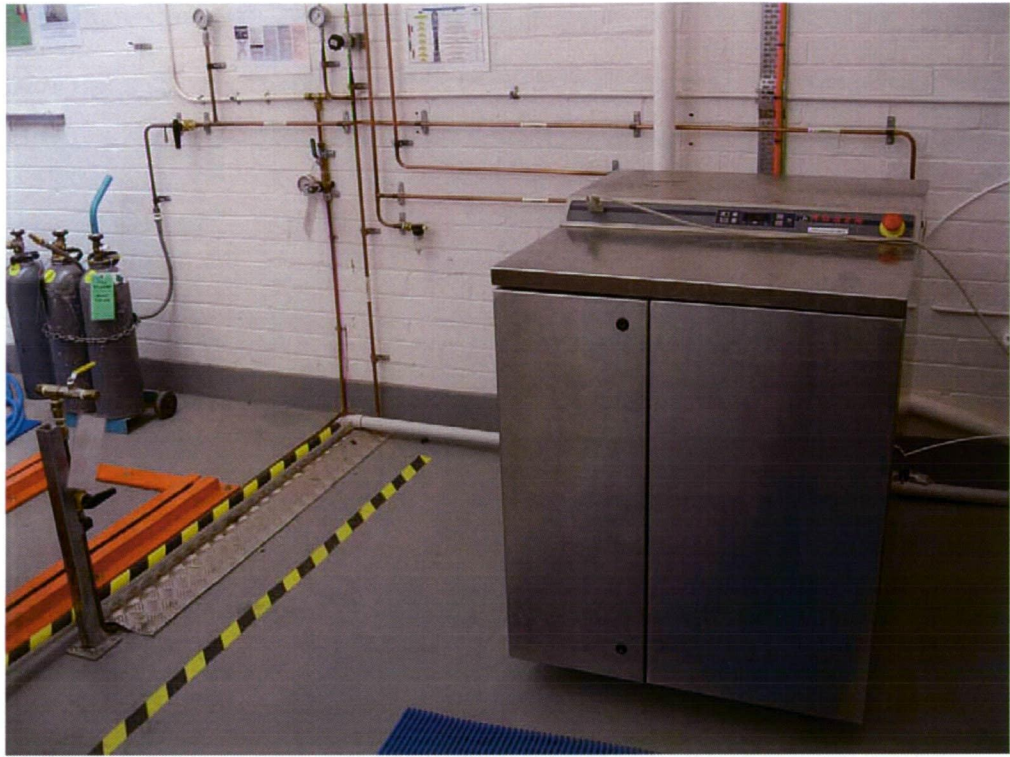


Figure 4.3: Hogen® 20 PEM-electrolyzer setup in hydrogen laboratory

The electrolyzer is capable of operating in two modes:

- Load following and
- Tank filling mode.

In the load following mode the electrolyzer follows a prior set pressure set point. If the output pressure falls below or rises above the pressure set point, it automatically adjusts the output pressure to its set value. In tank filling mode the output pressure rises to the maximum pressure set point before going into idle state. If the pressure falls below the pressure set point, it will start generating hydrogen once the minimum pressure set point (refill point) is reached.

Specifications of the Hogen® 20 electrolyzer are given in table 4.1 [158]. In addition, table 4.1 also includes specifications for an electrolyzer type Hogen® RE, a

similar aggregate, but specially designed for handling fluctuating power input from renewable sources, such as photovoltaic for comparison.

Table 4.1: Specifications for Hogen®RE and Hogen®20

Specifications	Hogen® RE (20/40)	Hogen® 20
Hydrogen output	0,5 or 1.05Nm ³ /h	0.53Nm ³ /h
Max. delivery pressure	200psi	200psi
Hydrogen purity	> 99,9%-99,999%	> 99,9%-99,999%
Water usage	Approx. 11,4l or 22,7l/24h	Approx. 11,4l/24h
Water quality required	Deionised (ASTM Type II)	Deionised (ASTM Type II)
Power consumption	6,6kWh/Nm ³	6.3-9kWh/Nm ³
Electrical supply required	AC: 190-240VAC, 1 phase, 50/60Hz, 7.2 or 12kVA DC: 60-200VDC, 150A(max)	AC: 190-240VAC, 1 phase, 50/60Hz
Operating environment	Indoor (optionally outdoor)	Indoor (optionally outdoor)
Dimensions	970mm*1050mm*1056mm	970mm*785mm*1056mm
Weight	220kg	227kg
Installation	“Plug and play”	“Plug and play”
Controls and automation	Fully automatic & unattended	Fully automatic and & unattended

The inside view of the electrolyzer is given in figure 4.4 [157]. It shows the location of the main components:

- A200 Oxygen/ water phase separator,

- A300 Hydrogen/water phase separator,
- X334 Dryer,
- Z350 Hydrogen management manifold

in correspondence with the flow schematic of figure 4.5 [158]. Additionally the combustible gas detector (CG 220), the guard bed resin cartridge (GB 208), the coalescing filter (F 328) and the cell stack (EM 100) have also been located from figure 4.5 for better transparency and understanding.

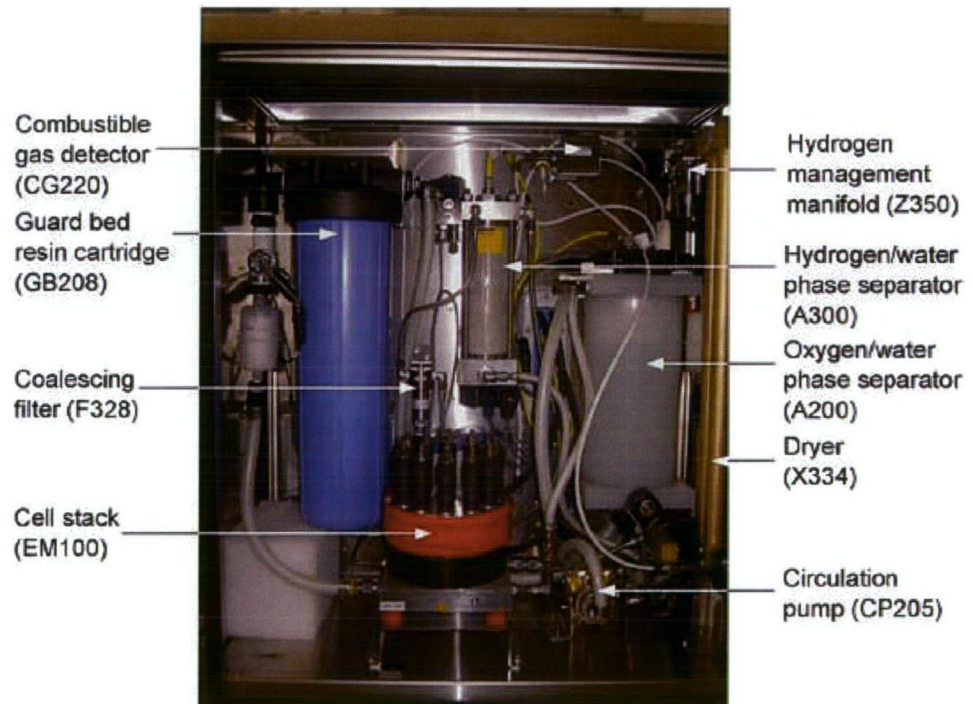


Figure 4.4: Inside view of electrolyzer with location of components

The fluid and gas flow schematic is shown in figure 4.5 [158]. The feed water inlet port is given with A, B corresponds to the Oxygen vent port, C to the Water outlet port and D to the Product hydrogen outlet port. In start up operation, in other words

before the system is fully operational, hydrogen is vented out to the hydrogen vent port (E).

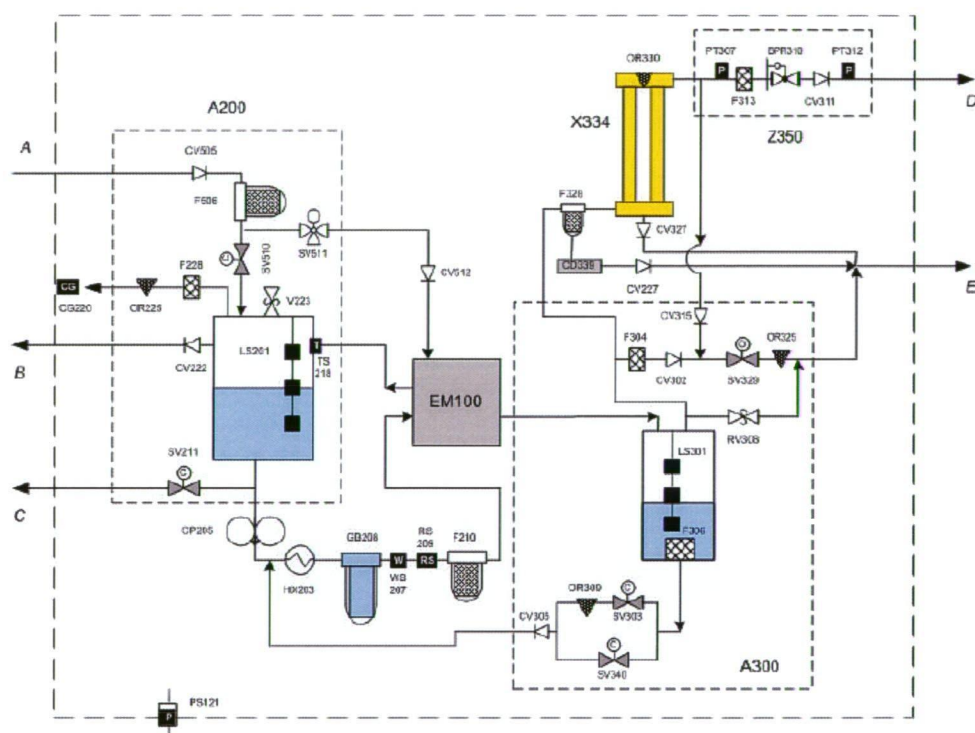


Figure 4.5: Flow schematic of Hogen® 20 electrolyzer

4.3.2 Storage unit

In order to investigate the Hogen® 20 PEM-electrolyzer a suitable storage unit has been developed. Figure 4.6 shows the assembly drawing of the hydrogen storage unit trolley. It consists of seven 12,2l tanks joint together as one storage unit with a physical volume of approx. 85.4l. It has been designed with an inlet port (Swagelok quick connector) for storage and an outlet port for application usage. A needle valve and swaged connections ensure to keep leakage of hydrogen gas to a minimum. A pressure gauge serves as a reference value to the output pressure given by the

manufacturers' internal diagnostic software (see section 4.4.1). The tanks are placed in a trolley to enable mobility of the storage unit for various hydrogen applications.

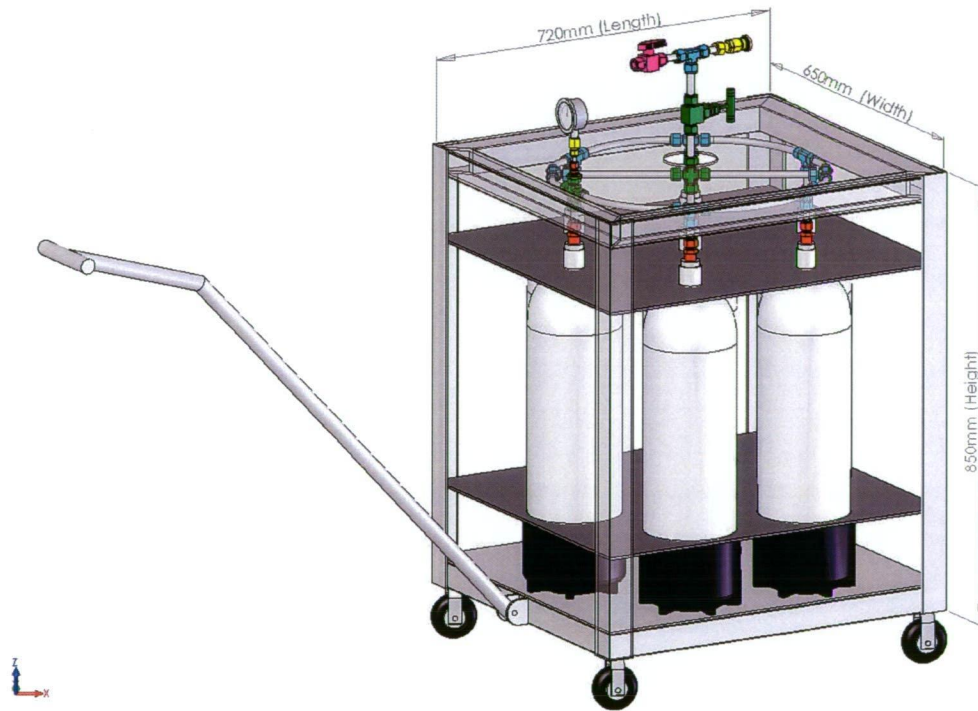


Figure 4.6: Hydrogen storage unit trolley

4.3.2.1 Material and assembly

The components and materials used for the storage unit had to be suitable for hydrogen use and the related operating conditions of the electrolyzer. The operating conditions to be considered and expected throughout the experimental rig are as follows:

- temperature range of operating environment (5-40°C),
- temperature of product hydrogen gas (5-40°C) and

- pressure range (0 up to 250psi) and maximum hydrogen flow rate (up to 12l/min) of product hydrogen gas.

The components and materials for the storage unit are listed in Table 4.2. Swagelok Fluid Systems technologies has been the main provider for the piping of the separate tanks, valves and pressure gauge respectively. The stainless steel tanks are provided by Faber.

Table 4.2: Part list of hydrogen storage unit

Quantity	Part	Unit price AUS	Price AUS	Supplier
7	Weld Connector	22.2	155.4	Swagelok
8	Tube Fitting Union Tee	61.3	490.4	Swagelok
2	Tube Fitting Union Cross	80.5	161	Swagelok
1	Tube Stub Reducer	14.6	14.6	Swagelok
1	Pressure Gauge	57.5	57.5	Swagelok
1	Female Connector	15.7	15.7	Swagelok
1	Turn Plug Valve	141	141	Swagelok
1	Needle Valve	275.5	275.5	Swagelok
1	Quick Connect Body	96	96	Swagelok
1	Quick Connect Stem	74.2	74.2	Swagelok
1	6 m of 0.5 Inch Tubing	56.1	56.1	Swagelok
7	Storage Tanks	289	2023	Faber
	Estimated Trolley costs (steel, roles, sheets, labour etc.)		500	UTAS Workshop
Total costs			4060.4	

The components for the trolley from table 4.2 have been assembled to the hydrogen storage unit as shown in figure 4.7 and 4.6 including trolley respectively.

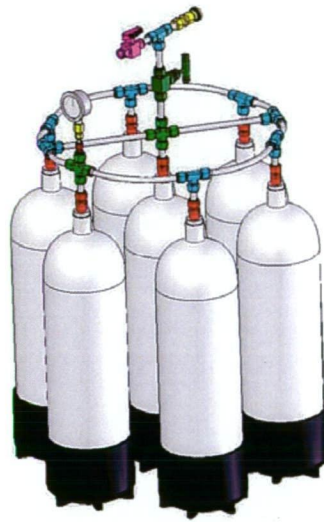


Figure 4.7: Connected tanks and piping

The parts are basically all of the shelf components, provided by Swagelok with swaged sealed (metal to metal) connections, to ensure to keep leakage of hydrogen gas to a minimum. Except for the connection from the tanks to the pipe work a custom designed connector was used. Figure 4.8 and 4.9 show the connector (custom designed to fit the storage tank thread) and weld connector assembly (Swagelok).

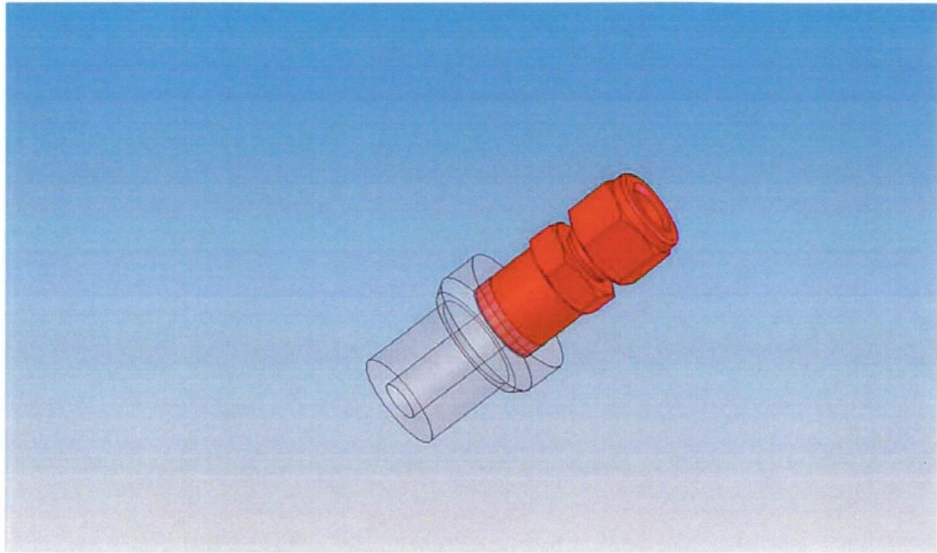


Figure 4.8: Connector and weld connector assembly



Figure 4.9: Connector welded with thread for each storage tank including o-ring

Figure 4.10 illustrates the main valve of the storage unit. This type of valve is a needle valve, which integrates a special safety feature. It can be closed even if the sealing in the valve fails, because the tip of the needle (see red circle) blocks the inlet of the valve when it is closed with a metal against metal solution.

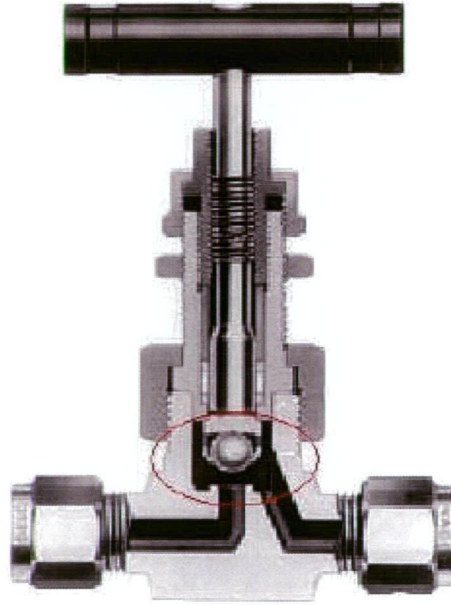


Figure 4.10: Main needle valve with metal against metal solution for safety

4.3.2.2 Permeability and sealing

As most of the components are swaged fitted as a solution from the provider (Swagelok), leakage is expected to be a minimum, except where the sealing is carried out with an o-ring solution. Materials for those o-rings have to be selected in order to provide minimum leaking. Leaking is usually represented by permeation of the gas through and passing around the sealing material. Therefore permeability is defined as the rate of which a permeate (liquid or gas) passes through a solid material by diffusion. An approximate leak rate can be calculated by using the following equation from Parker Seal Group [159]:

$$L = 0.7 \cdot F \cdot D \cdot P \cdot Q \cdot (1 - S)^2 \quad (4.1)$$

Where:

- L = is the approximate leak rate of the seal (std. cm^3/sec)
- F = Permeability rate of the gas through the elastomer at the anticipated operating temperature (std. $\text{cm}^3 \text{ cm}/\text{cm}^2 \text{ sec bar}$)
- D = Inside diameter of the o-ring, in inches (1")
- P = Pressure differential across the seal, (200 PSI)
- Q = Factor depending on the percent squeeze and whether the o-ring is lubricated or dry (1.2)
- S = Percent squeeze on the o-ring cross section expressed as a decimal (25% squeeze is recommended, $S = 0.25$)

The above formula contains mixed units, as D and P are given in inches or pounds per square inch respectively and the permeability rate is given in metric units. The factor of 0.7 resolves these inconsistencies. Furthermore the permeability is expressed in atmospheric cm^3 per second, thorough an elastomeric material of one centimetre squared and one centimetre thickness. It also varies between compounds in the same polymer and therefore gives only a rough order of magnitude approximation. Permeability rates of hydrogen for several materials can be found in table 4.3 [159].

Table 4.3: Permeability of hydrogen for several o-ring materials

Sealing material	Working temperature °C	Permeability ($\times 10^{-8}$)
Butadine	25	31.6
Butyl (IIR)	35	16.1
Ethylene Propylene (EPR)	40	111
Fluorocarbon (Viton)	93	160
Neoprene (CR)	38	180
Nitrile (NBR)	39	11.9
Polyacrylate (ACM)	38	49.6

Chapter 4: Experimental Setup and Design

Polysulfide (PSR)	25	1.2
Polyurethane (EU)	39	4.89
Styrene butadiene (SBR)	38	46.2
Silicone (PVMQ)	39	2070
FEP Teflon	38	10.1
TFE Teflon	30	42

From the above table fluorocarbon (Viton) was chosen as a suitable o-ring material for the storage unit (connector in figure 4.9). It has a higher working temperature (90 °C) as most of the materials are very close to the 40 °C operating temperature boundary of the test rig and creates an additional safety zone.

According to equation 4.1, the leak rate through one o-ring for fluorocarbon is approximately $1.51 \times 10^{-4} \text{ cm}^3/\text{s}$ and for the entire storage unit, taking into account seven o-rings, equals 0.3816l/hr. In accordance with the safety aspects from section 4.2, the installed fan with an air drag capacity of 1700l/s or $6.12 \times 10^6 \text{ l/hr}$ respectively, removes approximately 16 million times the amount of hydrogen from possible leaking. It is therefore not considered to be a safety risk.

4.3.2.3 Purification procedure and pressurisation

Before the first use of the unit, the safety and quality of the hydrogen to store have to be taken into account. To ensure elimination of remaining air from the storage system, the unit was connected to a vacuum pump, type ‘Speedivac’ by W. Edwards and Company (London) Ltd as shown in Figure 4.11.



Figure 4.11: Vacuum pump

After the vacuuming process to -100kPa the storage unit was pressurised with nitrogen of up to 2500kPa or 25bar respectively. A reference value for the inserted pressure was given by the pressure gauge of the nitrogen dispenser and pressure regulator as shown in figure 4.12.



Figure 4.12: Pressurisation with nitrogen

Thus the pressure can be seen as an accurate value. The pressurisation with nitrogen is mainly performed to check for possible leaks in the system and to bind any remaining contaminating elements from air. No leaks have been found during the pressurization test. Therefore the system is ready for initial fill process after releasing the nitrogen and vacuuming to 0kPa as illustrated in figure 4.13.

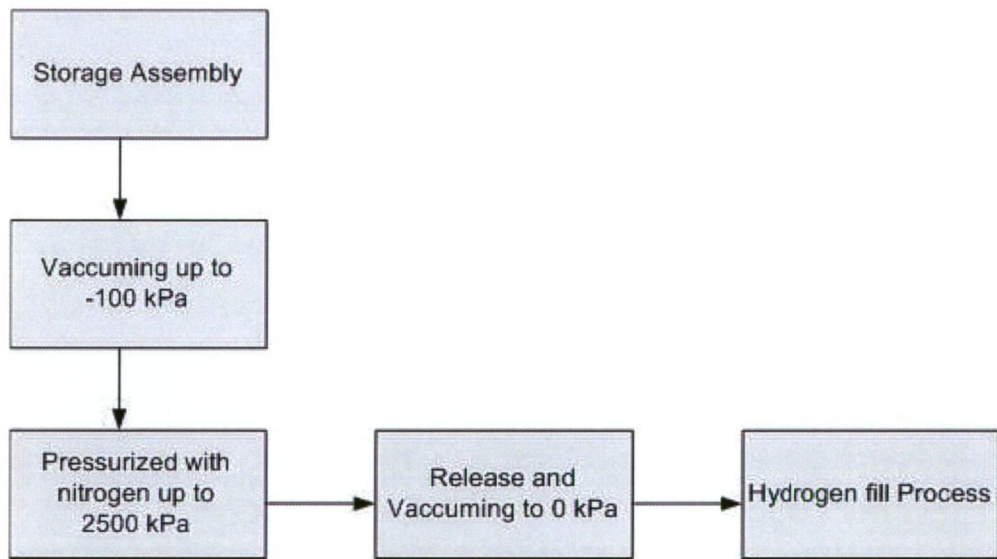


Figure 4.13: Hydrogen storage purification procedure before initial operation of the storage unit to ensure safety handling and quality of hydrogen

4.3.3 Water deionisation

Due to the fact that the PEM-electrolyzer requires deionised (distilled) water, a purification unit in figure 4.14 is directly coupled to the hydrogen generator water inlet port.

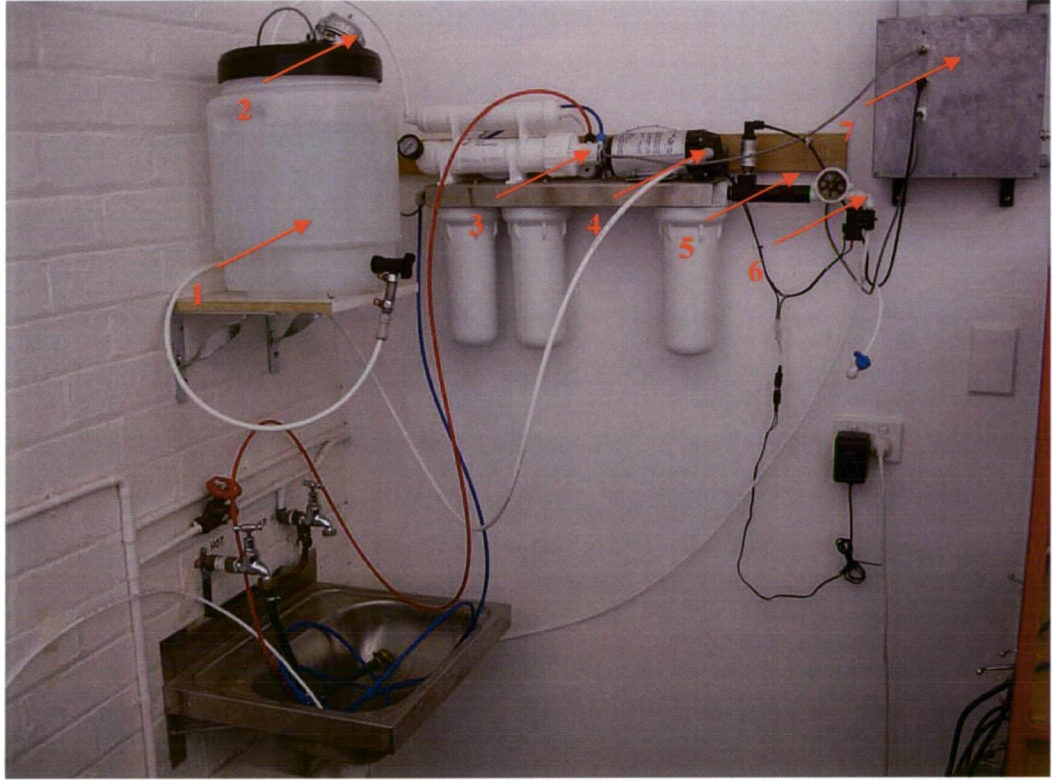


Figure 4.14: Water deionisation system with water container (1),RTD (resistance temperature device) (2), water deionisation (3), feed-water pump (4), pressure transducer (5), flow-meter (6) and data-acquisition connection box (7)

The above figure displays the basic setup of the water purifying unit. Tap water is fed into the deionisation (3) and enters the water container (1) after the process. An RTD (PT 100) (2) measures water temperature. A feed water pump (4) operates on demand for the electrolyzer feed water requirements. Connections of each sensor, such as RTD, pressure transducer and flow meter to the data-acquisition box (7) have been made to obtain feed water parameters.

4.3.4 Power analyser

For the purpose of overall power monitoring a power analyser, type PM 3000 (Voltech Instruments), has been employed to measure voltage, amps, power factor and watt-hours respectively. This will give an indication of the system-efficiency. Accuracy according to the manufacturers specifications are 0.1% for reading, 0.1% for range and 200 mA or 1 mV respectively [160].

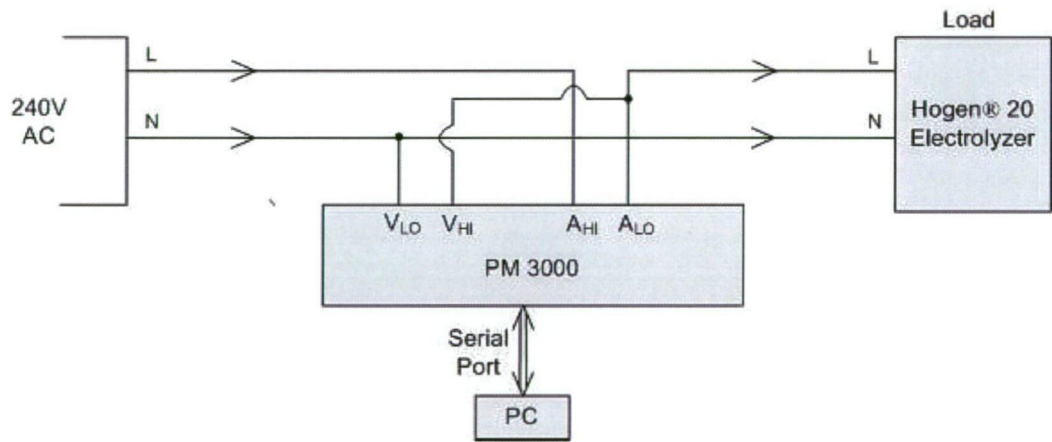


Figure 4.15: PM 3000 wiring diagram

The wiring diagram for the measurement of the power parameters is shown in figure 4.15. The PM 3000 power analyser measures the 240 VAC line voltage and line current flowing into the Hogen® 20 (load). These parameters, along with power factor and watt-hours (which are calculated by the PM 3000) are passed to the PC via serial interface.

4.4 Data-Acquisition

Data-acquisition was controlled with National Instruments (NI) LabVIEW software, which ensured synchronous data collection from the electrolyzer, power analyser and feed water sensors. Feed water parameters were acquired by an NI 6025 E data-acquisition card, with 12-bit input resolution and a maximum sample rate of 200kS/s, as shown in figure 4.16. Internal electrolyzer system parameters and power parameters are acquired by the PC via serial port.

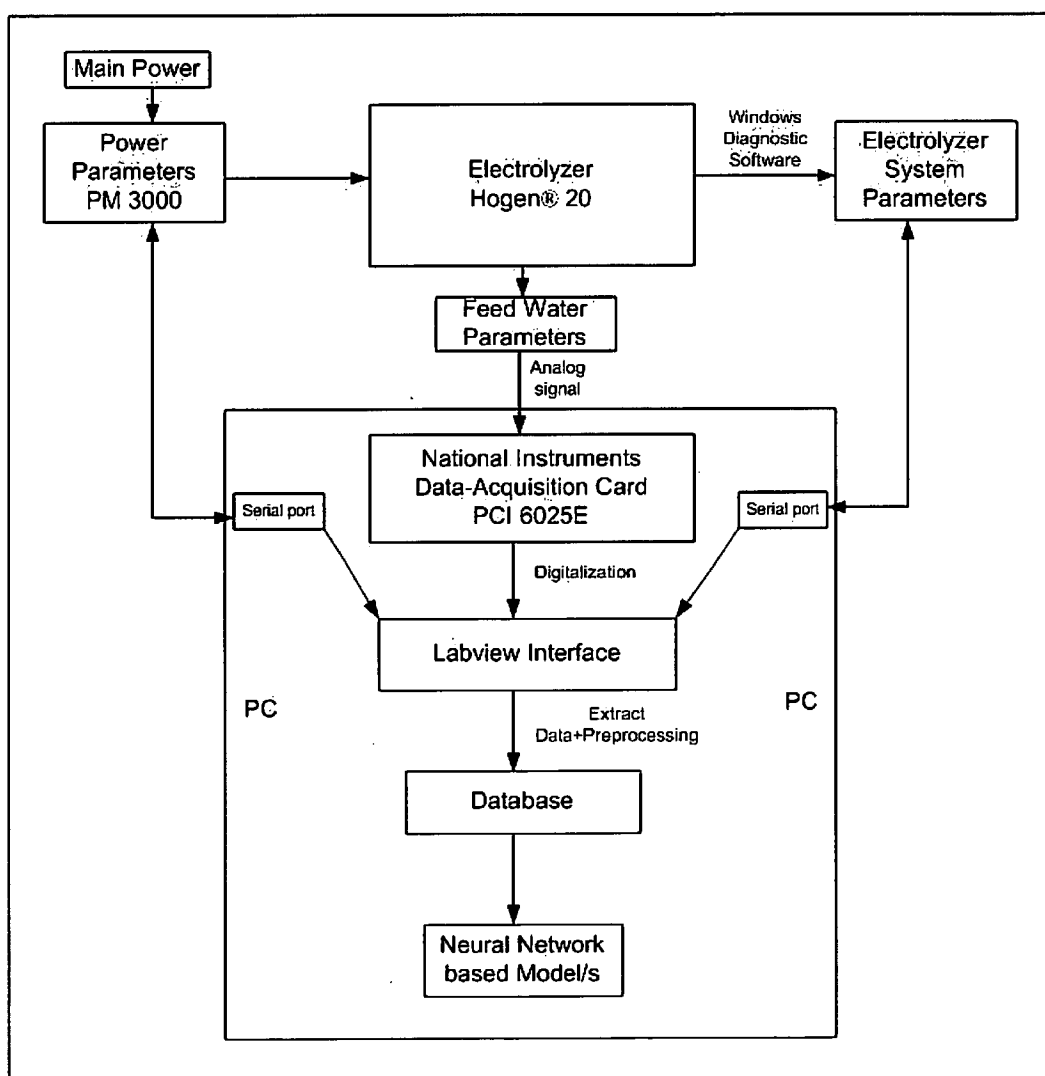


Figure 4.16: Data-acquisition schematic

4.4.1 On board diagnostic software of electrolyzer

The electrolyzer internal operating parameters can be programmed and/or monitored from a PC via an RS232 serial link. (Windows-based diagnostic software provided by the manufacturer is installed on the PC). A screenshot of the diagnostic software running under Windows is given in figure 4.17. This software allows sampling of the operating parameters from the electrolyzer. However, feed water and power parameters detailed in sections 4.3.3 and 4.3.4 respectively, are obtained from additional external sensors and cannot be sampled with the manufacturer's Windows diagnostic software. Therefore, new software which acquired power, flow and electrolyzer system parameters was developed and is outlined in section 4.4.2. Reverse engineering was employed to determine the serial communications link parameters and serial data protocols for the electrolyzer.

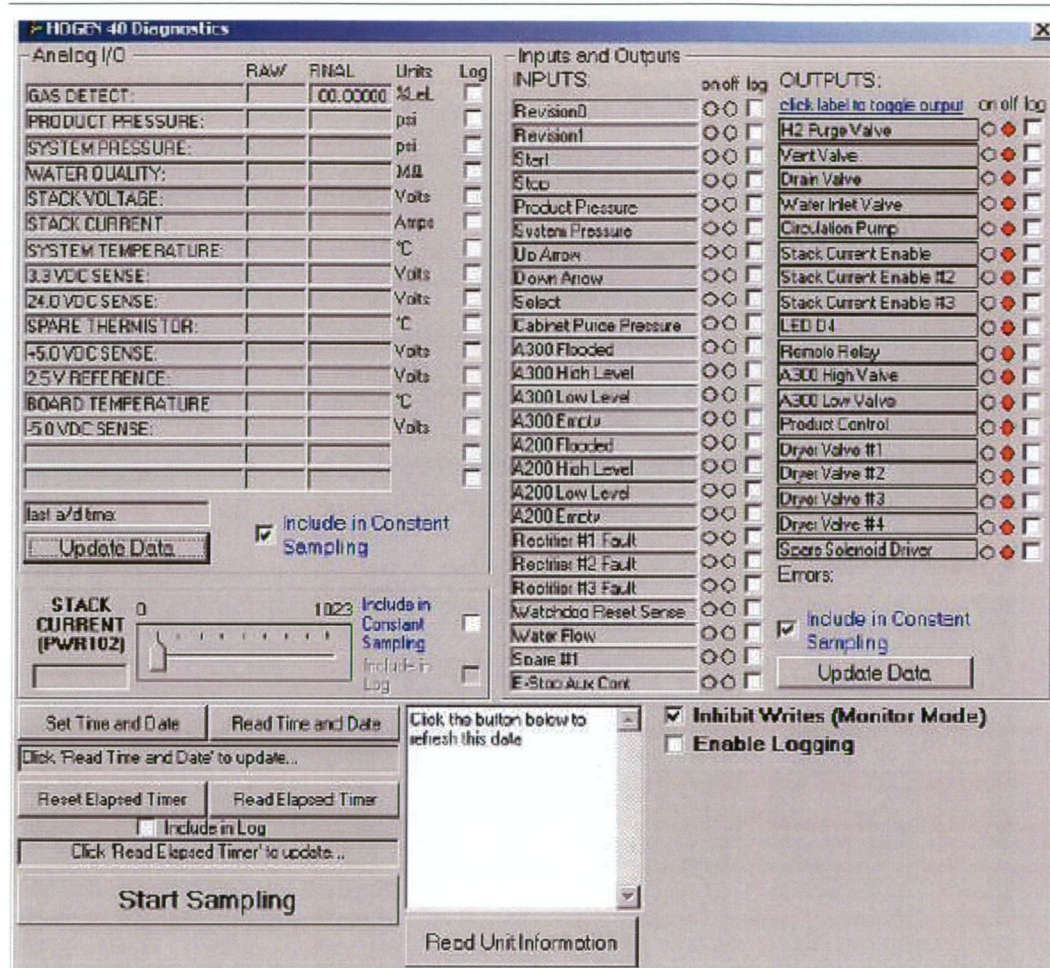


Figure 4.17: Electrolyzer diagnostic software

4.4.2 Determination of electrolyzer serial link parameters and data protocols

Serial communications and data protocols for the electrolyzer needed to be determined for their incorporation into LabVIEW software. Firstly, the serial communications parameters for the electrolyzer were determined, by using an oscilloscope to observe serial traffic between the host PC and electrolyzer. This was achieved whilst the PC was running commercial software provided by the electrolyzer manufacturer.

Hogen®20 serial communications parameters:

- 115200 bits/sec
- 8 data bits
- No parity
- 1 stop bit

Following the determination of the serial communication parameters, an interrogator byte sequence was then deduced by running the commercial software and simultaneously monitoring serial traffic with a second serial port on the host PC as shown in figure 4.18.

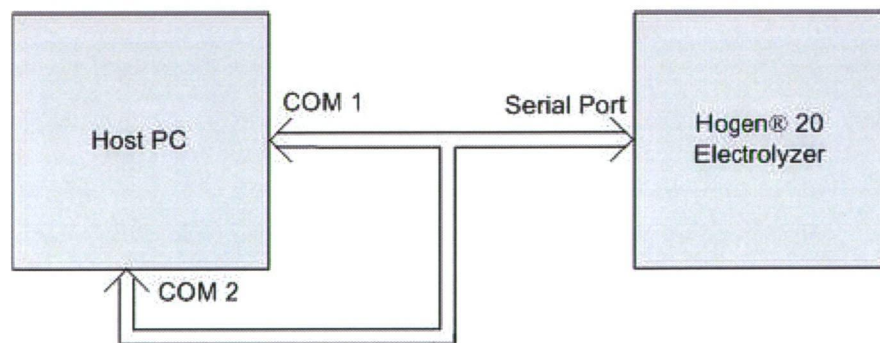


Figure 4.18: Hardware setup for deduction of interrogator byte sequence

Interrogator byte sequence for communication between host PC and electrolyzer:

2A 07 52 FF E0 F0 20 8D 80

Further reverse engineering yielded the following data format used by the electrolyzer in replying to the interrogator sequence:

06 $X_1 X_2 X_3 X_4 \dots X_{34}$

Where X_n is a byte and $n \in [1, 2, 3, 4, \dots, 34]$.

Pairs of bytes, where $X_{2n-1} X_{2n}$ and $n \in [1, 2, 3, 4, \dots, 17]$, are concatenated (linked together as a unit) to produce 16-bit binary words representing various electrolyzer parameters as given in table 4.4 and table 4.5.

Table 4.4: Concatenated data pairs (1-7) representing electrolyzer system parameters

$X_1 + X_2$	$X_3 + X_4$	$X_5 + X_6$	$X_7 + X_8$	$X_9 + X_{10}$	$X_{11} + X_{12}$	$X_{13} + X_{14}$
Gas Detect	Product Pressure	System pressure	Water quality	Stack voltage	Stack current	System temperature

Table 4.5: Data pairs (8-14) for electrolyzer system parameters

$X_{15} + X_{16}$	$X_{17} + X_{18}$	$X_{19} + X_{20}$	$X_{21} + X_{22}$	$X_{23} + X_{24}$	$X_{25} + X_{26}$	$X_{27} + X_{28}$
3.3V DC Sense	24V DC Sense	Spare thermistor	5V DC sense	2.5V reference	Board temperature	-5V DC sense

4.4.3 Implementation with National Instruments LabVIEW software

Custom software was written in LabVIEW to enable synchronous acquisition of electrolyzer, power and feed water parameters. Virtual Instruments were created for each of the following tasks:

- Acquisition of data pertaining to feed water flow into the electrolyzer
- Acquisition of data pertaining to electrical power flow into the electrolyzer
- Acquisition of electrolyzer process parameters

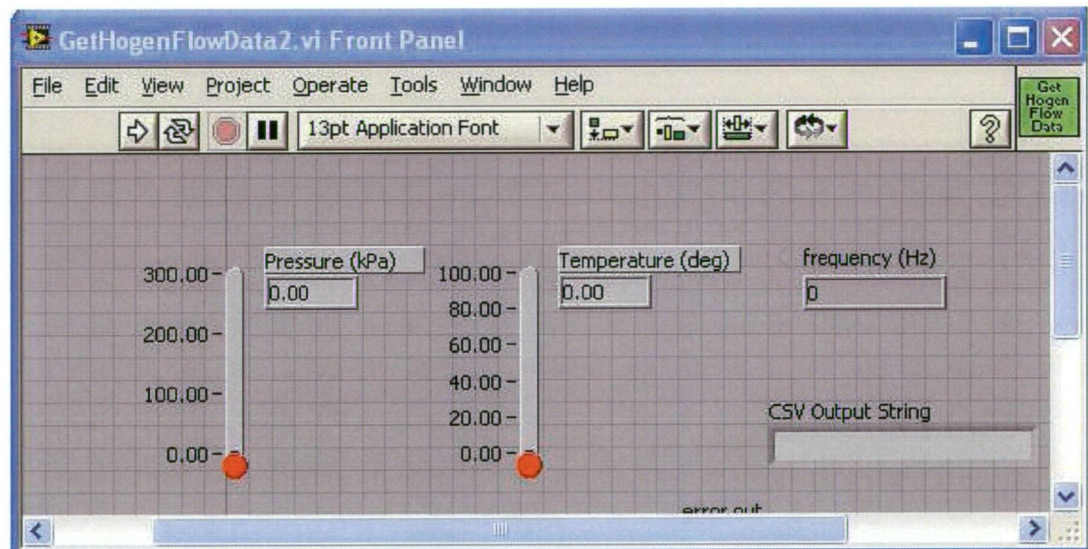


Figure 4.19: Feed water parameters front panel

The front panel of the feed water parameter virtual instrument is shown in figure 4.19. Water pressure, water temperature and flow sensor output frequency are monitored directly. Actual flow rate is subsequently calculated from frequency data.

The power analyser virtual instrument is depicted in figure 4.20. Power analyser output parameters are selected for subsequent storage in the PC database

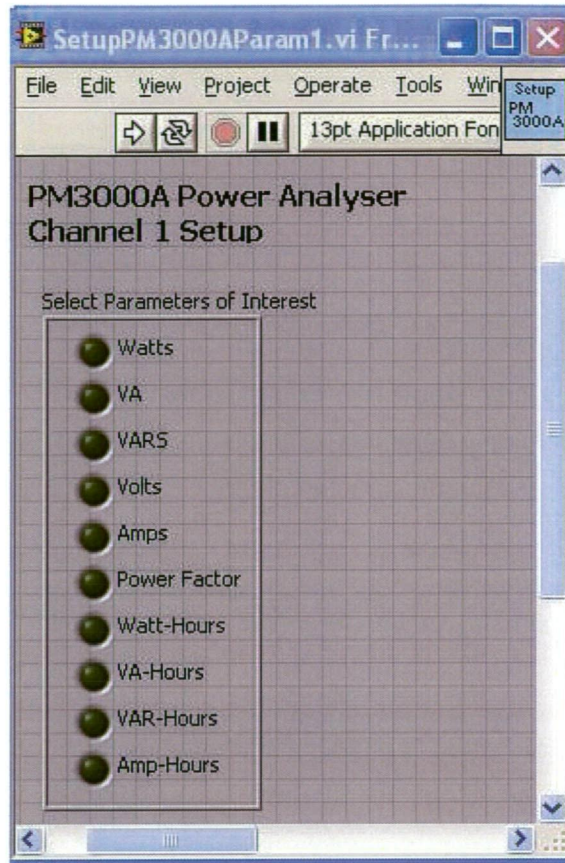


Figure 4.20: Power analyser setup front panel

The front panel of the electrolyzer system parameter virtual instrument is shown in figure 4.21. The interrogator byte sequence (which is depicted on the front panel) is sent to the electrolyzer. The electrolyzer reply is read and system parameters are decoded and displayed. The front panel in figure 4.21 shows the electrolyzer system parameters, the interrogator string and the electrolyzer reply string (decoded).

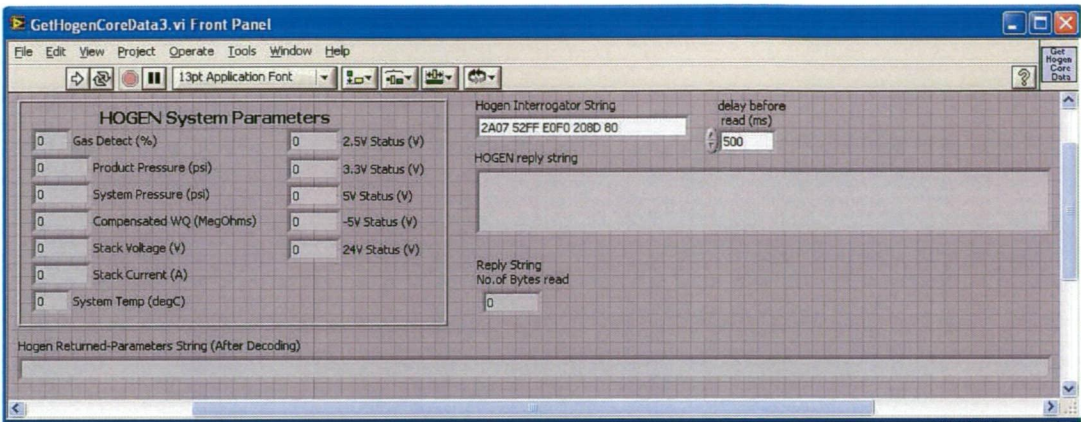


Figure 4.21: Electrolyzer system parameter front panel

The three virtual instruments detailed above were then integrated into the “main program” virtual instrument which is shown in figure 4.22. Data-acquisition start/stop and system sample rate are controlled from the front panel. The main program concatenates text-string data from the feed water, power analyser, and electrolyzer system virtual instruments. Furthermore the main program dates and time stamp data, before storing the concatenated string into a text file on the PC hard drive.

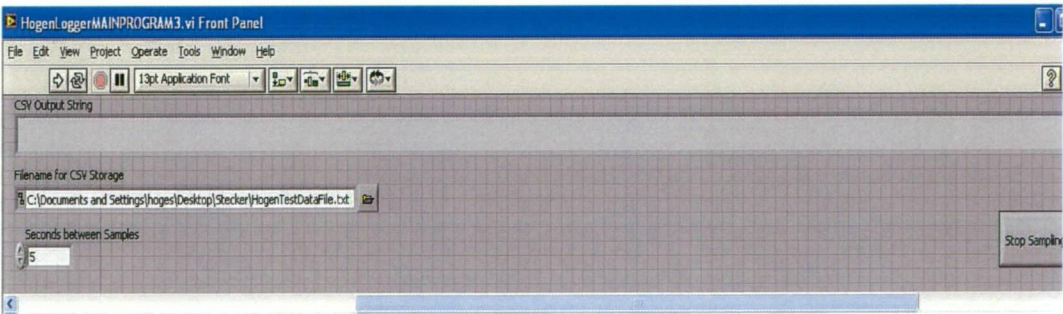


Figure 4.22: Virtual instrument front panel of main program

4.5 Range of Operating Conditions and Testing

The range of various operating conditions can be found in the appendix. It comprises of 244 cases resulting in a 12×244 operation condition matrix. The experimental data has been published in the following references [150-152].

The manufacturers' specification for the hydrogen flow rate of the electrolyzer was provided with an average value of 0.53Nm³/h or 8.833l/min, respectively [158]. Given that this value is averaged over the period of one hour, a more accurate method to estimate the hydrogen flow has been used. The ideal gas law is given in equation 4.2 and 4.3 below:

$$PV = nRT \quad (4.2)$$

$$n = \frac{m}{M} \quad (4.3)$$

where

- P pressure in storage (kPa),
- V volume (physical) of the storage (85.4l),
- n number of moles,
- M molar mass of hydrogen molecule (2.01588g/mol),
- m mass (g),
- R Universal gas constant, 8.31451 (J*K⁻¹*mol⁻¹) and
- T temperature of gas (298K).

According to equation 4.2 and 4.3, the mass of the produced hydrogen can be calculated. The experiments were conducted for a filling process of a storage tank

($V=\text{const.}$) over a period of approximately two hours. The gas temperature was assumed to be constant at 298K and the pressure was obtained from the experimental setup as described in the previous section(s). A plot of the hydrogen flow rate over the output pressure (equals storage pressure) is depicted in figure 4.23.

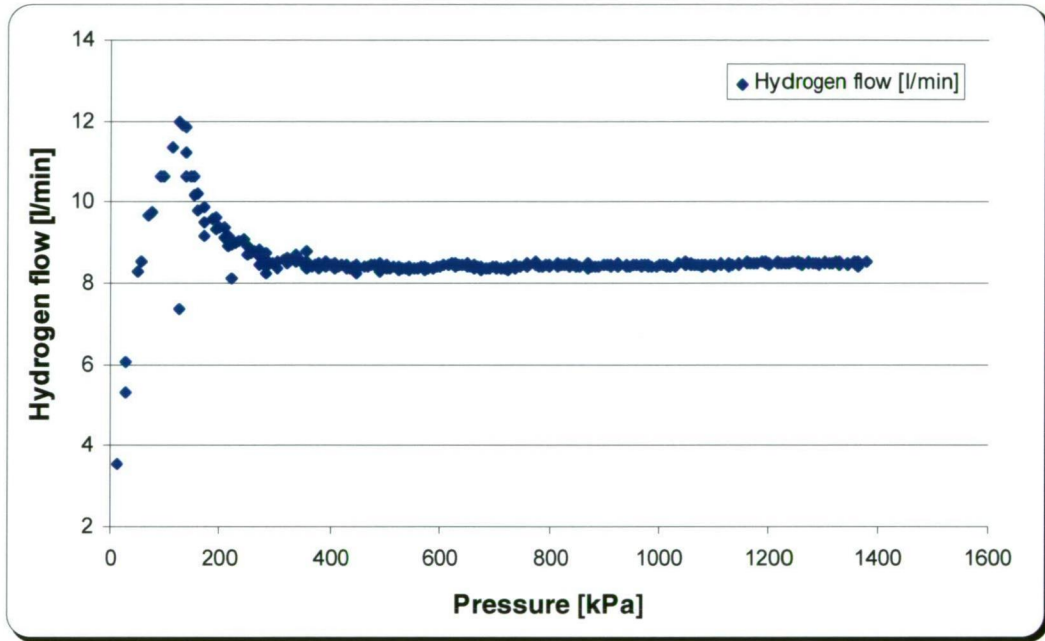


Figure 4.23: Experimental hydrogen flow for tank filling process

These results show an average hydrogen flow rate of 8.62l/min and a more accurate estimation of individual values. The experimental results replicate the averaged manufacturers' specification of 8.833l/min by $\pm 3\%$. Therefore the gathered data are reliable and present a more accurate estimation of hydrogen flow rate.

The power consumption given by the manufacturer with 6.3–9kWh/Nm³ corresponds to an average system-efficiency of 39-56% [158]. The experimental system-efficiency with an average 46% (0.46) lies within the manufacturers' specifications and is therefore considered reliable. The average stack-efficiency was found to be at 55% as it includes only the power consumed by the stack and not the

entire electrolysis system compared the system-efficiency. Therefore, the peripheral devices account for an average loss of approximately 9% efficiency.

A comprehensive range of experimental conditions were tested as part of the investigation that covers a wide range of input variables and their influence on the output performance. The various input parameters that have been obtained include feed water quality (WTQ, Mean = 36.17M Ω), water pressure (Mean = 275.93kPa), system temperature (STM, Mean = 27.56° C), stack current (SCT, Mean = 142.78A), stack voltage (SVG, Mean = 23.72V), system power (Mean = 4172.28W), system pressure (SPS, Mean = 1332.69kPa), product pressure (PPS, Mean = 706.19kPa) and lower explosive limit (LEL, Mean = 36.17%).

The obtained experimental data represent a realistic hydrogen production process using a commercial PEM-electrolyzer. The hydrogen production performance parameter, such as hydrogen flow rate, system-efficiency and stack-efficiency can be seen as a function of various input parameter.

4.6 Concluding Remarks

This chapter provided a detailed description of the experimental setup and individual components in the hydrogen laboratory. The development of the hydrogen storage unit has been outlined in detail. Furthermore, custom built software incorporating virtual instruments of various sensors to enable synchronous data-acquisition has been presented for NI LabVIEW.

The software signifies a new approach for obtaining electrolyzer system parameters through LabVIEW and can be useful for further research using the Hogen® 20 PEM-electrolyzer. The data-acquisition system has been successfully applied to obtain a database comprising of various operating conditions, which characterise the dynamic behaviour of the electrolysis process.

As reviewed in section 4.5, the obtained data are reliable and represent a realistic hydrogen production process using a commercial PEM-electrolyzer. The experimental database is therefore suitable for predictive modelling of hydrogen production performance parameters. This database provides the foundation for the development of predictive models, which will be discussed in the following chapter.

CHAPTER 5
PREDICTIVE MODELS FOR HYDROGEN PRODUCTION
PERFORMANCE IN A PEM-ELECTROLYZER

5.1 Introduction

This chapter presents the development of a Performance Prediction Model (PPM) of a PEM-electrolyzer. The common procedure of modelling will be presented and described under consideration of the fundamentals from chapter 3 and the obtained experimental data in chapter 4.

The experimental data were used to train and test the developed models. Various approaches using ANN and ANFIS hybrid models for electrolyzer production performance parameter prediction, such as hydrogen flow rate, system-efficiency and stack-efficiency have been investigated and discussed. Comparison and assessment of those developed models has also been conducted based on error between experimental and predicted data. Results and appraisal for each performance parameter will be presented followed by summary and conclusion. Based on the error generated, the most suitable model for each performance parameter was selected for the PPM.

Neural Network modelling process has been implemented on the *Neural Network Analysis Package* and the ANFIS time-series prediction models have been built in Matlab Simulink. Results of this chapter have been partially published in the International Journal of Hydrogen Energy and international conferences [150-152].

5.2 Hydrogen Production Performance Prediction Model of a PEM-Electrolyzer

The Performance Prediction Model (PPM) consists of 3 different neural network based models corresponding to each hydrogen production performance parameter, such as hydrogen flow rate, system-efficiency and stack-efficiency (see figure 5.1) Three individual types of models have been applied in order to determine the best suitable model.

Implementation of the PPM has been performed using the *Neural Network Analysis Package* tool for the ANN and Matlab Simulink environment for the hybrid network ANFIS. The analysis package was developed by the HART Research Team from the School of Engineering, University of Tasmania for Neural Network approaches. The following sections (5.2.1; 5.2.2) present a summary of pertinent information regarding this analysis tool. Additional literature can be found in the following references [161-163].

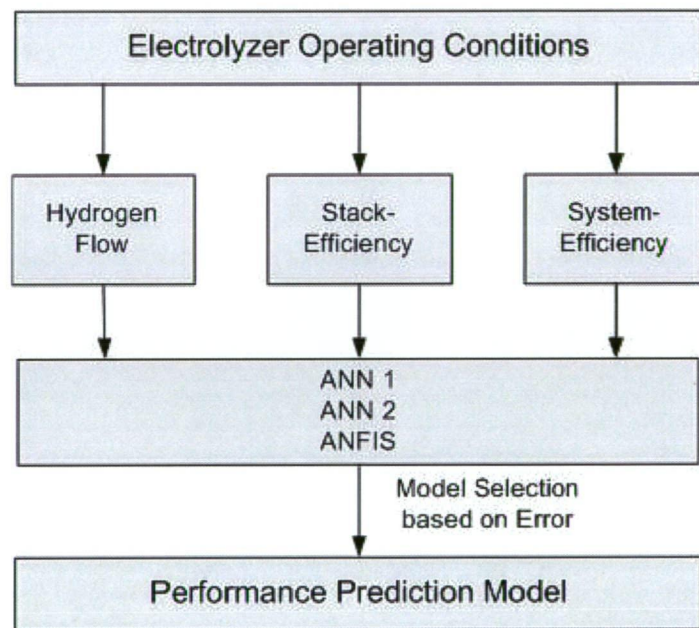


Figure 5.1: Performance Prediction Model (PPM) schematic

5.2.1 Neural Network Analysis Package

The Neural Network Analysis Package has been implemented in Microsoft Excel with the user interface based on Visual Basic macros. The Pascal programmed kernel

does most of the Neural Network processing tasks. The following summary describes the processing steps to perform an analysis with this tool:

1. Conducting analysis and choose number of data patterns, number of inputs and outputs to be filled into spreadsheet.
2. Insert test data.
3. Normalisation of test data patterns from 0 to 1 and automatically saving into a separate work sheet without altering the original test data.
4. Manually or randomly separation of normalised data patterns into training and testing data.
5. Selection of a Neural Network model for a given application from figure 5.2 following the definition of specific parameter such as number of hidden nodes, iterations etc..
6. Generation of output files after successful network training and testing of the chosen model with its corresponding parameters.
7. Finally results can be uploaded including RMS errors and graphical charts.

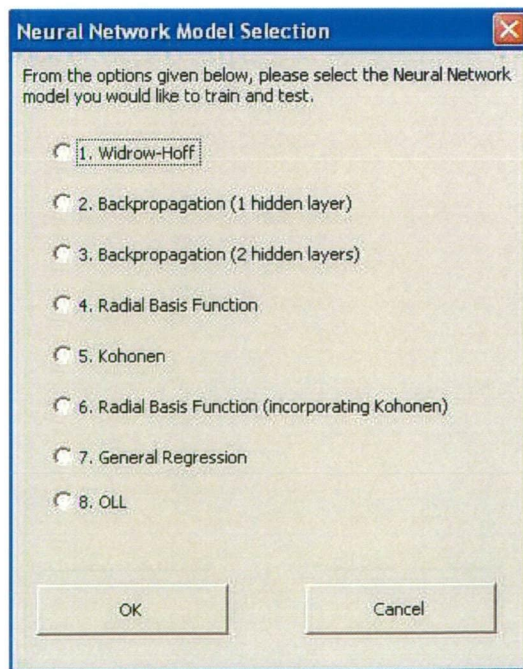


Figure 5.2: User interface of Neural Network Model Selection

5.2.2 General procedure of performance prediction modelling using ANN

Hydrogen production performance parameters, such as hydrogen flow rate (l/min), stack-efficiency (%) and system-efficiency (%) have been obtained according to experimental setup previously discussed in chapter 4. Each of those parameters has been modelled based on experimental data collection (operating conditions). Figure 5.3 shows the input and output parameters in a general neural network organisation for the PPM.

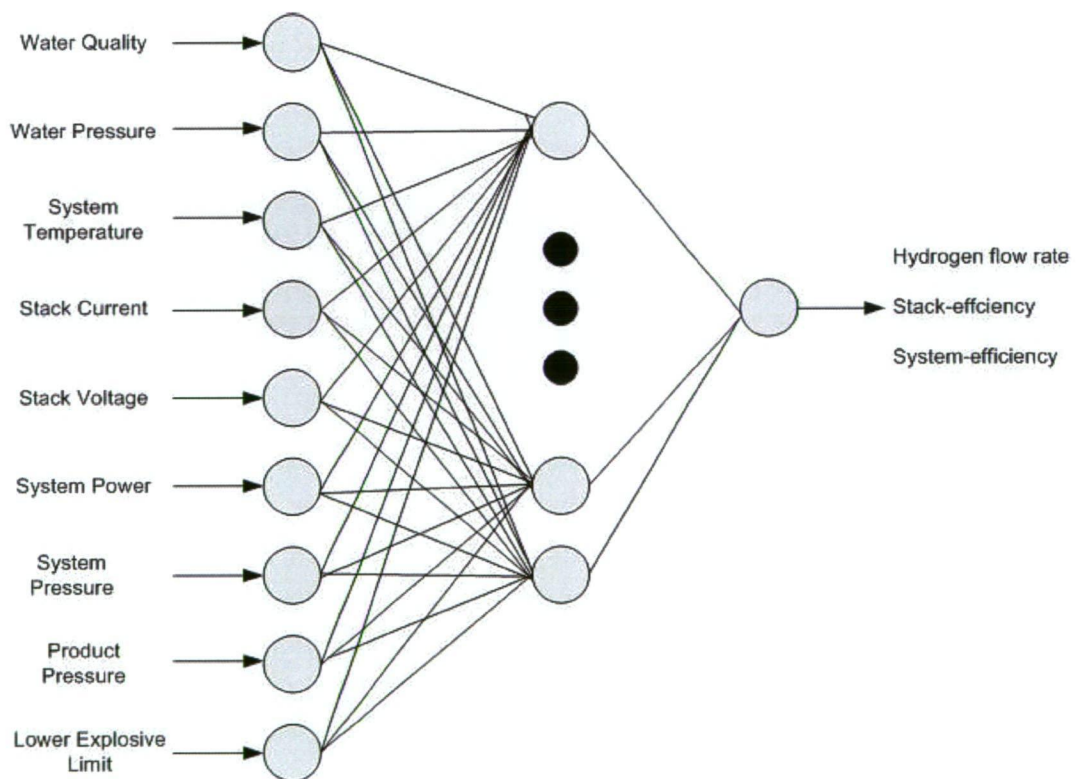


Figure 5.3: General Neural Network structure for PPM

For each of the performance parameter to be modelled, two different Neural Networks such as

- Back-propagation Neural Network with one and two hidden layers (BP1; BP2) and
- Optimisation Layer-by-Layer Neural Network

have been applied. Their functionality and logic has been widely described in chapter 3.

The following steps were applied to model each performance parameter using the *Neural Network Analysis Package*:

1. Processing of experimental data
2. Neural Network training and testing
3. Network selection

Step 1 – Processing of experimental data

Normalisation of experimental data, ranging from 0-1 (see equation 3.3), was performed on a total of 244 data patterns produced by the experiments at different operating conditions. Subsequent to the normalisation process 80% (220 data patterns) of the data was assigned to training and the remaining 20% was reserved for testing.

Step 2 – Neural Network training and testing

Following a network model chosen from figure 5.2, specific parameters such as number of hidden nodes and iterations have to be defined. Those individual network settings were tested and yielding in an average RMS error (equation 3.10) between the experimental and predicted data.

Step 3 - Network Selection

The RMS error can be seen as an overall performance parameter or qualitative measure of the individually tested model. Thus, the specific model with the

minimum RMS error can be identified. Testing results can be graphically depicted and assist the selection process of the most suitable model for each performance parameter.

5.2.3 ANFIS implementation

In addition to the Neural Network models, ANFIS time-series prediction hybrid model as discussed in chapter 3 has been developed and tested using the Matlab Simulink environment. Unlike ANN the data are not normalised and randomised. A set of 134 data has been used for testing of the models and the remaining 101 accounted for training and checking. ANFIS is used as a tool to predict future values of hydrogen flow rate, stack-efficiency and system-efficiency based on precision data collection of the experiments in tank filling mode (TF). The time-series prediction uses past values of the parameters until time t in order to predict the value at a point in the future $(t + 1)$ as follows:

$$x(t + 1) = f[(x(t - 3)x(t - 2)x(t - 1)x(t))]$$
(5.1)

5.2.4 ANFIS parameter selection

The ANFIS network parameters, such as the order of the Membership Function (MF) and epochs, have been varied to obtain best results in terms of model validation corresponding to a low average RMS error. A number of distributions were tested to obtain the most suitable type of MF. The generalised bell function gives the distribution of parameters close to its mean value. Due to the nature of the data-sets and their distribution close to its mean value, the generalized bell function was found to be the most suitable for the parameter prediction. One epoch or iteration is a single pass through the entire training set followed by testing. Increasing the number of

epochs might improve the performance of the ANFIS, however it increases the training time. Changing the MF to a higher order can improve the performance slightly, but also adds significantly to the training and evaluation time. It should also be noted to consider the capacity of the computational facilities when training the model with a higher order of MFs.

5.3 Results and Model Evaluation

5.3.1 Stack-efficiency prediction model

Back-propagation Neural Networks with one hidden layer (BP1) and a changing architecture of 2-10 neurons in the hidden layer were tested first. Figure 5.4 shows the RMS errors for training and testing in this category. From this figure, the network with 2 hidden neurons has resulted in the minimum RMS error with a corresponding value of 8.43% for the testing set and 7.22% for the training set. As a result it was chosen as the optimal one hidden layer Back-propagation network for prediction of stack-efficiency.

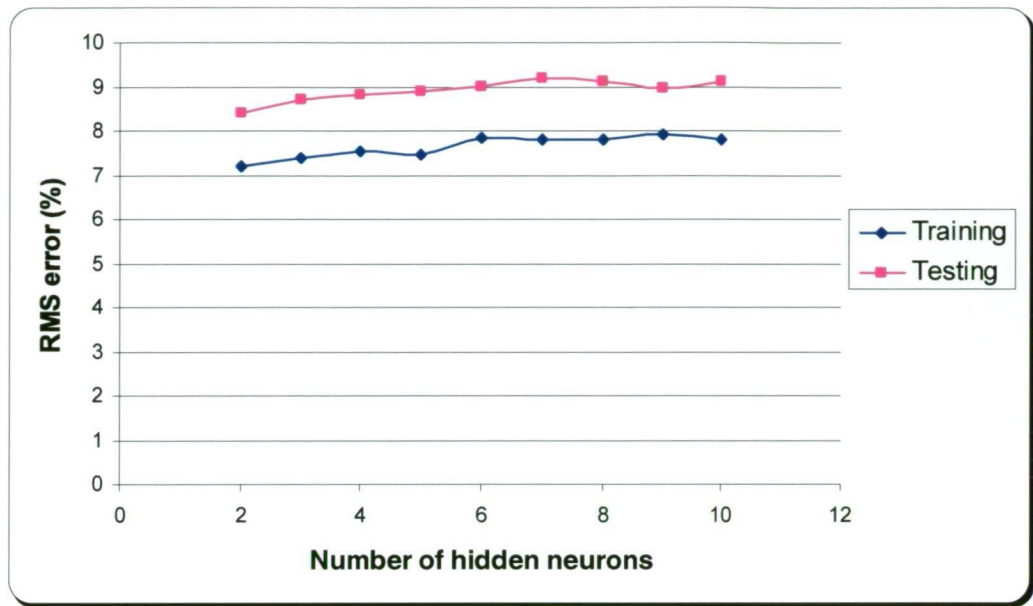


Figure 5.4: Back-propagation Neural Network (BP1) RMS error with changing architecture for prediction of Stack-efficiency

Testing results for the two hidden layer Back-propagation network (BP2) are shown in figure 5.5. The network with 13 neurons in the first hidden layer and 3 neurons in the second hidden layer has resulted in the minimum RMS error for the two hidden layer Back-propagation Neural Networks. This optimum network was selected for the prediction of the stack-efficiency. It yielded in a slightly lower RMS error compared to the one hidden layer Back-propagation network with RMS error values of 6.53% and 7.96% for the training set and testing set, respectively.

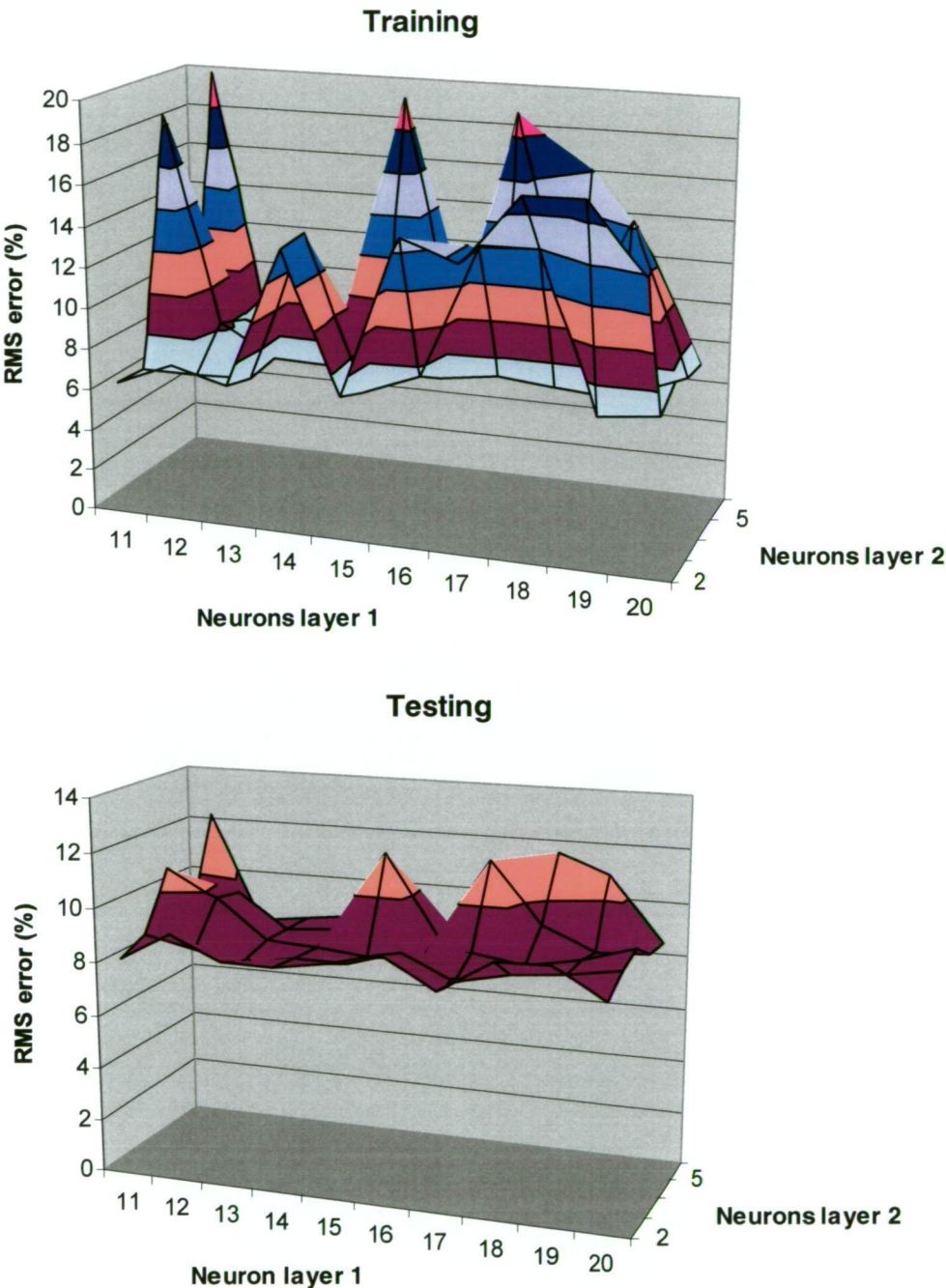


Figure 5.5: Two hidden layer Back-propagation Neural Network (BP2) RMS error with changing architecture for prediction of Stack-efficiency

The testing results for the Optimisation Layer-by-Layer (OLL) Neural Network are depicted in figure 5.6. This category presented an improvement compared to the Back-propagation Neural Networks. The network with 5 hidden neurons was chosen as the best of this category for prediction of stack-efficiency. It resulted in RMS errors of 2.96% for the training set and 1.95% for the testing set.

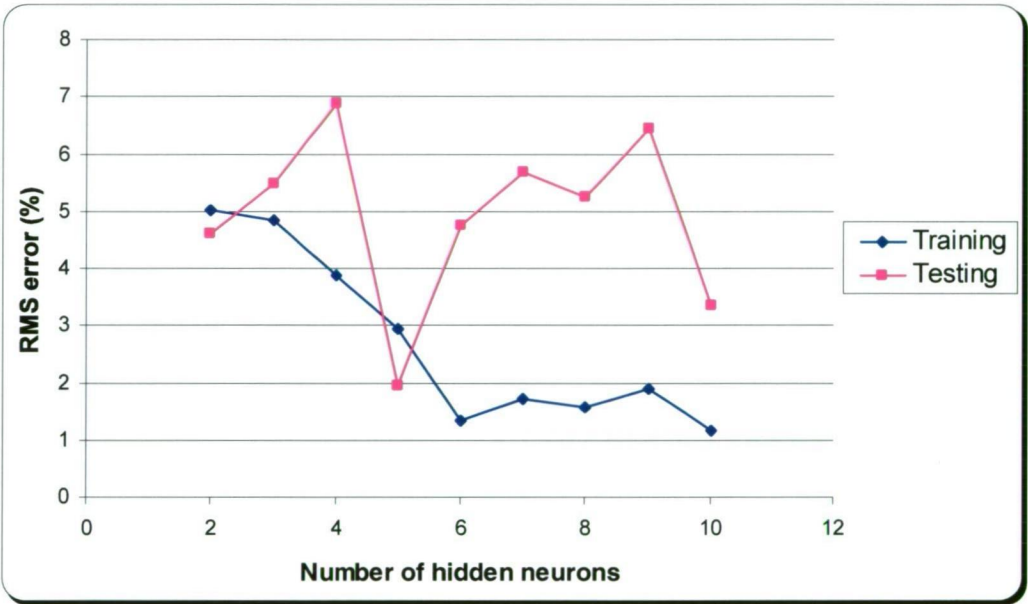


Figure 5.6: OLL Neural Network RMS error with changing architecture for prediction of Stack-efficiency

In the hybrid category, the approach with ANFIS produced the following results as shown in table 5.1. The number of epochs and MFs have been varied to obtain optimum results.

Table 5.1: ANFIS performance for prediction of stack-efficiency with variation of MFs and epochs based on RMS error

Number of Epochs	Stack-efficiency RMS error (%)		
	MF 2	MF 3	MF 4
3	0.36	0.7	0.77
5	0.5	0.77	3.04
10	0.87	0.8	1.89

The best results based on RMS error were achieved by using MF 2 ranging from 0.36%-0.87%. However, models which follow the trend at best are essential for control strategies. In order to identify those models, a comparison of the plotted diagrams for each of the investigated models from table 1 was conducted. The predictive model with the best performance in terms of trend following was found for MF 3 with an average RMS testing error of 0.7%. A plot of the testing data with actual and predicted parameters is shown in figure 5.7. Additionally the numerical error between the actual and predicted data is also depicted in this figure [151].

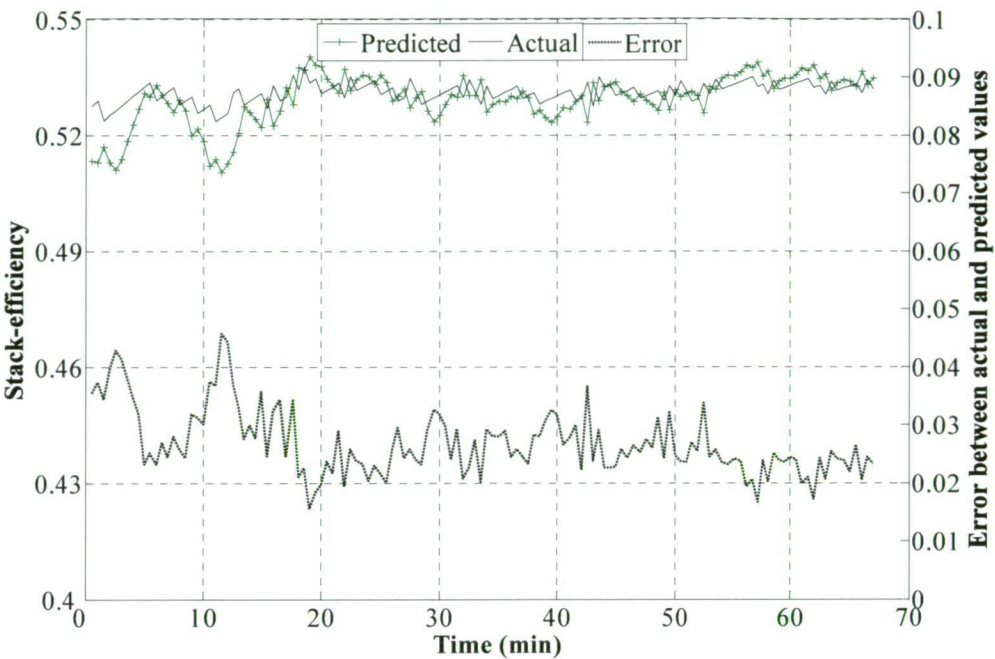


Figure 5.7: ANFIS network with 3 membership functions for prediction of stack-efficiency

A summary of the optimum models for the prediction of stack-efficiency is presented in table 2 below.

Table 5.2: Summary of best performing model in each category

Model	Architecture	RMS testing error (%)
BP1	2 hidden neurons	8.43
BP2	13 hidden neurons 1 st layer; 2 hidden neurons 2 nd layer	7.96
OLL	5 hidden neurons	1.95
ANFIS	3 MF	0.7

From those results, it can be concluded that the OLL and ANFIS networks show excellent results with an average RMS error of 1.95% and 0.7% respectively. The performance of those models is significantly better compared to the Back-propagation models.

5.3.2 Hydrogen flow rate prediction model

For the prediction of hydrogen flow rate, Back-propagation Neural Networks with one hidden layer (BP1) and a changing architecture of 2-10 neurons in the hidden layer were initially tested as shown in figure 5.8. From this figure, the optimum network with 10 neurons in the hidden layer resulted in a minimum RMS error of 6.47% for the training set and 6.09% for the testing set. It was therefore chosen as the optimum model for hydrogen flow rate prediction in this network category.

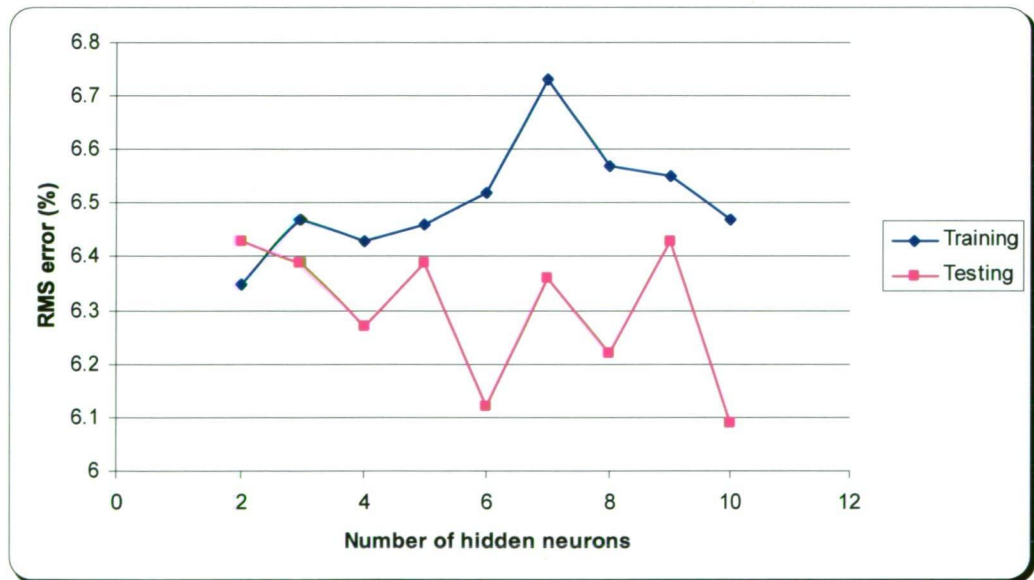


Figure 5.8: Back-propagation Neural Network (BP1) RMS error with changing architecture for prediction of Hydrogen flow rate

The testing results with changing architecture for the two hidden layer Back-propagation network (BP2) are illustrated in figure 5.9. The model with 11 neurons in the first hidden layer and 3 neurons in the second hidden layer resulted in the minimum RMS error and was selected as the optimum model for hydrogen flow rate prediction. This particular model architecture produced RMS errors of 6.92% for the training set and 6.39% for the testing set. In comparison to the BP1 model, no further improvement could be made.

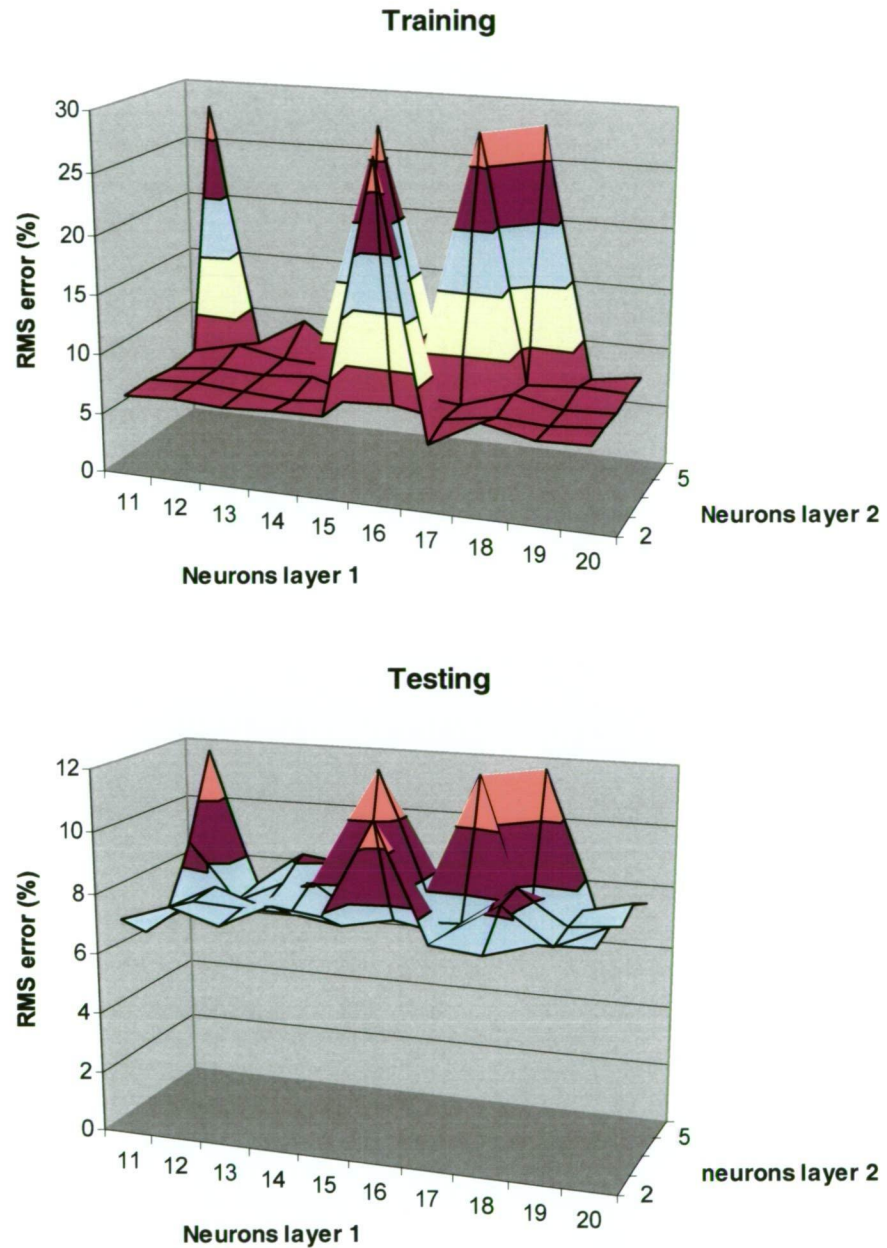


Figure 5.9: Two hidden layer Back-propagation Neural Network (BP2) RMS error with changing architecture for prediction of Hydrogen flow rate

Based on the testing results for the OLL neural network in figure 5.10, accuracy of this model category has improved compared to the BP1 and BP2 models. The best

model for prediction of hydrogen flow rate contained 8 neurons in the hidden layer and yielded RMS errors of 0.71% for the training set and 2.13% for the testing set.

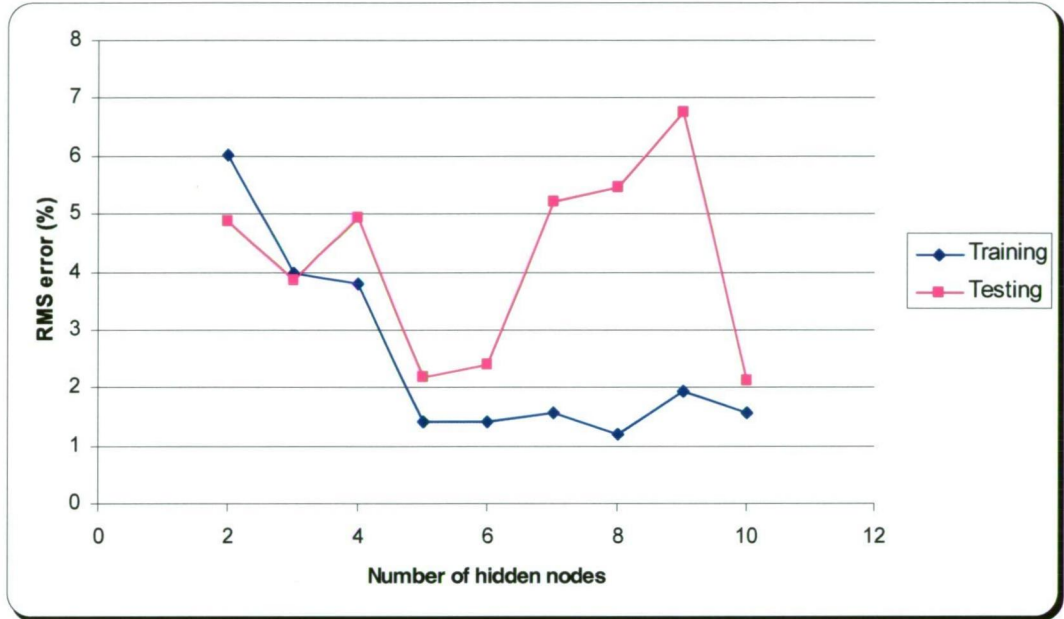


Figure 5.10: OLL Neural Network RMS error with changing architecture for prediction of Hydrogen flow rate

Table 5.3 highlights the results produced with ANFIS in the hybrid network category. The best result could be achieved using 4 MFs and produced an average RMS testing error of 3.47%. This network was selected as the optimum model in the time-series prediction of hydrogen flow rate.

Table 5.3: ANFIS performance for prediction of hydrogen flow rate with variation of MFs and epochs

Number of Epochs	Hydrogen flow rate RMS error (%)		
	MF 2	MF 3	MF 4
3	4.5	4.71	4.83
5	4.29	4.59	7.77

10	4.82	4.58	3.47
----	------	------	------

According to the summary of the optimum models in each category presented in table 5.4, the OLL network and the ANFIS approach outperform Back-propagation models. In the hybrid category, the ANFIS network achieved acceptable results with an RMS error of 3.47%. On the other hand the OLL Neural Network produced excellent results with an average RMS error of 2.13%.

Table 5.4: Summary of best performing model for hydrogen flow rate prediction in each category

Model	Architecture	RMS testing error (%)
BP1	10 hidden neurons	6.09
BP2	11 hidden neurons 1 st layer; 3 hidden neurons 2 nd layer	6.39
OLL	8 hidden neurons	2.13
ANFIS	4 MF	3.47

A plot of the best model for the prediction of hydrogen flow rate is shown in figure 5.11. It can be seen, that qualitative and quantitative trends between predicted and experimental data are matched accurately.

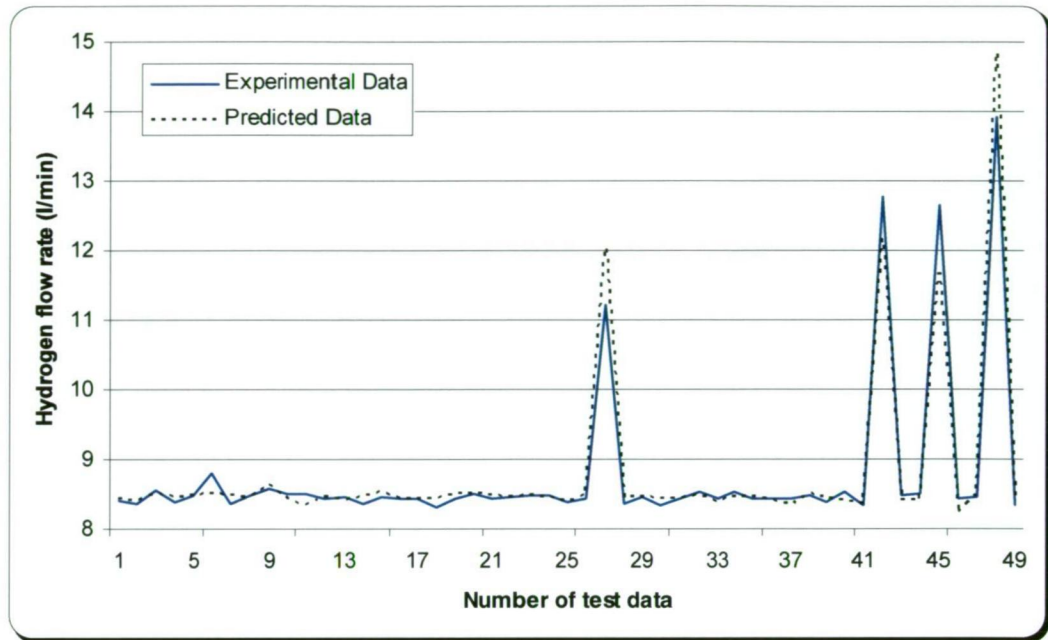


Figure 5.11: Experimental and predicted data for OLL Neural Network with 8 neurons in hidden layer for Hydrogen flow rate prediction

5.3.3 System-efficiency prediction model

Back-propagation Neural Networks with one hidden layer (BP1) were initially tested for the prediction of system-efficiency. The results of the investigated models are shown in figure 5.12. The network with 10 hidden neurons produced minimal RMS error in this network category. Consequently, this model was chosen as the optimum network for system-efficiency prediction with RMS errors of 6.91% for the training set and 3.05% for the testing set respectively.

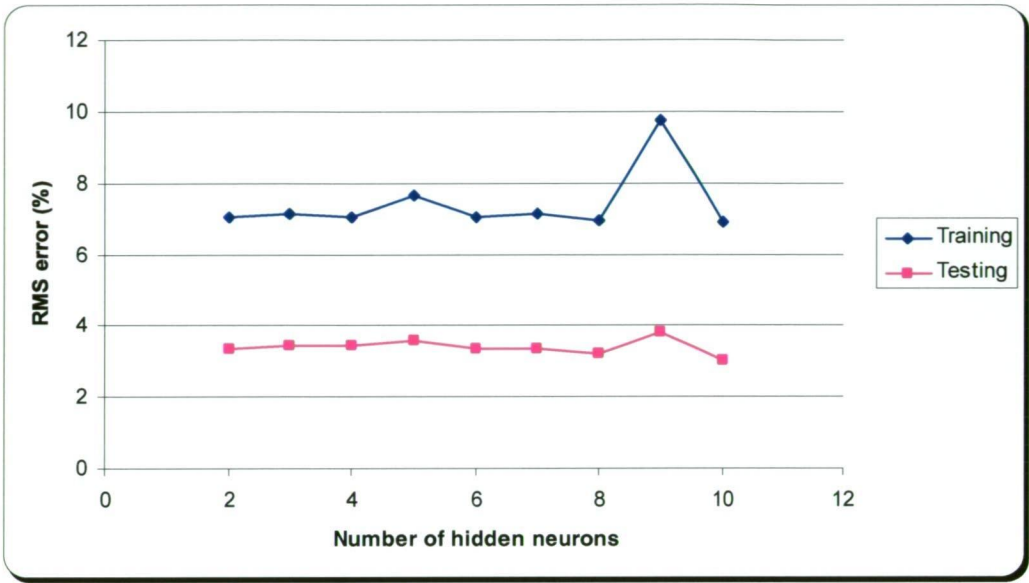


Figure 5.12: Back-propagation Neural Network (BP1) RMS error with changing architecture for prediction of System-efficiency

Training and testing results for the two hidden layer Back-propagation Neural Network are presented in figure 5.13. The RMS error varied according to the changing architecture and a slight improvement compared to BP1 could be made. The best performing model, with 20 neurons in the first layer and 6 neurons in the second layer yielded minimum RMS error of 6.79% for the training set and 2.4% for the testing set. Thus it was selected as the optimum model for system-efficiency prediction in this network category.

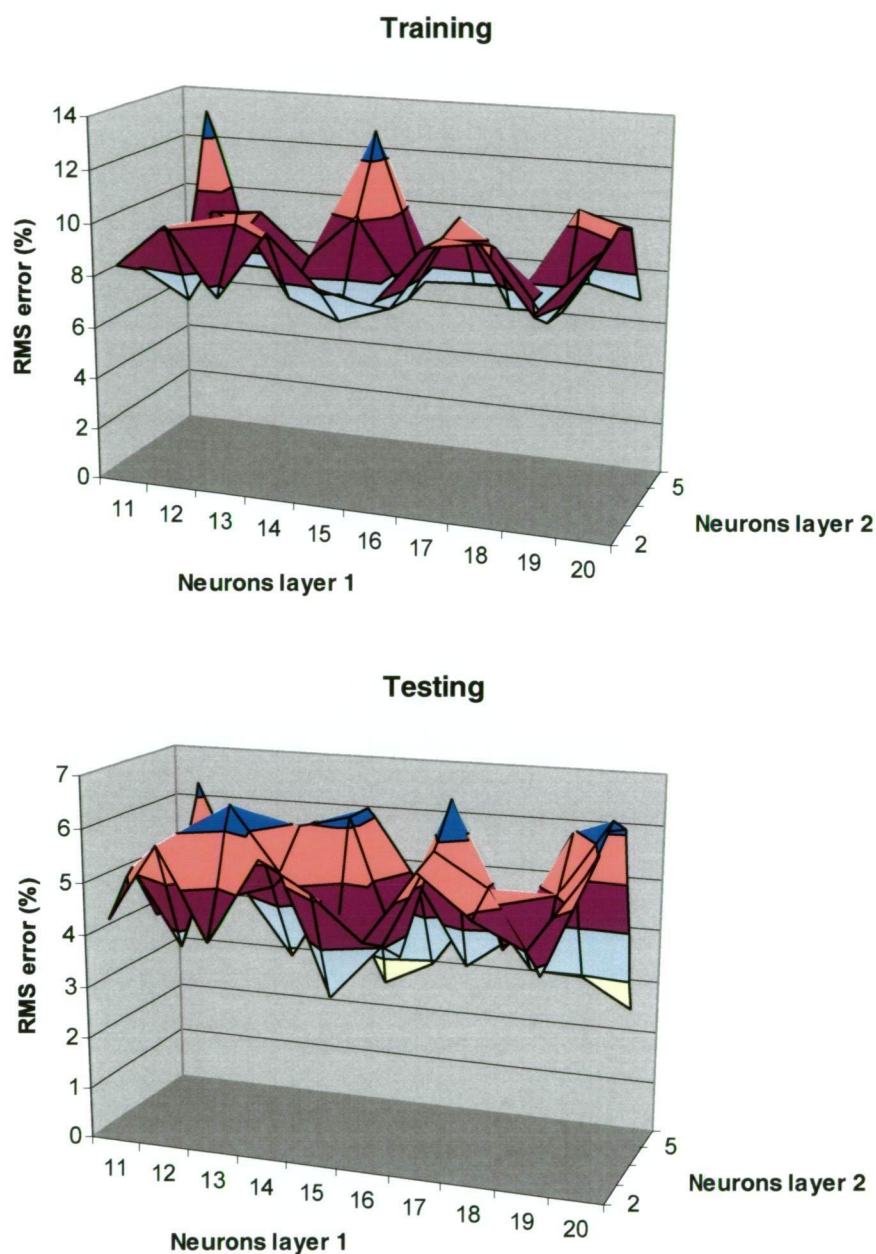


Figure 5.13: Two hidden layer Back-propagation Neural Network (BP2) RMS error with changing architecture for prediction of System-efficiency

Significant improvement in comparison to BP1 and BP2 for prediction of system-efficiency was achieved using the OLL Neural Network. Based on the results from figure 5.14, the model with 9 neurons in the hidden layer yielded minimum RMS

error. This model, with a corresponding RMS error of 1.21% and 1.54% for the training and testing set respectively, was selected as the optimum model in this network category.

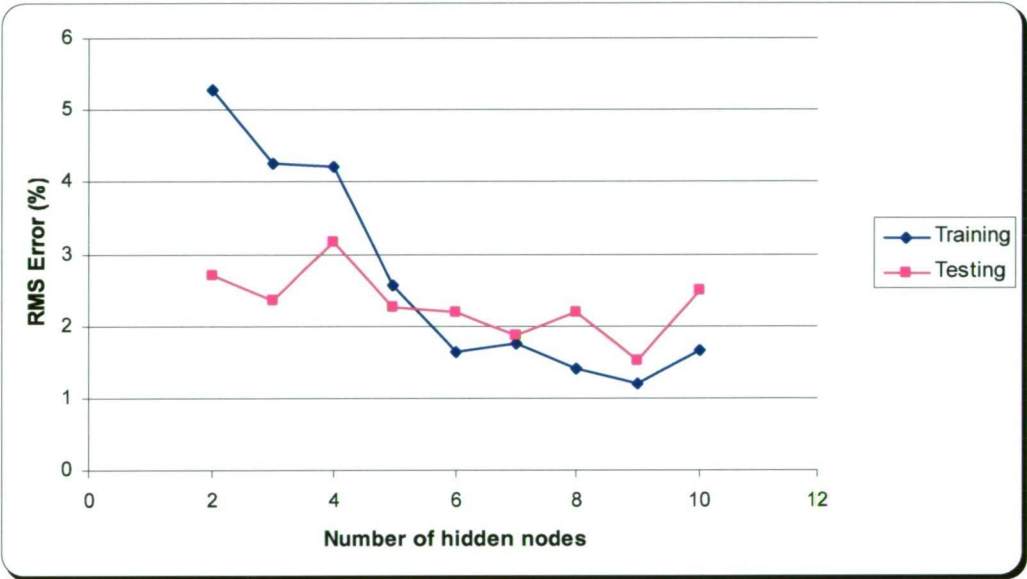


Figure 5.14: OLL Neural Network RMS error with changing architecture for prediction of System-efficiency

The results of the ANFIS network in the hybrid category are shown in table 5.5. Further improvement compared to the OLL model was achieved. Excellent results of 0.38% RMS testing error were produced using 3 MFs.

Table 5.5: ANFIS hybrid network performance for prediction of system-efficiency with variation of MFs and epochs

Number of Epochs	System-efficiency RMS error (%)		
	MF 2	MF 3	MF 4
3	1.49	0.39	0.75
5	1.67	0.38	0.68
10	2.22	0.59	1.59

Following the summary of the optimum models from each category in table 5.6, the ANFIS time-series prediction model using 3 MFs was selected as the best performing model for the prediction of electrolyzer system-efficiency.

Table 5.6: Summary of best performing model for system-efficiency in each category

Model	Architecture	RMS testing error (%)
BP1	10 hidden neurons	3.05
BP2	20 hidden neurons 1 st layer; 6 hidden neuron 2 nd layer	2.4
OLL	9 hidden neurons	1.54
ANFIS	3 MF	0.38

A plot of the ANFIS prediction model is shown in figure 5.15. It can be seen, that the predicted data (green) are following the qualitative and quantitative trend of the actual data (black) at a very high accuracy.

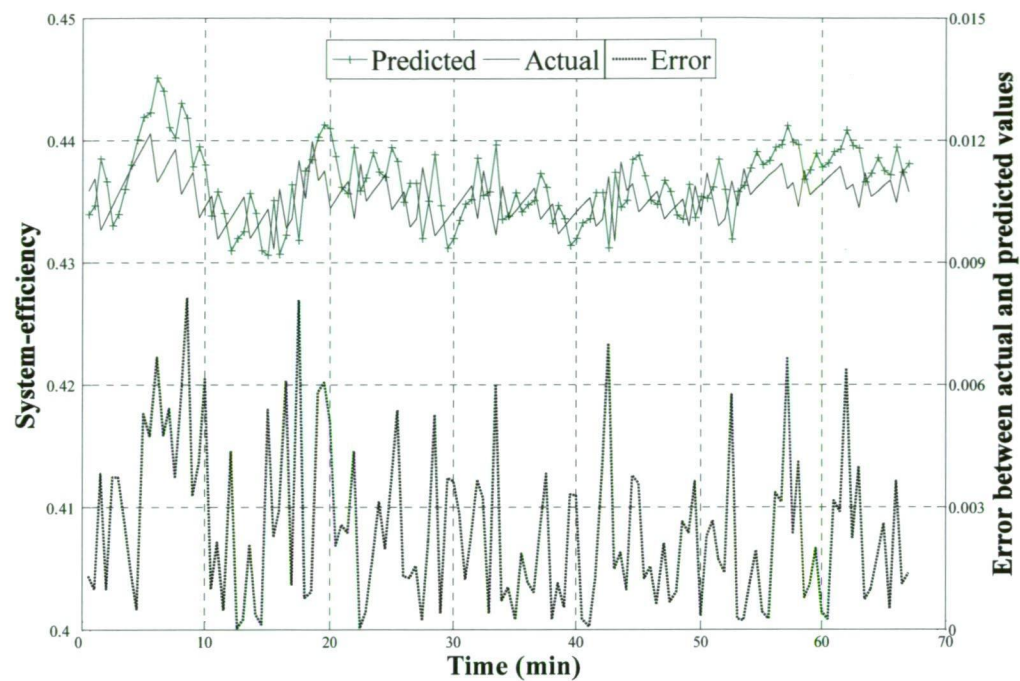


Figure 5.15: ANFIS network with 3 membership functions for prediction of system-efficiency

5.4 Concluding Remarks

Various neural network based models have been investigated to predict three specific hydrogen production performance parameters, such as stack-efficiency, hydrogen flow rate and system-efficiency. The models for the PPM proved to be highly accurate with very low average RMS error as shown in table 5.7.

Table 5.7: Selected models for the PPM of the PEM-electrolyzer

Performance Parameter	RMS testing error (%)	Prediction Model
Stack-efficiency	0.7	ANFIS (3 MF)
Hydrogen flow rate	2.13	OLL (8 hidden neurons)
System-efficiency	0.38	ANFIS (3 MF)

The ANFIS model, using 3 MFs has been chosen as the best suitable model for the prediction of the stack-efficiency with an average RMS testing error of 0.7%. For the prediction of hydrogen flow rate the OLL neural network model with 8 neurons in the hidden layer was selected as the optimum model for the PPM. It yielded average RMS error of 2.13%. Finally, the most suitable model for prediction of system-efficiency could be identified as the ANFIS hybrid network with 3 MFs and an average RMS testing error of 0.38%.

This study of performance prediction modelling for an industrial process of a PEM-electrolyzer provides an alternative method to conventional mathematical modelling approaches, where operating conditions have to be determined initially. The PPM, consisting of neural network based models, utilised the operating conditions from experimental database in order to predict the hydrogen performance parameters.

The high accuracy of those predictive models enables on-line adaptation for wider monitor and safety application, where the PPM could be implemented as a virtual sensor and replace expensive instrumentation for hydrogen production.

CHAPTER 6
FINAL CONCLUDING REMARKS AND PROPOSED FUTURE
WORK

Increasing global warming and pollution present a serious problem of mankind in today's world. The decrease of fossil fuels accompanied by increasing global energy demand requires alternative energy solutions. Hydrogen production technologies are gaining increasing importance in the search of an alternative energy supply for the future. Electrolytic hydrogen production can be seen as the binding element in utilising and storing fluctuating renewable energies towards a sustainable and environmentally compatible energy supply.

This thesis provided a comprehensive study in predictive performance modelling for a commercial PEM-electrolyzer. An extensive literature survey on the most common and widely used hydrogen production technologies was presented. A special emphasises on the process of water electrolysis and electrolyzer technology was also provided. Furthermore, various existing electrolyzer models and modelling approaches, which are mainly based on fundamental theories, have been discussed. Due to the complexity of those mathematical models, which rely on extensive and expensive experimental investigations, an approach with intelligent techniques, such as Neural Networks and hybrid models was suggested.

As part of the literature review, neural network based models and their application for non-linear processes have been investigated. A general knowledge about Artificial Neural Networks and hybrid model ANFIS was presented. The theory and mathematical logic behind each of the models used in this work has also been discussed. By using the *Neural Networks Analysis Package*, which was developed by the School of Engineering at the University of Tasmania and the Matlab Simulink environment for the development of the ANFIS models, a good understanding of neural network based models has been demonstrated.

The design and development of the experimental test facility has been described. The test rig was used to measure and predict specific electrolyzer performance parameters, such as hydrogen flow rate, stack-efficiency and system-efficiency. Comprehensive experimental data, which cover a wide range of operating conditions, were obtained with National Instruments LabVIEW software. The database formed the foundation for the training and verification of the predictive

performance models. The verification was carried out between by comparison of the experimental and predicted values.

Various neural network based models have been investigated to predict three specific hydrogen production performance parameters, such as stack-efficiency, hydrogen flow rate and system-efficiency. The models for the PPM proved to be highly accurate with very low average RMS error.

The ANFIS model, using 3 MFs has been chosen as the best suitable model for the prediction of the stack-efficiency with an average RMS testing error of 0.7%.

For the prediction of hydrogen flow rate the OLL neural network model with 8 neurons in the hidden layer was selected as the optimum model for the PPM. It yielded average RMS error of 2.13%.

The most suitable model for prediction of the system-efficiency could be identified as the ANFIS hybrid network with 3 MFs and an average RMS testing error of 0.38%.

This study of performance prediction modelling for an industrial process of a PEM-electrolyzer provides an alternative method to conventional mathematical modelling approaches, where operating conditions have to be determined initially. The PPM, consisting of neural network based models, utilised the operating conditions from experimental database in order to predict the hydrogen performance parameters.

Based on this work further research could be conducted. The dynamic electrolyzer behaviour could be further investigated, especially when coupled directly with a renewable source, such as wind generator or a photovoltaic system. This would provide a greater range of data, where the capability of neural network based predictive models could be further investigated. The high accuracy of the predictive models presented here enables on-line adaptation for wider monitor and safety application, where the PPM could be implemented as a virtual sensor and replace expensive instrumentation for hydrogen production.

REFERENCES

- [1] <http://www.eia.doe.gov/emeu/cabs/Australia/Electricity.html>, accessed on 27/07/2009
- [2] <http://www.eia.doe.gov/oiaf/ieo/transportation.html>, accessed on 22/07/09, Energy Information Administration, Official Energy Statistics from the U.S. Government
- [3] Intergovernmental Panel on Climate Change (IPCC), Fourth Assessment Report (AR4) 2007
- [4] Lewtas, J., Human exposure to complex mixtures of air pollutants. *Toxicology Letters*, 1994. 72(1-3): p. 163-169.
- [5] Ghose, M.K., R. Paul, and S.K. Banerjee, Assessment of the impacts of vehicular emissions on urban air quality and its management in Indian context: the case of Kolkata (Calcutta). *Environmental Science & Policy*, 2004. 7(4): p. 345-351.
- [6] Mohamed, M.F., D. Kang, and V.P. Aneja, Volatile organic compounds in some urban locations in United States. *Chemosphere*, 2002. 47(8): p. 863-882.
- [7] Lewtas, J., Air pollution combustion emissions: Characterization of causative agents and mechanisms associated with cancer, reproductive, and cardiovascular effects. *Mutation Research/Reviews in Mutation Research*. 636(1-3): p. 95-133.
- [8] Atimtay, A.T., et al., Urban CO Exposure and Its Health Effects on Traffic Policemen in Ankara. *Environmental Research*, 2000. 82(3): p. 222-230.
- [9] Nielsen, T., et al., City air pollution of polycyclic aromatic hydrocarbons and other mutagens: occurrence, sources and health effects. *Science of The Total Environment*, 1996. 189-190: p. 41-49.
- [10] Latza, U., S. Gerdes, and X. Baur, Effects of nitrogen dioxide on human health: Systematic review of experimental and epidemiological studies conducted between 2002 and 2006. *International Journal of Hygiene and Environmental Health*, 2009. 212(3): p. 271-287.

References

- [11] Shafiee, S. and E. Topal, When will fossil fuel reserves be diminished? *Energy Policy*, 2009. 37(1): p. 181-189.
- [12] Hubbert, M.K., 1949. Energy from fossil fuels. *Science* 109(2823), 103–109.
- [13] de Almeida, P. and P.D. Silva, The peak of oil production--Timings and market recognition. *Energy Policy*, 2009. 37(4): p. 1267-1276.
- [14] Bardi, U., Peak oil: The four stages of a new idea. *Energy*, 2009. 34(3): p. 323-326.
- [15] Peak Oil: an Outlook on Crude Oil Depletion, Colin J. Campbell, online, accessed October 2007, <http://www.greatchange.org/ov-campbell,outlook.html>
- [16] Campbell, C., 2003. Industry urged to watch for regular oil production peaks, depletion signals. *Oil and Gas Journal* 101(27), 38–45.
- [17] http://www.ens.dk/en-US/policy/delegations/Documents/Renewable_Energy_Danish-Solutions.pdf
Accessed on 20/08/09
- [18] Danish Energy Authority, Energy Statistics 2005, http://193.88.185.141/Graphics/Publikationer/Statistik_UK/Energy_statistics_2005/html/chapter03.htm accessed 20/08/09
- [19] Australian Bureau of Statistics, online, accessed 27/07/09, <http://www.abs.gov.au/AUSSTATS/abs@.nsf/2f762f95845417aeca25706c00834efa/7D4C023D72C58A37CA2573C5000DA88B?opendocument>
- [20] Midilli, A. and I. Dincer, Hydrogen as a renewable and sustainable solution in reducing global fossil fuel consumption. *International Journal of Hydrogen Energy*, 2008. 33(16): p. 4209-4222.
- [21] Veziroglu, T.N., Hydrogen movement and the next action: Fossil fuels industry and sustainability economics. *International Journal of Hydrogen Energy*, 1997. 22(6): p. 551-556.
- [22] Meher L.C., Sagar D>V., Naik S.N. Technical aspects of biodiesel production by transesterification- a review, *Renew Sustain Energy Rev* 2006, 10:248
- [23] Veziroglu, T.N., Hydrogen Energy, Part A. 1975, New York: Plenum.
- [24] Wikipedia, Hydrogen, online, accessed 21/05/2008; available from: <http://en.wikipedia.org/wiki/Hydrogen>.

References

- [25] Zuettel, A., Borgschulte A., Schlappbach, L. Hydrogen as a future energy carrier. 2008 WILEY-VCH verlag GmbH and Co. KGaA, Wannheim
- [26] Balat, M. hydrogen in fueled systems and the significance of hydrogen in vehicular transportation. *Energy Source Part B* 2007, 2:49
- [27] Aceves, S.M., et al., Vehicular storage of hydrogen in insulated pressure vessels. *International Journal of Hydrogen Energy*, 2006. 31(15): p. 2274-2283.
- [28] Maddalena, A., et al., Study of Mg-based materials to be used in a functional solid state hydrogen reservoir for vehicular applications. *International Journal of Hydrogen Energy*, 2006. 31(14): p. 2097-2103.
- [29] Peschka, W., Liquid hydrogen as a vehicular fuel- a challenge for cryogenic engineering. *International Journal of Hydrogen Energy*, 1984. 9(6): p. 515-523.
- [30] Aceves SM, Smith JR. Hybrid and conventional hydrogen engines that meet EZEV emissions SAE Paper 970290, SAE Transactions. J Passenger Cars 1997;106:486–97.
- [31] Australian Standard 2430.1-1987. Classification of hazardous areas—part 1: explosive gas atmospheres.
- [32] Hay, D.R. Safety guide for hydrogen. National Research Council Hydrogen Safety Committee (1987), Ottawa
- [33] Gregory, F.D. Safety standard for hydrogen and hydrogen systems. Guidelines for hydrogen system design, material selection, operations, storage and transportation. office of safety and mission assurance (1997), Washington, DC 20546, Natianal Aeronautics and Space Administration NASA.
- [34] Lippman, T.E. What will power the hydrogen economy? Analysis and report prepared for the Natural Resources Defense Council. Publication no. UCD-ITS-RR-04-10. University of California, July 2004
- [35] Universal Industrial Gases, Inc. (UIG), USA, Hydrogen properties, uses, applications, hydrogen gas and liquid hydrogen.
<http://www.uigi.com/hydrogen.html>, accessed: 26 Feb 2009.

References

- [36] Dehkordi, A.M. and M. Memari, Compartment model for steam reforming of methane in a membrane-assisted bubbling fluidized-bed reactor. *International Journal of Hydrogen Energy*, 2009. 34(3): p. 1275-1291.
- [37] Yu, W., et al., A comparative simulation study of methane steam reforming in a porous ceramic membrane reactor using nitrogen and steam as sweep gases. *International Journal of Hydrogen Energy*, 2008. 33(2): p. 685-692.
- [38] Levent, M., D. J. Gunn, and M. Ali El-Bousiffi, Production of hydrogen-rich gases from steam reforming of methane in an automatic catalytic microreactor. *International Journal of Hydrogen Energy*, 2003. 28(9): p. 945-959.
- [39] Simpson, A.P. and A.E. Lutz, Exergy analysis of hydrogen production via steam methane reforming. *International Journal of Hydrogen Energy*, 2007. 32(18): p. 4811-4820.
- [40] Kumar, S., S. Kumar, and J.K. Prajapati, Hydrogen production by partial oxidation of methane: Modeling and simulation. *International Journal of Hydrogen Energy*, 2009. 34(16): p. 6655-6668.
- [41] Dobrego, K.V., et al., Partial oxidation of methane in a reverse flow porous media reactor. Water admixing optimization. *International Journal of Hydrogen Energy*, 2008. 33(20): p. 5535-5544.
- [42] Koh, A.C.W., et al., Hydrogen or synthesis gas production via the partial oxidation of methane over supported nickel-cobalt catalysts. *International Journal of Hydrogen Energy*, 2007. 32(6): p. 725-730.
- [43] Corbo, P. and F. Migliardini, Hydrogen production by catalytic partial oxidation of methane and propane on Ni and Pt catalysts. *International Journal of Hydrogen Energy*, 2007. 32(1): p. 55-66.
- [44] Lutz, A.E., et al., Thermodynamic analysis of hydrogen production by partial oxidation reforming. *International Journal of Hydrogen Energy*, 2004. 29(8): p. 809-816.
- [45] Jin H, Xu Y, Lin R, Han W. A proposal for a novel multifunctional energy system for the production of hydrogen and power. *Int J Hydrogen Energy* 2008;33:9.

References

- [46] Belghit, A., E.D. Gordillo, and S. El Issami, Coal steam-gasification model in chemical regime to produce hydrogen in a gas-solid moving bed reactor using nuclear heat. *International Journal of Hydrogen Energy*, 2009. 34(15): p. 6114-6119.
- [47] Li, K., R. Zhang, and J. Bi, Experimental study on syngas production by co-gasification of coal and biomass in a fluidized bed. *International Journal of Hydrogen Energy*. In Press, Corrected Proof.
- [48] Z'Graggen, A. and A. Steinfeld, Hydrogen production by steam-gasification of carbonaceous materials using concentrated solar energy - V. Reactor modeling, optimization, and scale-up. *International Journal of Hydrogen Energy*, 2008. 33(20): p. 5484-5492.
- [49] Yang, L., et al., Field test of large-scale hydrogen manufacturing from underground coal gasification (UCG). *International Journal of Hydrogen Energy*, 2008. 33(4): p. 1275-1285.
- [50] Guan, Y., et al., Steam catalytic gasification of municipal solid waste for producing tar-free fuel gas. *International Journal of Hydrogen Energy*. In Press, Corrected Proof.
- [51] He, M., et al., Hydrogen-rich gas from catalytic steam gasification of municipal solid waste (MSW): Influence of steam to MSW ratios and weight hourly space velocity on gas production and composition. *International Journal of Hydrogen Energy*, 2009. 34(5): p. 2174-2183.
- [52] Luo, S., et al., Hydrogen-rich gas from catalytic steam gasification of biomass in a fixed bed reactor: Influence of particle size on gasification performance. *International Journal of Hydrogen Energy*, 2009. 34(3): p. 1260-1264.
- [53] Mahishi, M.R. and D.Y. Goswami, An experimental study of hydrogen production by gasification of biomass in the presence of a CO₂ sorbent. *International Journal of Hydrogen Energy*, 2007. 32(14): p. 2803-2808.
- [54] Wei, L., et al., Steam gasification of biomass for hydrogen-rich gas in a free-fall reactor. *International Journal of Hydrogen Energy*, 2007. 32(1): p. 24-31.

References

- [55] Cormos, C.-C., et al., Innovative concepts for hydrogen production processes based on coal gasification with CO₂ capture. *International Journal of Hydrogen Energy*, 2008. 33(4): p. 1286-1294.
- [56] Gnanapragasam, N.V., B.V. Reddy, and M.A. Rosen, Hydrogen production from coal gasification for effective downstream CO₂ capture. *International Journal of Hydrogen Energy*. In Press, Corrected Proof.
- [57] European Hydrogen and Fuel Cell Technology Platform. Strategic research agenda, <https://www.hfpeurope.org/>; 2005.
- [58] E. Shoko, B. McLellan, A.L. Dicks and J.C. Diniz da Costa, Hydrogen from coal production and utilisation technologies, *Int. J. Coal Geol* 65 (2006), pp. 213–222
- [59] Zabaniotou, A., et al., Experimental study of pyrolysis for potential energy, hydrogen and carbon material production from lignocellulosic biomass. *International Journal of Hydrogen Energy*, 2008. 33(10): p. 2433-2444.
- [60] Ahmed, I.I. and A.K. Gupta, Hydrogen production from polystyrene pyrolysis and gasification: Characteristics and kinetics. *International Journal of Hydrogen Energy*, 2009. 34(15): p. 6253-6264.
- [61] Zhao, B., et al., Hydrogen production from biomass combining pyrolysis and the secondary decomposition. *International Journal of Hydrogen Energy*. In Press, Corrected Proof.
- [62] Marda, J.R., et al., Non-catalytic partial oxidation of bio-oil to synthesis gas for distributed hydrogen production. *International Journal of Hydrogen Energy*, 2009. 34(20): p. 8519-8534.
- [63] Le Valant, A., et al., Hydrogen production from raw bioethanol steam reforming: Optimization of catalyst composition with improved stability against various impurities. *International Journal of Hydrogen Energy*. In Press, Corrected Proof.
- [64] Chen, H., et al., Thermodynamic analyses of adsorption-enhanced steam reforming of glycerol for hydrogen production. *International Journal of Hydrogen Energy*, 2009. 34(17): p. 7208-7222.

References

- [65] Rossi, C.C.R.S., et al., Thermodynamic analysis of steam reforming of ethanol and glycerine for hydrogen production. *International Journal of Hydrogen Energy*, 2009. 34(1): p. 323-332.
- [66] Su, H., et al., Combination of dark- and photo-fermentation to enhance hydrogen production and energy conversion efficiency. *International Journal of Hydrogen Energy*, 2009. 34(21): p. 8846-8853.
- [67] Gavala, H.N., I.V. Skiadas, and B.K. Ahring, Biological hydrogen production in suspended and attached growth anaerobic reactor systems. *International Journal of Hydrogen Energy*, 2006. 31(9): p. 1164-1175.
- [68] Yoon, J.H., et al., Evaluation of conversion efficiency of light to hydrogen energy by *Anabaena variabilis*. *International Journal of Hydrogen Energy*, 2006. 31(6): p. 721-727.
- [69] Kalinci, Y., A. Hepbasli, and I. Dincer, Biomass-based hydrogen production: A review and analysis. *International Journal of Hydrogen Energy*, 2009. 34(21): p. 8799-8817.
- [70] Wang, G., J.M. Ogden, and M.A. Nicholas, Lifecycle impacts of natural gas to hydrogen pathways on urban air quality. *International Journal of Hydrogen Energy*, 2007. 32(14): p. 2731-2742.
- [71] El-Bassuoni, A.M.A., J.W. Sheffield, and T.N. Veziroglu, Hydrogen and fresh water production from sea water. *International Journal of Hydrogen Energy*, 1982. 7(12): p. 919-923.
- [72] Ivy, J. Summary of Electrolytic Hydrogen Production, Milestone Completion Report, 2004, National Renewable Energy Laboratory
- [73] Yildiz, B. and M.S. Kazimi, Efficiency of hydrogen production systems using alternative nuclear energy technologies. *International Journal of Hydrogen Energy*, 2006. 31(1): p. 77-92.
- [74] O'Brien, J.E., et al., High-temperature electrolysis for large-scale hydrogen and syngas production from nuclear energy - summary of system simulation and economic analyses. *International Journal of Hydrogen Energy*. In Press, Corrected Proof.

References

- [75] Utgikar, V. and T. Thiesen, Life cycle assessment of high temperature electrolysis for hydrogen production via nuclear energy. *International Journal of Hydrogen Energy*, 2006. 31(7): p. 939-944.
- [76] Sakurai, M. and S. Ueno, Preliminary analysis of transportation cost of nuclear off-peak power for hydrogen production based on water electrolysis. *International Journal of Hydrogen Energy*, 2006. 31(15): p. 2378-2385.
- [77] Pregger, T., et al., Prospects of solar thermal hydrogen production processes. *International Journal of Hydrogen Energy*, 2009. 34(10): p. 4256-4267.
- [78] Arriaga, L.G., et al., Direct coupling of a solar-hydrogen system in Mexico. *International Journal of Hydrogen Energy*, 2007. 32(13): p. 2247-2252.
- [79] Nowotny, J., et al., Solar-hydrogen: Environmentally safe fuel for the future. *International Journal of Hydrogen Energy*, 2005. 30(5): p. 521-544.
- [80] Aiche-Hamane, L., et al., Feasibility study of hydrogen production from wind power in the region of Ghardaia. *International Journal of Hydrogen Energy*, 2009. 34(11): p. 4947-4952.
- [81] Bockris, J.O.M. and T.N. Veziroglu, Estimates of the price of hydrogen as a medium for wind and solar sources. *International Journal of Hydrogen Energy*, 2007. 32(12): p. 1605-1610.
- [82] Greiner, C.J., M. KorpAs, and A.T. Holen, A Norwegian case study on the production of hydrogen from wind power. *International Journal of Hydrogen Energy*. 32(10-11): p. 1500-1507.
- [83] Balta, M.T., I. Dincer, and A. Hepbasli, Potential methods for geothermal-based hydrogen production. *International Journal of Hydrogen Energy*. In Press, Corrected Proof.
- [84] Tolga Balta, M., I. Dincer, and A. Hepbasli, Thermodynamic assessment of geothermal energy use in hydrogen production. *International Journal of Hydrogen Energy*, 2009. 34(7): p. 2925-2939.
- [85] Yumurtaci, Z. and E. Bilgen, Hydrogen production from excess power in small hydroelectric installations. *International Journal of Hydrogen Energy*, 2004. 29(7): p. 687-693.

References

- [86] Tarnay, D.S., Hydrogen production at hydro-power plants. *International Journal of Hydrogen Energy*, 1985. 10(9): p. 577-584.
- [87] La Roche, U., The greenland hydropower as a source of electrolytic hydrogen. *International Journal of Hydrogen Energy*, 1977. 2(4): p. 405-411.
- [88] Wikipedia, electrolysis, <http://en.wikipedia.org/wiki/Electrolysis#History>, accessed 13 Feb 2008
- [89] Wikipedia, hofmann voltameter, http://en.wikipedia.org/wiki/Hofmann_voltameter, accessed 13 Feb 2008
- [90] Ulleberg, Ø., Modeling of advanced alkaline electrolyzers: a system simulation approach. *International Journal of Hydrogen Energy*, 2003. 28(1): p. 21-33.
- [91] Ganley, J.C., High temperature and pressure alkaline electrolysis. *International Journal of Hydrogen Energy*, 2009. 34(9): p. 3604-3611.
- [92] Fujiwara, S., et al., Hydrogen production by high temperature electrolysis with nuclear reactor. *Progress in Nuclear Energy*. 50(2-6): p. 422-426.
- [93] Shin, Y., et al., Evaluation of the high temperature electrolysis of steam to produce hydrogen. *International Journal of Hydrogen Energy*. 32(10-11): p. 1486-1491.
- [94] Wendt, H., *Electrochemical hydrogen technologies*. Elsevier, Amsterdam (1990), pp. 1-14.
- [95] Barbir, F., PEM electrolysis for production of hydrogen from renewable energy sources. *Solar Energy Solar Hydrogen*, 2005. 78(5): p. 661-669.
- [96] Divisek J., Steffen B., Schmitz H. Theoretical analysis and evaluation of the operating data of a bipolar water electrolyser. *Int. J. Hydrogen Energy*, vol. 19 (7), 1994, pp. 579-586
- [97] Divisek, J. and H. Schmitz, A bipolar cell for advanced alkaline water electrolysis. *International Journal of Hydrogen Energy*, 1982. 7(9): p. 703-710
- [98] ELT Elektrolyse Technik GmbH, <http://www.elektrolyse.de/vkp/modules.php?name=Content&pa=showpage&pid=5>, accessed 15 October 2009

References

- [99] Linde AG, [http://www.linde-gas.com/International/Web/LG/COM/likeigcom30.nsf/repositorybyalias/pdf_onsite_hydross/\\$file/HYDROSS.pdf](http://www.linde-gas.com/International/Web/LG/COM/likeigcom30.nsf/repositorybyalias/pdf_onsite_hydross/$file/HYDROSS.pdf), accessed 15 October 2009
- [100] Hydrogenics Corporation, http://www.hydrogenics.com/hydro/hystat_a, accessed 15 October 2009
- [101] Solid Polymer Electrolyte Water Electrolysis Technology Development for Large Scale Hydrogen Production, General Electric Coy (1981), DOE report no. DOE/ET/26 202-1.
- [102] Proton Energy Systems, products, <http://www.protonenergy.com/>, accessed 20 October 2009.
- [103] Giner, Inc. and Giner Electrochemical Systems, LLC, <http://www.ginerinc.com/products.php?a=HPH2>, accessed 20 October 2009
- [104] Mitsubishi generates 350 bar hydrogen without compressor, 2004, Fuel Cells Bulletin, number 6: p. 8.
- [105] h-tech Wasserstoff-Energie-Systeme GmbH, <http://www.h-tec.com/html/web/industrial/index.asp>, accessed 20 October 2009
- [106] Treadwell Corporation, <http://www.treadwellcorp.com/pemhg.htm>, accessed 20 October 2009.
- [107] Grigoriev, S.A., et al., Hydrogen safety aspects related to high-pressure polymer electrolyte membrane water electrolysis. *International Journal of Hydrogen Energy*, 2009. 34(14): p. 5986-5991.
- [108] Marshall, A.T., et al., Performance of a PEM water electrolysis cell using IrxRuyTazO2 electrocatalysts for the oxygen evolution electrode. *International Journal of Hydrogen Energy*, 2007. 32(13): p. 2320-2324.
- [109] Grigoriev, S.A., V.I. Porembsky, and V.N. Fateev, Pure hydrogen production by PEM electrolysis for hydrogen energy. *International Journal of Hydrogen Energy*, 2006. 31(2): p. 171-175.
- [110] PEM electrolysis efficiency takes a leap forward. *Membrane Technology*, 2009. 2009(5): p. 3-3.

References

- [111] Santarelli, M., P. Medina, and M. Calì, Fitting regression model and experimental validation for a high-pressure PEM electrolyzer. *International Journal of Hydrogen Energy*, 2009. 34(6): p. 2519-2530.
- [112] Grigoriev SA, Lyutikova EK, Martemianov S, Fateev VN. On the possibility of replacement of Pt by Pd on a hydrogen electrode of PEM fuel cells. *Int J Hydrogen Energy* 2007;32: 4438–42.
- [113] Millet, P., et al., PEM water electrolyzers: From electrocatalysis to stack development. *International Journal of Hydrogen Energy*. In Press, Corrected Proof.
- [114] Brown, T.M., et al., Dynamic first principles model of a complete reversible fuel cell system. *Journal of Power Sources*, 2008. 182(1): p. 240-253.
- [115] Marshall, A., et al., Hydrogen production by advanced proton exchange membrane (PEM) water electrolyzers--Reduced energy consumption by improved electrocatalysis. *Energy*, 2007. 32(4): p. 431-436.
- [116] Shapiro, D., et al., Solar-powered regenerative PEM electrolyzer/fuel cell system. *Solar Energy*, 2005. 79(5): p. 544-550.
- [117] Clarke, R.E., et al., Direct coupling of an electrolyser to a solar PV system for generating hydrogen. *International Journal of Hydrogen Energy*, 2009. 34(6): p. 2531-2542.
- [118] Doucet, G., et al., Hydrogen-based PEM auxiliary power unit. *International Journal of Hydrogen Energy*, 2009. 34(11): p. 4983-4989.
- [119] Paul, B. and J. Andrews, Optimal coupling of PV arrays to PEM electrolyzers in solar-hydrogen systems for remote area power supply. *International Journal of Hydrogen Energy*, 2008. 33(2): p. 490-498.
- [120] Ipsakis, D., et al., Power management strategies for a stand-alone power system using renewable energy sources and hydrogen storage. *International Journal of Hydrogen Energy*, 2009. 34(16): p. 7081-7095.
- [121] Sopian, K., et al., Performance of a PV-wind hybrid system for hydrogen production. *Renewable Energy*, 2009. 34(8): p. 1973-1978.

References

- [122] Peharz, G., F., Dimroth, and U. Wittstadt, Solar hydrogen production by water splitting with a conversion efficiency of 18%. *International Journal of Hydrogen Energy*, 2007. 32(15): p. 3248-3252.
- [123] Görgün, H., Dynamic modelling of a proton exchange membrane (PEM) electrolyzer. *International Journal of Hydrogen Energy*, 2006. 31(1): p. 29-38.
- [124] Onda K. et al., Performance analysis of polymer-electrolyte water electrolysis cell at a small-unit test cell and performance prediction of large stacked cell, *Journal of The Electrochemical Society*, 149 (2001) A1069-A1078.
- [125] Nguyen V. Predictive models for emissions in petrol–hydrogen engine. PhD dissertation. University of Tasmania; 2007.
- [126] Burke P. Performance appraisal of a hydrogen combustion engine. Master thesis. University of Tasmania; 2005.
- [127] Lebbal, M.E. and S. Lecoëuche, Identification and monitoring of a PEM electrolyser based on dynamical modelling. *International Journal of Hydrogen Energy*, 2009. 34(14): p. 5992-5999.
- [128] Karri V, et al. Artificial neural networks and neuro-fuzzy inference systems as virtual sensors for hydrogen safety prediction. *Int J Hydrogen Energy* 2008; 33:2857–67.
- [129] Crockett RGM, Newborough M, Highgate DJ, Probert SD. Electrolyser-based electricity management. *Appl Energy* 1995;51:249–63.
- [130] Leaver RH, Thomas TR. Analysis and presentation of experimental results. London: The Macmillan Press Ltd; 1974.
- [131] Padhy NP. Artificial intelligence and intelligent systems. New Delhi: Oxford University Press; 2005.
- [132] Haykin S. Neural networks: a comprehensive foundation. 2nd ed. New Jersey: Prentice Hall; 1999.
- [133] Negnevitsky M. Artificial intelligence –a guide to intelligent systems. 2nd ed. Harlow, England: Pearson Education Limited; 2005.
- [134] Kendall, G., "Neural Networks," *Introduction to Artificial Intelligence*, 2001

References

- [135] Jurada, JM. Introduction to artificial neural systems, West Publishing Company, 1992
- [136] Hebb, DO. Organization of behaviour, Wiley, 1949
- [137] Rumelhart, D & McClelland, J 1986, Parallel distributed processing: exploitations in the micro-structure of cognition, vol. 1 and 2, MIT Press, Cambridge.
- [138] Hopfield, JJ 1982, „Neural networks and physical systems with emergent collecting computational abilities“, Proceedings of the National Academy of Sciences, vol. 79, pp. 2554-2558.
- [139] Elman, JL 1990, „Finding structure in time“, Cognitive Science, vol. 14, pp. 179-211.
- [140] Lowe, D. Adaptive radial basis function nonlinearities and the problem of generalization, Proc. 1st IEEE International Conference on Artificial Networks, London, 1989, UK
- [141] Ergezinger, S. Thomsen, E. An accelerated learning algorithm for multilayer perceptrons: Optimization Layer-by-Layer. IEEE Transactions on Neural Networks, vol. 6, no. 1, 1995, pp. 31-42.
- [142] Kohonen, T. “Self Organisation and Associative Memory”. Third Edition, Springer-Verlag, New York, 1989.
- [143] Dayhoff, J. E. “Neural Network Architectures – An Introduction”, Van Nostrand Reinhold, 1990.
- [144] Brunelli, R., “Training Neural Nets Through Stochastic Minimisation”. Journal Neural Networks, vol. 7, no. 9, 1994, pp. 1405-1412.
- [145] Karri, V, Kiatcharoenpol, T. Prediction of Thrust and Torque in Drilling Using Conventional and an Optimised Layer by Layer Neural Network, Proceedings of the 3rd Asia Pacific Conference on Systems Integrity and Maintenance (Systems Integrity and Maintenance - ACSIM 2002), Cairns, Australia, 178-183

References

- [146] Karri, V, Kiatcharoenpol, T. Prediction of Internal Surface Roughness in Drilling using Three Feedforward Neural Networks - A Comparison, CD-Rom Proceedings of 9th International Conference on Neural Information Processing, Singapore, EJ (2002).
- [147] Zadeh, Lofti A. Fuzzy Sets, *Information and Control*, vol.8, 1965, pp. 385-353
- [148] Jang, J.-S.R. ANFIS: Adaptive Network based Fuzzy-Inference Systems, *IEEE Transactions on Systems, Man and Cybernetics*, vol.23, no.3, 1993, pp. 665-685
- [149] Matlab neural networks and ANFIS, version 2006. Mathworks Inc; 2006.
- [150] Becker, S. and V. Karri. Neural network based predictive models for PEM-electrolyzer performance, *Proceedings Hypothesis 8, Hydrogen Systems and Materials for Sustainability*, Lisbon (2009), April 1-3
- [151] Becker, S. and V. Karri, Predictive models for PEM-electrolyzer performance using adaptive neuro-fuzzy inference systems. *International Journal of Hydrogen Energy*. In Press, Corrected Proof.
- [152] Becker, S. and V. Karri, Modelling of hydrogen production efficiency for a PEM-electrolyzer using Neural Networks. *The 3rd International Workshop on Artificial Intelligence in Science and Technology (AISAT)*, Hobart (2009), 23-24 November
- [153] Haruni AMO, Muttaqi KM, Negnevitsky M. Artificial intelligent approach to arc furnace response prediction. In: *Proc. of international conference on intelligent technologies*, Sydney; 2007. p. 189–94.
- [154] Karri, V, 'Drilling Performance Prediction Using General Regression Neural Networks', *Proceedings of the 13th International Conference on Industrial and Engineering Applications of Artificial Intelligence and Expert Systems: ntelligent Problem Solving - Methodologies and Approaches*, New Orleans, Louisiana, USA, 67-72 (2000) [F1]
- [155] Huang SH, Zang HC. Artificial neural networks in manufacturing: concepts, applications and perspectives. *IEEE Trans Compon Packag Manuf Technol* 1994; 17(2): 212–28.

References

- [156] Karri V. Design and development of hydrogen laboratory, vols. 1–3. University of Tasmania research report; 2004.
- [157] Petersen MG. Installation of a hydrogen generator. University of Tasmania research report; 2004.
- [158] Hogen 40 series 2 hydrogen generator. Installation and operation instruction manual. Distributed Energy Systems; 2004.
- [159] Parker Seal Group, O-Ring Handbook, Parker Hannifin Corporation 1992, online http://www.parker.com/literature/ORD%205700%20Parker_O-Ring_Handbook.pdf, accessed November 2008
- [160] PM 3000 ACE user manual, version 10. Voltech Instruments Inc.
- [161] Kiatcharoenpol, T (2004), Applications of neural-fuzzy systems to tool condition monitoring in drilling operations, PhD. Thesis, University of Tasmania.
- [162] Frost, F (2001), Neural network applications to aluminium manufacturing for auto part, PhD. Thesis, University of Tasmania.
- [163] Karri, V and Kiatcharoenpol, T (2003), Tool condition monitoring in drilling using artificial neural network, Lecture Notes in Computer Science, vol. 2903, pp, 293-301.

APPENDIX

EXPERIMENTAL DATA

LEL	Lower Explosive Limit
PPS	Product Pressure
SPS	System Pressure
WTQ	Feed Water Quality
SVG	Stack Voltage
SCT	Stack Current
STM	Electrolyzer System Temperature

Appendix: Experimental Data

LEL [%]	PPS [kPa]	SPS [kPa]	WTQ [MΩ]	SVG [V]	SCT [A]	STM [°C]	Water- pressure [kPa]	System Power [W]	System- efficiency	Hydrogen flow [l/min]	Stack- efficiency
31	13.7898	1089.394	15.1	24.7	144.1	21	268.95	4279	0.3141	3.5523	0.4192
31	27.5796	1344.506	15.1	24.6	144.1	21	268.55	4286	0.4857	6.0896	0.5808
31	27.5796	1344.506	15.2	24.5	144.1	22	268.55	4309	0.3949	5.3284	0.4860
31	48.2643	1344.506	15	24.4	143.7	22	268.55	4260	0.5828	8.2887	0.6399
31	55.1592	1330.716	15.2	24.4	144.1	22	268.75	4266	0.5756	8.5255	0.6404
31	68.949	1344.506	15.1	24.4	144.1	23	268.36	4258	0.6335	9.6880	0.7120
31	75.8439	1344.506	15.2	24.4	144.1	23	268.55	4254	0.6226	9.7688	0.7052
32	89.6337	1344.506	15.5	24.3	144.1	23	268.55	4249	0.6651	10.6568	0.7582
32	96.5286	1344.506	15.3	24.3	144.1	23	268.55	4245	0.6532	10.6568	0.7490
32	110.3184	1344.506	15.4	24.3	143.9	24	268.75	4241	0.6866	11.3673	0.7906
32	124.1082	1344.506	15.1	24.3	143.9	24	268.55	4220	0.7150	11.9890	0.8264

Appendix: Experimental Data

33	137.898	1323.821	15.3	24.2	144.1	24	268.75	4236	0.6916	11.8409	0.8046
33	137.898	1344.506	15.3	24.2	144.1	24	268.75	4231	0.6498	11.2177	0.7576
33	137.898	1344.506	15.1	24.2	144.1	24	268.75	4227	0.6126	10.6568	0.7158
34	144.7929	1344.506	15.5	24.2	144.1	25	268.55	4225	0.6083	10.6568	0.7124
34	151.6878	1351.4	15.3	24.1	144.1	25	268.16	4223	0.6045	10.6568	0.7094
35	151.6878	1344.506	15.5	24.1	144.1	25	268.55	4219	0.5751	10.1935	0.6759
35	158.5827	1351.4	15.2	24.1	144.1	25	268.36	4200	0.5733	10.2128	0.6748
35	158.5827	1344.506	15.4	24.1	143.7	25	268.36	4198	0.5478	9.8043	0.6459
35	124.1082	1310.031	15.2	24.1	144.1	25	269.34	4217	0.4105	7.3778	0.4846
36	172.3725	1344.506	15.3	24.1	144.1	25	268.16	4214	0.5471	9.8674	0.6463
36	172.3725	1344.506	15.3	24.1	144.1	25	268.36	4212	0.5257	9.5150	0.6217
36	172.3725	1344.506	15.2	24.1	144.1	26	268.16	4202	0.5059	9.1869	0.5988
37	186.1623	1351.4	15.4	23.9	143.7	26	268.55	4192	0.5265	9.5912	0.6241
37	193.0572	1351.4	15.3	23.9	143.7	26	268.75	4192	0.5269	9.6255	0.6252
36	193.0572	1344.506	15.4	23.9	143.7	26	268.36	4171	0.5093	9.3247	0.6048
34	199.9521	1351.4	15.3	23.9	143.5	26	268.16	4172	0.5103	9.3651	0.6065

Appendix: Experimental Data

32	206.847	1351.4	15.3	23.9	143.9	26	268.16	4205	0.4956	9.1344	0.5900
32	213.7419	1330.716	15.3	23.9	144.1	26	268.36	4204	0.4970	9.1767	0.5919
32	213.7419	1323.821	15.2	23.9	144.1	26	268.16	4204	0.4826	8.9287	0.5752
32	220.6368	1330.716	15.4	23.9	144.1	26	267.97	4202	0.4841	8.9742	0.5775
34	227.5317	1330.716	15.2	23.9	144.1	26	268.55	4202	0.4856	9.0173	0.5796
35	234.4266	1330.716	15.3	23.9	144.1	26	268.36	4183	0.4870	9.0583	0.5816
36	241.3215	1330.716	15.2	23.9	143.7	26	268.16	4183	0.4884	9.0973	0.5836
36	220.6368	1275.557	15.1	23.9	143.7	26	268.16	4202	0.4353	8.1195	0.5204
37	248.2164	1344.506	15.3	23.9	144.1	26	268.36	4201	0.4777	8.9220	0.5713
37	248.2164	1344.506	15.4	23.9	144.1	26	268.55	4202	0.4662	8.7192	0.5579
37	255.1113	1344.506	15.5	23.9	144.1	27	267.97	4200	0.4679	8.7623	0.5601
37	262.0062	1344.506	15.4	23.9	144.1	27	268.16	4198	0.4695	8.8035	0.5623
37	268.9011	1344.506	15.1	23.9	144.1	27	268.55	4198	0.4711	8.8429	0.5644
37	268.9011	1344.506	15.4	23.9	144.1	27	268.36	4181	0.4608	8.6587	0.5523
37	268.9011	1344.506	15.3	23.9	143.7	27	267.97	4180	0.4509	8.4820	0.5407
37	282.6909	1344.506	15.2	23.9	143.9	27	268.16	4200	0.4642	8.7386	0.5567

Appendix: Experimental Data

37	282.6909	1344.506	15.5	23.9	144.1	27	267.97	4198	0.4455	8.4025	0.5346
37	282.6909	1344.506	15.5	23.9	144.1	27	267.38	4197	0.4367	8.2440	0.5242
37	296.4807	1344.506	15.3	23.9	144.1	27	268.16	4195	0.4491	8.4860	0.5393
37	303.3756	1344.506	15.3	23.9	144.1	27	267.97	4196	0.4508	8.5255	0.5415
37	303.3756	1344.506	15.3	23.9	144.1	27	267.97	4178	0.4424	8.3732	0.5315
37	317.1654	1344.506	15.2	23.9	143.7	27	268.75	4162	0.4541	8.6003	0.5457
37	324.0603	1344.506	15.2	23.8	143.5	27	267.97	4182	0.4556	8.6357	0.5477
37	324.0603	1344.506	15.4	23.9	143.9	27	267.77	4178	0.4476	8.4894	0.5382
37	337.8501	1344.506	15.5	23.8	143.7	27	267.97	4177	0.4587	8.7031	0.5516
35	337.8501	1344.506	15.4	23.8	143.7	27	267.58	4177	0.4509	8.5604	0.5423
34	344.745	1344.506	15.4	23.8	143.7	27	267.38	4176	0.4524	8.5942	0.5443
33	358.5348	1344.506	15.1	23.8	143.7	27	267.58	4193	0.4627	8.7961	0.5569
33	351.6399	1316.926	15.2	23.8	144.1	27	267.19	4175	0.4464	8.4922	0.5375
33	358.5348	1316.926	15.1	23.8	143.7	27	266.99	4175	0.4481	8.5255	0.5394
33	358.5348	1323.821	15.4	23.8	143.7	27	267.38	4194	0.4411	8.3963	0.5311
35	365.4297	1344.506	15.3	23.8	144.1	27	267.58	4193	0.4426	8.4300	0.5331

Appendix: Experimental Data

37	379.2195	1344.506	15.4	23.8	144.1	27	267.19	4193	0.4455	8.4946	0.5368
37	379.2195	1344.506	15.1	23.8	144.1	27	267.58	4192	0.4389	8.3732	0.5290
37	393.0093	1344.506	15	23.8	144.1	27	267.58	4192	0.4482	8.5555	0.5404
37	393.0093	1344.506	15.1	23.8	144.1	27	267.38	4175	0.4418	8.4367	0.5327
37	399.9042	1344.506	15.2	23.8	143.7	27	267.77	4175	0.4432	8.4671	0.5345
37	406.7991	1344.506	15.3	23.8	143.7	27	267.77	4194	0.4445	8.4967	0.5363
37	406.7991	1344.506	15.1	23.8	144.1	27	267.38	4193	0.4385	8.3834	0.5290
37	413.694	1344.506	15.2	23.8	144.1	27	267.38	4193	0.4399	8.4133	0.5307
37	420.5889	1344.506	15.3	23.8	144.1	27	266.8	4191	0.4412	8.4424	0.5325
37	427.4838	1344.506	15.1	23.8	144.1	27	266.99	4190	0.4425	8.4708	0.5341
37	427.4838	1344.506	15.2	23.8	144.1	27	267.19	4191	0.4367	8.3636	0.5272
37	434.3787	1344.506	15.1	23.8	144.1	27	267.58	4173	0.4381	8.3923	0.5289
37	441.2736	1337.611	15.1	23.8	143.7	27	266.99	4173	0.4394	8.4202	0.5306
37	448.1685	1344.506	15.2	23.8	143.7	27	266.6	4193	0.4406	8.4475	0.5322
38	448.1685	1344.506	15	23.8	144.1	28	266.41	4192	0.4351	8.3457	0.5257
37	448.1685	1344.506	15.3	23.8	144.1	28	265.43	4173	0.4299	8.2464	0.5193

Appendix: Experimental Data

37	468.8532	1344.506	15.3	23.8	143.7	28	266.6	4173	0.4390	8.4263	0.5305
36	475.7481	1344.506	15.2	23.8	143.9	28	266.8	4172	0.4402	8.4520	0.5320
35	482.643	1344.506	15.2	23.8	143.7	28	266.6	4154	0.4414	8.4770	0.5335
34	489.5379	1344.506	15.1	23.8	143.5	28	266.41	4170	0.4426	8.5015	0.5350
33	489.5379	1323.821	15.2	23.8	143.7	28	266.6	4191	0.4376	8.4071	0.5290
33	489.5379	1344.506	15.1	23.8	144.1	28	266.41	4190	0.4326	8.3147	0.5230
33	503.3277	1344.506	15	23.8	144.1	28	266.8	4188	0.4398	8.4560	0.5318
35	503.3277	1337.611	15.1	23.8	144.1	28	266.21	4188	0.4350	8.3651	0.5260
37	510.2226	1337.611	15.2	23.8	144.1	28	266.6	4188	0.4361	8.3894	0.5275
37	517.1175	1337.611	15.4	23.8	144.1	28	266.41	4186	0.4372	8.4133	0.5289
37	524.0124	1337.611	15	23.8	144.1	28	266.6	4169	0.4384	8.4367	0.5303
37	524.0124	1337.611	15.3	23.8	143.7	28	266.41	4170	0.4338	8.3497	0.5248
37	530.9073	1337.611	15.2	23.8	143.7	28	266.21	4190	0.4349	8.3732	0.5262
37	537.8022	1337.611	15	23.8	144.1	28	266.21	4187	0.4360	8.3963	0.5275
37	544.6971	1330.716	15.1	23.8	144.1	28	266.41	4187	0.4370	8.4189	0.5289
37	544.6971	1330.716	15	23.8	144.1	28	266.41	4187	0.4326	8.3356	0.5236

Appendix: Experimental Data

37	558.4869	1337.611	15	23.8	144.1	28	266.41	4184	0.4347	8.3806	0.5263
37	565.3818	1330.716	15.2	23.8	144.1	28	266.41	4170	0.4359	8.4025	0.5276
37	572.2767	1330.716	15.1	23.8	143.7	28	266.41	4168	0.4369	8.4240	0.5289
37	572.2767	1337.611	15.3	23.8	143.7	28	266.21	4188	0.4327	8.3445	0.5238
38	579.1716	1337.611	15.3	23.8	144.1	28	266.02	4185	0.4337	8.3661	0.5251
37	586.0665	1330.716	15.3	23.8	144.1	28	265.62	4185	0.4347	8.3873	0.5264
37	592.9614	1337.611	15.2	23.8	144.1	28	266.21	4177	0.4356	8.4082	0.5276
37	599.8563	1337.611	15.2	23.8	143.7	28	266.02	4169	0.4367	8.4286	0.5289
38	606.7512	1337.611	15.2	23.8	143.7	28	266.02	4168	0.4377	8.4487	0.5301
37	613.6461	1337.611	15.1	23.8	143.7	28	265.82	4155	0.4386	8.4684	0.5313
36	620.541	1330.716	15.2	23.8	143.5	28	265.82	4151	0.4395	8.4878	0.5324
35	627.4359	1330.716	15.1	23.8	143.5	28	266.02	4172	0.4405	8.5068	0.5336
34	627.4359	1337.611	15.2	23.8	143.9	28	266.21	4187	0.4366	8.4328	0.5289
33	634.3308	1316.926	15.3	23.8	144.1	28	265.82	4186	0.4375	8.4520	0.5300
33	641.2257	1310.031	15.3	23.8	144.1	28	265.82	4186	0.4384	8.4708	0.5312
34	648.1206	1310.031	15.1	23.8	144.1	28	266.02	4185	0.4393	8.4894	0.5323

Appendix: Experimental Data

37	655.0155	1316.926	15.2	23.8	144.1	28	265.82	4175	0.4365	8.4367	0.5289
37	661.9104	1310.031	15	23.8	143.7	28	266.41	4169	0.4373	8.4550	0.5300
37	661.9104	1316.926	15.1	23.8	143.7	28	265.82	4188	0.4337	8.3857	0.5256
37	668.8053	1337.611	15.3	23.8	144.1	28	266.02	4186	0.4345	8.4042	0.5267
37	675.7002	1330.716	15	23.8	144.1	28	266.02	4186	0.4354	8.4223	0.5278
37	675.7002	1330.716	15	23.8	144.1	28	266.02	4186	0.4318	8.3550	0.5235
38	682.5951	1330.716	14.9	23.8	144.1	28	266.02	4185	0.4328	8.3732	0.5246
37	689.49	1330.716	15	23.8	144.1	28	265.82	4184	0.4337	8.3912	0.5257
38	696.3849	1330.716	15.2	23.8	144.1	28	265.82	4174	0.4345	8.4089	0.5309
37	703.2798	1330.716	15.4	23.8	143.7	28	267.38	4166	0.4353	8.4263	0.5320
38	703.2798	1330.716	15.4	23.8	143.7	28	265.82	4189	0.4319	8.3615	0.5278
38	710.1747	1330.716	15	23.8	144.1	28	265.62	4187	0.4328	8.3790	0.5288
38	717.0696	1330.716	15.1	23.8	144.1	28	265.82	4186	0.4336	8.3963	0.5299
38	723.9645	1330.716	15.1	23.8	144.1	28	265.82	4186	0.4344	8.4133	0.5308
38	723.9645	1330.716	15.2	23.8	144.1	28	265.62	4185	0.4311	8.3505	0.5268
38	737.7543	1330.716	14.9	23.8	144.1	28	265.62	4181	0.4360	8.4465	0.5328

Appendix: Experimental Data

38	744.6492	1330.716	15	23.8	143.5	28	265.82	4152	0.4336	8.4010	0.5298
38	758.439	1330.716	15	23.8	143.5	28	265.43	4171	0.4383	8.4946	0.5357
37	758.439	1330.716	15.1	23.8	143.9	28	265.62	4169	0.4352	8.4335	0.5317
35	772.2288	1337.611	15.3	23.8	143.9	28	265.43	4177	0.4399	8.5255	0.5375
35	772.2288	1330.716	15.1	23.8	143.9	28	288.67	4184	0.4367	8.4650	0.5336
34	779.1237	1310.031	15.1	23.8	144.1	28	285.35	4186	0.4375	8.4804	0.5345
34	779.1237	1310.031	15.1	23.8	144.1	28	284.18	4185	0.4344	8.4211	0.5307
34	786.0186	1310.031	15	23.8	144.1	28	284.37	4181	0.4352	8.4367	0.5316
36	792.9135	1310.031	15.1	23.8	143.7	28	284.18	4168	0.4359	8.4520	0.5325
37	799.8084	1310.031	15.1	23.8	143.7	28	283.79	4189	0.4366	8.4671	0.5334
37	799.8084	1330.716	15.2	23.8	144.1	28	284.18	4187	0.4336	8.4095	0.5297
37	813.5982	1330.716	15.1	23.8	144.1	28	284.18	4185	0.4380	8.4967	0.5352
37	813.5982	1330.716	15.2	23.8	144.1	28	284.18	4184	0.4350	8.4396	0.5315
37	820.4931	1330.716	15.2	23.8	144.1	28	284.37	4185	0.4358	8.4544	0.5324
37	827.388	1330.716	15.1	23.8	144.1	28	284.37	4184	0.4365	8.4690	0.5332
38	834.2829	1330.716	15.2	23.8	144.1	28	284.18	4182	0.4372	8.4834	0.5341

Appendix: Experimental Data

38	841.1778	1330.716	15.2	23.8	143.7	28	284.37	4187	0.4350	8.4424	0.5314
38	848.0727	1330.716	15.3	23.8	144.1	28	284.57	4185	0.4357	8.4567	0.5323
38	848.0727	1330.716	15	23.8	144.1	28	284.37	4185	0.4329	8.4025	0.5288
38	854.9676	1330.716	15.2	23.8	144.1	28	284.18	4184	0.4336	8.4169	0.5296
38	868.7574	1330.716	14.9	23.8	144.1	28	284.57	4184	0.4377	8.4985	0.5347
38	868.7574	1330.716	15.3	23.8	144.1	28	284.37	4184	0.4349	8.4450	0.5313
37	868.7574	1330.716	15.2	23.8	144.1	28	284.18	4183	0.4322	8.3923	0.5279
37	875.6523	1330.716	14.9	23.8	143.7	28	284.57	4150	0.4328	8.4063	0.5288
38	882.5472	1330.716	15.2	23.8	143.5	28	284.57	4172	0.4336	8.4202	0.5296
38	889.4421	1330.716	15.1	23.8	143.9	28	282.81	4171	0.4342	8.4339	0.5304
37	896.337	1330.716	15.1	23.8	143.9	28	284.37	4168	0.4349	8.4475	0.5312
35	903.2319	1330.716	14.9	23.8	143.7	28	284.77	4168	0.4355	8.4609	0.5320
35	910.1268	1330.716	15.1	23.8	143.9	28	284.77	4184	0.4363	8.4741	0.5328
34	910.1268	1316.926	15	23.8	144.1	28	284.77	4184	0.4336	8.4234	0.5296
34	923.9166	1310.031	14.9	23.8	144.1	28	284.77	4184	0.4375	8.5001	0.5344
34	923.9166	1310.031	14.9	23.8	144.1	28	284.96	4168	0.4349	8.4498	0.5312

Appendix: Experimental Data

37	937.7064	1330.716	15.2	23.8	144.1	28	284.77	4187	0.4362	8.4756	0.5327
37	937.7064	1330.716	14.9	23.8	144.1	28	284.96	4187	0.4336	8.4263	0.5296
37	944.6013	1330.716	15.1	23.8	144.1	28	284.77	4184	0.4342	8.4392	0.5303
37	951.4962	1330.716	15.1	23.8	144.1	28	284.96	4186	0.4348	8.4520	0.5311
37	958.3911	1330.716	15	23.8	144.1	28	284.77	4186	0.4354	8.4646	0.5318
37	965.286	1330.716	14.9	23.8	144.1	28	284.77	4184	0.4360	8.4770	0.5326
37	965.286	1330.716	15	23.8	144.1	28	285.16	4168	0.4335	8.4291	0.5295
37	972.1809	1330.716	15.1	23.8	143.7	28	284.37	4189	0.4341	8.4417	0.5303
37	979.0758	1330.716	15.2	23.8	144.1	28	282.23	4189	0.4348	8.4540	0.5310
37	979.0758	1323.821	15.2	23.8	144.1	28	284.96	4187	0.4323	8.4071	0.5280
38	985.9707	1323.821	14.9	23.8	144.1	28	284.57	4185	0.4329	8.4195	0.5287
38	992.8656	1330.716	15.1	23.8	144.1	28	284.57	4185	0.4335	8.4318	0.5295
38	999.7605	1323.821	15.1	23.8	144.1	28	284.57	4186	0.4341	8.4439	0.5302
38	1006.655	1330.716	14.9	23.8	144.1	28	285.74	4186	0.4347	8.4560	0.5309
37	1013.55	1323.821	14.9	23.8	143.9	28	284.57	4168	0.4353	8.4679	0.5316
38	1013.55	1330.716	15	23.8	143.7	28	285.16	4175	0.4330	8.4223	0.5287

Appendix: Experimental Data

38	1034.235	1330.716	14.9	23.8	143.9	28	284.18	4171	0.4370	8.5028	0.5337
37	1027.34	1330.716	15.1	23.8	143.7	28	284.37	4171	0.4318	8.4014	0.5273
35	1048.025	1330.716	15.1	23.8	143.7	28	284.57	4170	0.4382	8.5255	0.5351
35	1048.025	1330.716	15.1	23.8	143.7	28	284.57	4191	0.4358	8.4808	0.5323
35	1054.92	1330.716	15	23.8	144.3	28	285.75	4187	0.4364	8.4922	0.5329
34	1054.92	1310.031	15	23.8	144.1	28	293.55	4170	0.4341	8.4482	0.5301
34	1061.815	1316.926	15.3	23.8	143.7	28	293.36	4192	0.4346	8.4596	0.5308
35	1068.71	1323.821	15.3	23.8	144.1	28	293.16	4190	0.4352	8.4708	0.5315
37	1075.604	1330.716	15.1	23.8	144.1	28	293.36	4191	0.4358	8.4820	0.5322
37	1075.604	1330.716	15.1	23.8	144.1	28	293.36	4188	0.4335	8.4389	0.5294
37	1082.499	1330.716	15	23.8	144.1	28	293.55	4189	0.4341	8.4501	0.5301
37	1089.394	1330.716	15.2	23.8	144.1	28	293.75	4188	0.4346	8.4612	0.5307
37	1096.289	1330.716	15.3	23.8	144.1	28	294.34	4188	0.4351	8.4722	0.5314
37	1096.289	1330.716	15.2	23.8	144.1	28	294.14	4171	0.4329	8.4300	0.5287
37	1110.079	1330.716	15.2	23.8	143.7	28	294.14	4188	0.4362	8.4938	0.5327
38	1110.079	1330.716	14.9	23.8	144.1	28	294.34	4188	0.4340	8.4520	0.5300

Appendix: Experimental Data

38	1123.869	1330.716	15.2	23.8	144.1	28	294.53	4186	0.4350	8.4735	0.5313
38	1123.869	1330.716	15.2	23.8	144.1	29	294.73	4186	0.4330	8.4324	0.5287
38	1130.764	1330.716	15	23.8	144.1	28	294.53	4185	0.4335	8.4431	0.5294
38	1144.553	1330.716	15	23.8	144.1	28	294.73	4186	0.4366	8.5050	0.5332
37	1144.553	1330.716	14.9	23.8	144.1	28	294.73	4169	0.4346	8.4643	0.5306
37	1158.343	1330.716	15.3	23.8	143.7	28	294.73	4186	0.4376	8.5255	0.5344
38	1158.343	1330.716	15.1	23.8	144.1	28	293.95	4173	0.4355	8.4851	0.5319
37	1165.238	1330.716	14.8	23.8	143.7	28	294.53	4172	0.4361	8.4953	0.5325
38	1172.133	1330.716	15.1	23.8	143.9	28	294.73	4172	0.4366	8.5055	0.5331
37	1179.028	1337.611	15.1	23.8	143.7	28	294.34	4172	0.4371	8.5155	0.5337
35	1185.923	1337.611	15	23.8	143.9	28	294.34	4171	0.4375	8.5255	0.5343
35	1192.818	1344.506	15.1	23.8	143.9	28	294.34	4184	0.4381	8.5353	0.5349
35	1192.818	1330.716	15	23.8	144.1	28	294.14	4171	0.4360	8.4960	0.5324
34	1199.713	1330.716	15	23.8	143.7	28	294.34	4182	0.4365	8.5059	0.5330
34	1199.713	1330.716	14.9	23.8	144.1	28	293.95	4191	0.4345	8.4671	0.5305
35	1213.502	1330.716	15	23.8	144.1	28	292.97	4189	0.4375	8.5255	0.5342

Appendix: Experimental Data

37	1220.397	1344.506	15	23.8	144.1	28	294.34	4186	0.4360	8.4967	0.5323
37	1227.292	1344.506	15	23.8	144.1	28	294.34	4187	0.4364	8.5064	0.5329
37	1234.187	1344.506	14.9	23.8	144.1	28	293.95	4186	0.4369	8.5160	0.5335
37	1241.082	1344.506	14.9	23.8	144.1	28	294.73	4168	0.4374	8.5255	0.5340
38	1247.977	1344.506	15	23.8	143.7	28	294.34	4182	0.4379	8.5349	0.5346
38	1247.977	1330.716	15	23.8	144.1	28	294.14	4190	0.4359	8.4973	0.5322
38	1254.872	1344.506	15.1	23.8	144.1	28	294.34	4188	0.4364	8.5068	0.5328
37	1254.872	1344.506	15.3	23.8	144.1	28	294.34	4188	0.4344	8.4696	0.5304
38	1268.662	1344.506	15	23.8	144.1	28	294.53	4188	0.4373	8.5255	0.5339
38	1268.662	1344.506	15.1	23.8	144.1	28	294.14	4187	0.4354	8.4886	0.5316
38	1275.557	1344.506	15.1	23.8	144.1	28	294.34	4187	0.4358	8.4979	0.5321
38	1282.451	1351.4	14.8	23.8	144.1	28	291.99	4173	0.4363	8.5072	0.5327
38	1289.346	1344.506	14.8	23.8	143.7	28	293.75	4179	0.4367	8.5164	0.5332
38	1289.346	1344.506	14.9	23.8	144.1	28	293.95	4175	0.4349	8.4801	0.5310
38	1303.136	1358.295	14.9	23.8	143.9	28	293.95	4175	0.4376	8.5345	0.5343
38	1303.136	1358.295	15	23.8	143.9	28	293.36	4174	0.4358	8.4985	0.5321

Appendix: Experimental Data

36	1316.926	1365.19	14.9	23.8	143.7	28	293.55	4172	0.4366	8.5166	0.5332
35	1323.821	1365.19	15	23.8	143.7	28	293.75	4177	0.4371	8.5255	0.5337
34	1330.716	1365.19	14.8	23.8	144.3	28	294.77	4171	0.4376	8.5343	0.5342
34	1330.716	1365.19	14.8	23.8	143.7	28	295.51	4175	0.4357	8.4991	0.5320
34	1330.716	1337.611	15	23.8	144.1	28	295.51	4192	0.4339	8.4641	0.5298
35	1344.506	1372.085	14.8	23.8	144.1	28	295.9	4191	0.4366	8.5167	0.5331
37	1344.506	1372.085	15.1	23.8	144.1	28	296.09	4189	0.4348	8.4820	0.5309
37	1358.295	1378.98	14.8	23.8	144.1	28	296.48	4187	0.4374	8.5341	0.5341
37	1365.19	1378.98	15	23.8	144.1	28	296.68	4189	0.4379	8.5427	0.5346
38	1365.19	1385.875	14.8	23.8	144.1	28	296.09	4189	0.4361	8.5083	0.5324
38	1378.98	1385.875	15.1	23.8	144.1	28	296.68	4279	0.4387	8.5597	0.5356
38	1365.19	1365.19	14.2	14.9	0.5	26	296.68	363.7	0.4336	8.4402	0.5303